

**WASM: Minerals, Energy and Chemical Engineering**

**Fast Pyrolysis of Lignin and Its Derived Products at Low  
Temperatures**

**Yee Wen Chua**

**This thesis is presented for the Degree of  
Doctor of Philosophy  
of  
Curtin University**

**November 2019**

**Declaration**

To the best of my knowledge and belief this thesis contains no material previously published by any other person except where due acknowledgment has been made.

This thesis contains no material which has been accepted for the award of any other degree or diploma in any university.

Signature:.....

Date: 13/11/2019 .....

To my beloved family

**Abstract**

The increased energy consumption in the past decades leads to severe energy and environmental issues, such as global warming and fossil fuel depletion. Lignocellulosic biomass is considered as one of the promising alternative renewable resources for substituting at least part of fossil fuels. Due to the limitations of biomass itself as a fuel, such as low energy density and poor transportability, pyrolysis technology has been developed to convert biomass into biochar and bio-oil. However, the bio-oil produced from biomass fast pyrolysis exhibits poor quality such as low heating value, high acidity, high viscosity and poor stability. It is important to clearly understand the pyrolysis mechanism of biomass in order to produce a high-quality bio-oil. While the pyrolysis mechanism of cellulose has been extensively studied, the pyrolysis mechanism of lignin as one of the major components in biomass has not been well understood, mainly due to its complicated structures. Particularly, the formation of liquid intermediates easily takes place during lignin pyrolysis, leading to significant operation problems during pyrolysis in a fluidised bed reactor system. Therefore, the present research aims to carry out a systematic work on lignin pyrolysis, focusing on the structural changes of lignin and its derived products during pyrolysis at low temperatures where the formation of liquid intermediates becomes significant.

The main objectives of this study is to provide new understandings in the structural changes of solid products produced from the pyrolysis of lignin and its derived products (i.e., pyrolytic lignin, low- and high-molecular-weight portions of lignin) and the cellulose-lignin interactions during co-pyrolysis of cellulose and lignin at low temperatures. To achieve the above objectives, a drop-tube/fixed-bed reactor with pulsed-feeding system was employed to carry out the fast pyrolysis experiments of various lignin and cellulose-lignin samples. The solid products produced from the fast pyrolysis experiments were characterized by a series of analytical techniques.

First of all, the pyrolytic lignin, extracted from bio-oil via cold-water precipitation, was used as a model compound of lignin to understand its structural changes during

pyrolysis at low temperatures. In this study, the pyrolytic lignin was thermally decomposed in a drop-tube/fixed-bed reactor under inert conditions at 100–350 °C. It is found that the char yield of the pyrolytic lignin under such fast pyrolysis conditions decreases rapidly from ~82% at 100 °C to ~23% at 350 °C. The majority of the weight loss is contributed by the significant reduction in the fraction of light aromatic oligomers (i.e., the CH<sub>2</sub>Cl<sub>2</sub>-soluble fraction) retained in the pyrolytic lignin chars, with such reductions increasing with temperature. On the contrary, there is insignificant change in the fraction of heavy aromatic oligomers (i.e., the CH<sub>2</sub>Cl<sub>2</sub>-insoluble fraction) retained in the pyrolytic lignin chars during pyrolysis at such low temperatures. It is evidenced that there are strong interactions between the light and heavy aromatic oligomers during thermal decomposition of the pyrolytic lignin, leading to the observed additional char formation. The main reactions during thermal decomposition of the pyrolytic lignin are the release of aliphatic and small phenolic compounds (i.e., via demethylation and decarbonylation reactions), mainly due to the breaking of ether bonds in the pyrolytic lignin structure. The char structure becomes more aromatic as temperature increases, due to the enhanced polymerization reactions at high temperatures (> 250 °C).

Secondly, lignin pyrolysis was then carried out to understand the structural changes of lignin during pyrolysis at low temperatures. It is known that lignin experiences more complicated reactions because of its heterogeneous structure. Particularly, the low-molecular-weight portion easily melts at low temperatures during pyrolysis to form a liquid intermediate phase. This study presents a systematic study to understand the structural changes of the chars produced from lignin fast pyrolysis at 100–300 °C, focusing more on the low-molecular-weight portion (i.e., the THF-soluble portion) of lignin. The results show that low temperature lignin pyrolysis mainly proceeds with the THF-soluble portion via decomposition reactions into volatiles and polymerization reactions into the THF-insoluble portion. The decomposition of the THF-soluble portion starts at ~150 °C, mainly due to the loss of some thermally-labile structures such as hydroxyl groups and the alkyl aliphatic chains. Decomposition of the THF-soluble portion becomes significant as the pyrolysis temperature increases to ~175 °C, mainly because of the cleavage of weak ether bonds linked with  $\beta$ -carbon or  $\gamma$ -carbon to release phenolic monomers or oligomers. Meanwhile, significant polymerization also takes place at ~175 °C or

above, leading to an increase of the THF-insoluble portion from ~31% in the raw lignin to ~67% in the char at 250 °C. Further decomposition of the THF-insoluble portion occurs as pyrolysis temperature increases. Because of enhanced polymerization reactions at higher temperatures (> 250 °C), the char structure becomes more condensed with decreased H/C atomic ratio and increased aromaticity.

Thirdly, this study further investigated the interactions between the low- and high-molecular-weight portions of lignin during pyrolysis at 100–300 °C. THF extraction was employed to separate lignin into the low-molecular-weight (i.e., the THF-soluble portion) and high-molecular-weight (i.e., the THF-insoluble) portions. The raw, the THF-soluble and THF-insoluble lignin samples were all subjected to fast pyrolysis experiments individually to understand the structural changes of chars from each lignin sample. Then, the results from the whole lignin pyrolysis were compared with those calculated based on the THF-soluble and THF-insoluble lignin to examine the interactions between the low- and high-molecular-weight portions of lignin. As pyrolysis temperature increases, the char yield of the LMW lignin decreases more significantly than that of the HMW lignin. During fast pyrolysis, the experimentally-measured char yields from the whole lignin are consistently higher than those calculated from the respective char yields of the LMW and HMW portions via addition, increasing from ~0.5 wt % at 100 °C to ~10.7 wt % at 300 °C. Such char yield differences provide direct evidence on the existence of interactions between the LMW and HMW portions of lignin during fast pyrolysis of the whole lignin. The results suggest that the formation of liquid intermediate phase from the LMW portion suppresses the release of volatiles from both the LMW and HMW portions, resulting in a higher char yield during fast pyrolysis of the whole lignin. Experimental results further show that such interactions also result in changes in lignin char structures (especially at temperatures >150 °C) due to enhanced polymerization reactions of oxygenated functional groups and aromatic structures with fused rings of 2–5. As a result, more condensed char structures are formed, as evidenced by the decreased atomic O/C and H/C ratios for the chars produced from the whole lignin pyrolysis.

Fourthly, this study also investigated the cellulose-lignin interactions during fast pyrolysis at 100–350 °C to better understand the pyrolysis mechanism of lignocellulosic biomass. The results show that co-pyrolysis of cellulose and lignin

(with a mass ratio of 1:1) at temperatures  $\leq 250$  °C leads to a char yield lower than the char yield calculated from those of individual cellulose and lignin pyrolysis. The difference between the experimental and calculated char yields increases with temperature, from  $\sim 2\%$  at 150 °C to  $\sim 6\%$  at 250 °C. Such char yield differences provide direct evidences on the existence of cellulose-lignin interactions during co-pyrolysis of cellulose and lignin. At 250 °C or below, the retention of lignin functional groups decreases and the destruction of sugar structures in the char increases during co-pyrolysis of cellulose and lignin. This indicates that the reaction intermediates produced from cellulose pyrolysis can stabilize the reactive species from lignin pyrolysis as hydrogen donors, thus enhancing the release of lignin-derived species as volatiles. In contrast, at temperatures  $> 250$  °C, co-pyrolysis of cellulose and lignin increases char yields, i.e., with the difference between the experimental and calculated char yields increasing from  $\sim 1\%$  at 300 °C to  $\sim 8\%$  at 350 °C. This indicates that partially decomposed structures of cellulose lead to increased char formation from cellulose pyrolysis at above 250 °C, further supported by the increased retention of cellulose functional groups in the char from co-pyrolysis of cellulose and lignin.

Overall, the present research provides new insights on the pyrolysis mechanisms of lignin and its derived compounds, particularly at low temperatures. The pyrolysis of the low-molecular-weight portion of lignin plays a key role at low temperatures, largely affecting char structural changes during lignin pyrolysis. The interactions between the low- and high-molecular-weight portions of lignin also lead to the formation of more char with condensed structures. This study further elucidates the cellulose-lignin interactions during co-pyrolysis of cellulose and lignin, which lead to the formation of less char at low temperatures ( $\leq 250$  °C) due to enhanced evaporation of lignin-derived species, but more char at high temperatures ( $> 250$  °C) due to enhanced polymerization of cellulose-derived species.

### Acknowledgements

I gratefully acknowledge the Curtin International Postgraduate Research Scholarship (CIPRS) from Curtin University for my PhD research study, which is financially supported by the Australian Research Council via the Discovery Early Career Research Award (DECRA) scheme.

I express my deepest gratitude to my supervisors, Dr. Yun Yu and Prof. Hongwei Wu, for their invaluable guidance, advices, supports, patience and inspirations during the years of my research study. Without their supervision and constant support, my PhD research would not be possible. I would also like to thank my thesis chairperson, Prof. Shaomin Liu, for his assistant and advice throughout this study.

I would like to offer my appreciation to all the technical staffs in the Department of Chemical Engineering, Ms. Karen Haynes, Mr. Araya Abera, Mr. Jason Wright, Dr. Roshanak Doroushi, Mr. Xiao Hua, Mr. Andrew Chan, Ms Melina Miralles and Ms. Ann Carroll. Further, special thanks to my research group members, Dr. Sui Boon Liaw, Dr. Mingming Zhang, Dr. Bing Song, Dr. Matthew Witham, Mr. Yu Long, Mr. Mingyang Li, Ms Jinxiu Cao, Mr. Xujun Chen and Mr. Changya Deng for their help and suggestions.

Last but not least, I would like to thank my family and friends for their continuous encouragement and support. My sincere gratitude also goes to my close relatives, Mr. & Mrs. Kong, Ms. Elaine and Ms. Agnes for all the love and caring throughout my PhD research journey overseas.



**List of Publications**

1. **Yee Wen Chua**, Hongwei Wu and Yun Yu. Interactions between Low-and High-molecular-weight Portions of Lignin during Fast Pyrolysis at Low Temperatures, *Energy & Fuels* **2019**, DOI: 10.1021/acs.energyfuels.9b02813.
2. **Yee Wen Chua**, Yun Yu and Hongwei Wu. Structural Changes of Chars Produced from Fast Pyrolysis of Lignin at 100–300 °C, *Fuel* **2019**, 255: 115754.
3. **Yee Wen Chua**, Yun Yu and Hongwei Wu. Thermal Decomposition of Pyrolytic Lignin under Inert Conditions at Low Temperatures, *Fuel* **2017**, 200: 70-75.
4. **Yee Wen Chua**, Hongwei Wu and Yun Yu. Effect of Cellulose-lignin Interactions on Char Structural Changes during Fast Pyrolysis at 100–350 °C, Submitted to 38<sup>th</sup> International Symposium on Combustion.
5. Yun Yu, **Yee Wen Chua** and Hongwei Wu. Characterization of Pyrolytic Sugars in Bio-Oil Produced from Biomass Fast Pyrolysis, *Energy & Fuels* **2016**, 30: 4145-4149.
6. Yu Long, Yun Yu, **Yee Wen Chua** and Hongwei Wu. Acid-catalyzed Cellulose Pyrolysis at Low Temperatures, *Fuel* **2017**, 193: 460-466.

**Table of Contents**

<b>Declaration.....</b>	<b>I</b>
<b>Abstract.....</b>	<b>III</b>
<b>Acknowledgements.....</b>	<b>VII</b>
<b>List of Publications.....</b>	<b>VIII</b>
<b>Table of Contents.....</b>	<b>IX</b>
<b>List of Figures.....</b>	<b>XIV</b>
<b>List of Tables.....</b>	<b>XVII</b>
<b>Chapter 1 Introduction.....</b>	<b>1</b>
1.1 Background and Motives.....	1
1.2 Scope and Objectives.....	3
1.3 Thesis Outline.....	3
<b>Chapter 2 Literature Review.....</b>	<b>6</b>
2.1 Introduction.....	6
2.2 Lignocellulosic Biomass.....	6
2.2.1 Cellulose.....	7
2.2.2 Hemicellulose.....	8
2.2.3 Lignin.....	9
2.2.4 OtherComponents .....	12
2.3 Pyrolysis of Lignocellulosic Biomass.....	12
2.3.1 Properties of Pyrolysis Products.....	13
2.3.1.1 Bio-char.....	13
2.3.1.2 Bio-oil.....	15
2.3.1.3 Gaseous Products.....	17
2.3.2 Parameters Influencing Biomass Pyrolysis.....	18
2.3.2.1 Feedstock Property.....	18
2.3.2.2 Pyrolysis Temperature.....	19
2.3.2.3 Heating Rate.....	20
2.3.2.4 Inorganic Matters.....	21

## TABLE OF CONTENTS

---

2.3.3	Pyrolysis Mechanism of Biomass.....	21
2.4	Mechanisms of Lignin Pyrolysis.....	26
2.5	Interactions of Components during Biomass Pyrolysis.....	31
2.5.1	Cellulose-Hemicellulose Pyrolysis.....	32
2.5.2	Hemicellulose-Lignin Pyrolysis.....	32
2.5.3	Cellulose-Lignin Pyrolysis.....	33
2.6	Conclusions and Research Gaps.....	35
2.7	Research Objectives.....	36
<b>Chapter 3</b>	<b>Research Methodology and Analytical Techniques.....</b>	<b>37</b>
3.1	Introduction.....	37
3.2	Methodology.....	37
3.2.1	Thermal Decomposition of Pyrolytic Lignin under Inert Conditions at Low Temperatures.....	39
3.2.2	Structural Changes of Chars Produced from Fast Pyrolysis of Lignin at Low Temperatures.....	39
3.2.3	Interactions between Low- and High-molecular-weight Portions of Lignin during Fast Pyrolysis at Low Temperatures.....	39
3.2.4	Effect of Cellulose-lignin Interactions on Char Structural Changes during Fast Pyrolysis at Low Temperatures.....	40
3.3	Experimental.....	40
3.3.1	Raw Materials.....	40
3.3.2	Samples Preparation.....	40
3.3.3	Reactor System.....	42
3.4	Instrument and Analytic Techniques.....	45
3.4.1	Analysis of Solid Products.....	45
3.4.1.1	Proximate and Ultimate Analysis.....	45
3.4.1.2	Thermogravimetric (TGA) analysis.....	45
3.4.1.3	<sup>13</sup> C Cross-Polarization Magic Angle Spinning (CP/MAS) NMR Analysis.....	45
3.4.1.4	Fourier Transform Infrared (FT-IR) Spectroscopy.....	45
3.4.2	Analysis of Liquid Products.....	46
3.4.2.1	Two Dimensional (2D) <sup>1</sup> H- <sup>13</sup> C Heteronuclear Single Quantum Correlation Nuclear Magnetic Resonance (HSQC NMR).....	46
3.4.2.2	UV Fluorescence Spectroscopy.....	47
3.4.2.3	Gel Permeation Chromatography (GPC).....	48

---

3.4.2.4 High-Performance Anion Exchange Chromatography with Pulsed Amperometric Detection (HPAEC-PAD).....	48
3.4.3 Inorganic Species Analysis.....	49
3.5 Summary.....	50
<b>Chapter 4 Thermal Decomposition of Pyrolytic Lignin under Inert Conditions at Low Temperatures.....</b>	<b>51</b>
4.1 Introduction.....	51
4.2 Yields and Elemental Compositions of Chars Produced from Thermal Decomposition of the Pyrolytic Lignin.....	52
4.3 Char Yields of Thermal Decomposition of the Light and Heavy Aromatic Oligomers in the Pyrolytic Lignin.....	53
4.4 Structural Changes of Chars Produced from Thermal Decomposition of the Pyrolytic Lignin.....	55
4.4.1 FT-IR Analysis.....	55
4.4.2 <sup>13</sup> C CP/MAS NMR Analysis.....	57
4.4.3 UV Fluorescence Analysis.....	60
4.5 Discussions on Thermal Decomposition Mechanism of Pyrolytic Lignin...	61
4.6 Conclusions.....	62
<b>Chapter 5 Structural Changes of Chars Produced from Fast Pyrolysis of Lignin at Low Tempertaures.....</b>	<b>63</b>
5.1 Introduction.....	63
5.2 Char Yield of Lignin during Fast Pyrolysis and Distribution of the THF-Soluble and the THF-Insoluble Portions in the Char.....	65
5.3 Structural Changes of the THF-Soluble Portion in the Chars Produced from Lignin Fast Pyrolysis.....	66
5.3.1 Elemental Composition.....	66
5.3.2 TG Analysis.....	67
5.3.3 GPC Analysis.....	68
5.3.4 UV Fluorescence Analysis.....	69
5.3.5 2D <sup>1</sup> H- <sup>13</sup> C HSQC-NMR Analysis.....	70
5.4 Structural Changes of the Chars Produced from Lignin Fast Pyrolysis.....	70
5.4.1 Elemental Composition.....	70
5.4.2 FT-IR Analysis.....	73
5.4.3 <sup>13</sup> C CP/MAS NMR Analysis.....	74
5.5 Conclusions.....	76

---

## TABLE OF CONTENTS

<b>Chapter 6 Interactions between Low- and High-molecular-weight Portions of Lignin during Fast Pyrolysis at Low Temperatures.....</b>	<b>78</b>
6.1 Introduction.....	78
6.2 Characterization of the Raw, LMW and HMW Lignin Samples.....	79
6.3 Interactions between the LMW and HMW Portions of Lignin Evidenced by Char Yields.....	82
6.4 Interactions between the LMW and HMW Portions of Lignin Evidenced by Char Structural Changes.....	83
6.4.1 Changes in Elemental Composition.....	83
6.4.2 Changes in Functional Groups.....	84
6.4.3 Changes in Aromatic Structures.....	87
6.5 Discussion on the Interactions between the LMW and HMW Portions of Lignin during Pyrolysis.....	90
6.6 Conclusions.....	91
<b>Chapter 7 Effect of Cellulose-Lignin Interactions on Char Structural Changes during Fast Pyrolysis at Low Temperatures.....</b>	<b>93</b>
7.1 Introduction.....	93
7.2 Yields and Properties of the Chars Produced from the Fast Pyrolysis of Cellulose, Lignin and Cellulose-lignin Mixture.....	94
7.3 Structural Changes of the Chars Produced from the Fast Pyrolysis of Cellulose, Lignin and Cellulose-lignin Mixture.....	97
7.4 Discussion on the Cellulose-lignin Interactions during Co-pyrolysis of Cellulose and Lignin.....	105
7.5 Conclusions.....	106
<b>Chapter 8 Conclusions and Recommendations.....</b>	<b>107</b>
8.1 Conclusions.....	107
8.1.1 Thermal Decomposition of Pyrolytic Lignin under Inert Conditions at Low Temperatures.....	107
8.1.2 Structural Changes of Chars Produced from Fast Pyrolysis of Lignin at Low Temperatures.....	107
8.1.3 Interactions between Low- and High-molecular-weight Portions of Lignin during Fast Pyrolysis at Low Temperatures.....	108
8.1.4 Effect of Cellulose-lignin Interactions on Char Structural Changes during Fast Pyrolysis at Low Temperatures.....	108
8.2 Recommendations.....	109
<b>REFERENCES.....</b>	<b>110</b>

**TABLE OF CONTENTS**

---

**APPENDICES..... 128**  
    **APPENDIX A ATTRIBUTION OF AUTHORSHIP..... 128**  
    **APPENDIX B COPYRIGHT PERMISSION STATEMENTS..... 131**

---

**List of Figures**

Figure 1.1: Thesis map.....	5
Figure 2.1: The schematic structure of typical biomass structure [52].....	7
Figure 2.2: Main components in lignocellulosic biomass[53].....	7
Figure 2.3: The atomic structure of cellulose with hydrogen bonding network [54]..	8
Figure 2.4: Main components in hemicellulose [54].....	9
Figure 2.5: The three principal building blocks of lignin [59].....	9
Figure 2.6: Schematic structure of hardwood lignin with various linkages as indicated in dashed line: PiR (pinoresinol), PhC (phenylcoumaran), $\beta$ -O-4 (aryl glycerol-arylether), BiPh (biphenyl), DiArEt (diarylether) and LP (lignin-carbohydrate links) [76].....	11
Figure 2.7: The applications of products from fast pyrolysis [87].....	13
Figure 2.8: Solvent fractionation method of bio-oil [101, 102].....	15
Figure 2.9: Weight loss (%) of different biomass feedstock with temperatures [130].....	19
Figure 2.10: Typical yield of end products from biomass pyrolysis [134].....	20
Figure 2.11: The proposed pathway of biomass pyrolysis [159, 160].....	22
Figure 2.12: The three main primary reactions in biomass pyrolysis [153].....	23
Figure 2.13: TG and DTG curves of cellulose, hemicellulose and lignin [44].....	24
Figure 2.14: The proposed reaction mechanisms during cellulose pyrolysis [163]..	24
Figure 2.15: Types of linkages with their estimated bond dissociation enthalpies values that exist in lignin structure [169].....	26
Figure 2.16: Proposed pyrolysis mechanism from MWL pyrolysis with various model dimers [171].....	28
Figure 2.17: Types of reactions occurring over the temperature ranging from 100 to 800 °C [153].....	29
Figure 2.18: Rheological properties of lignin during thermal decomposition [36]....	30
Figure 2.19: The proposed pyrolysis mechanism of lignin [38].....	30
Figure 2.20: The proposed interactions between cellulose and lignin during pyrolysis [42].....	34
Figure 2.21: The proposed pyrolysis mechanism of the effect of cellulose-derived compounds on lignin pyrolysis of (a) tar formation; (b) char formation [184].....	34

## LIST OF FIGURES

Figure 2.22: The proposed pyrolysis mechanism of the effect of lignin-derived compounds on cellulose pyrolysis [184].....	35
Figure 3.1: Research methodology.....	38
Figure 3.2: Schematic of pulsed-feeding system.....	43
Figure 3.3: Schematic of drop-tube/fixed-bed reactor system for pyrolysis process.	44
Figure 3.4: Absorbance changes of the functional groups with different samples concentration for FT-IR analysis. (a) 1 mg of pyrolytic lignin ground with 150 mg KBr; (b) 2 mg of pyrolytic lignin ground with 150 mg KBr; (c) 3 mg of pyrolytic lignin ground with 150 mg KBr.....	46
Figure 3.5: Linear relationship of the functional groups with different samples concentration for FT-IR analysis.....	47
Figure 3.6: Calibration curve for glucose standard by HPAEC-PAD.....	49
Figure 3.7: Ashing temperature program for AAEM species analysis.....	50
Figure 4.1: Char yield from thermal decomposition of the pyrolytic lignin at 100–350 °C and the distribution of the CH <sub>2</sub> Cl <sub>2</sub> -soluble and CH <sub>2</sub> Cl <sub>2</sub> -insoluble fractions in the char samples.....	53
Figure 4.2: Char yields from thermal decomposition of the pyrolytic lignin and its CH <sub>2</sub> Cl <sub>2</sub> -soluble and CH <sub>2</sub> Cl <sub>2</sub> -insoluble fractions at 100–350 °C.....	54
Figure 4.3: Panel (A) FT-IR spectra of the pyrolytic lignin and its chars prepared at 100–350 °C; legends: (a) pyrolytic lignin; (b) char prepared at 100 °C; (c) char prepared at 150 °C; (d) char prepared at 200 °C; (e) char prepared at 250 °C; (f) char prepared at 300 °C; and (g) char prepared at 350 °C. Panel (B) % Functional groups in chars prepared at 100–350 °C, expressed as % the intensity of respective FT-IR spectra for the pyrolytic lignin.....	56
Figure 4.4: Solid <sup>13</sup> C CP/MAS NMR spectra of the pyrolytic lignin and its chars prepared at 100–350 °C. Legends: (a) pyrolytic lignin; (b) char prepared at 100 °C; (c) char prepared at 150 °C; (d) char prepared at 200 °C; (e) char prepared at 250 °C; (f) char prepared at 300 °C; and (g) char prepared at 350 °C.....	59
Figure 4.5: UV Fluorescence spectra of the solutions obtained from the extraction of pyrolytic lignin and its chars prepared at 100–350 °C using chloroform-methanol solvent mixture (4:1 v/v).....	61
Figure 5.1: Char yield from the pyrolysis of lignin at 100–300 °C and the distribution of the THF-soluble and THF-insoluble fractions in all samples.....	66



## LIST OF FIGURES

Figure 5.2: TG and DTG curves of the THF-soluble portion in the raw lignin and chars prepared at various temperatures.....	67
Figure 5.3: Weight-average molecular weight (Mw) and number-average molecular weight (Mn) of the THF-soluble portion in the raw lignin and chars prepared at various temperatures.....	68
Figure 5.4: UV Fluorescence spectra of the THF-soluble portion in the raw lignin and its chars prepared at 100–300 °C.....	69
Figure 5.5: 2D <sup>1</sup> H- <sup>13</sup> C HSQC spectra of the THF-soluble portion in the raw lignin and its chars prepared at 100–300 °C. (a) THF-soluble portion in the raw lignin; (b) THF-soluble portion in the char prepared at 100 °C; (c) THF-soluble portion in the char prepared at 150 °C; (d) THF-soluble portion in the char prepared at 175 °C; (e) THF-soluble portion in the char prepared at 200 °C; (f) THF-soluble portion in the char prepared at 250 °C.....	72
Figure 5.6: Panel (a) FT-IR spectra of the lignin and its chars prepared at 100–300 °C. Panel (b) % Functional groups in chars at 100–300 °C, expressed as % the intensity of respective FT-IR spectra for the raw lignin.....	73
Figure 5.7: Solid <sup>13</sup> C CP/MAS NMR spectra of the lignin and its chars prepared at 100–300 °C. Legends: (a) lignin; (b) char prepared at 100 °C; (c) char prepared at 200 °C; (d) char prepared at 300 °C.....	76
Figure 6.1: Weight losses and DTG curves of the raw, LMW and HMW lignin samples.....	80
Figure 6.2: FT-IR spectra of the raw, LMW and HMW lignin samples normalized to the unit mass (per mg on a dry basis) of each sample.....	81
Figure 6.3: Char yields from the pyrolysis of the raw, LMW and HMW lignin samples at 100–300 °C. The calculated char yields are based on percentages of the LMW and HMW portions in the raw lignin and their corresponding char yields.....	83
Figure 6.4: FT-IR spectra of the chars from the pyrolysis of the raw, LMW and HMW lignin samples at 100–300 °C, normalized to the unit mass (per mg on a dry basis) of each lignin sample. Panel (a) chars from the raw lignin: (1) raw lignin; (2) char at 100 °C; (3) char at 150 °C; (4) char at 200 °C; (5) char at 250 °C; (6) char at 300 °C. Panel (b) chars from the HMW lignin pyrolysis: (1) HMW lignin; (2) char at 100 °C; (3) char at 150 °C; (4) char at 200 °C; (5) char at 250 °C; (6) char at 300 °C. Panel (c) chars from the LMW lignin pyrolysis: (1) LMW lignin; (2) char at 100 °C; (3) char at 150 °C; (4) char at 200 °C; (5) char at 250 °C; (6) char at 300 °C.....	85

## LIST OF FIGURES

Figure 6.5: Differences between the FT-IR spectra of the raw lignin chars and the calculated spectra based on the percentages of the LMW and HMW portions in the raw lignin and their corresponding FT-IR spectra of chars produced at 100–300 °C. ....	87
Figure 6.6: UV Fluorescence spectra of the chars from the pyrolysis of the raw and LMW lignin samples at 100–300 °C. Panel (a) chars from the raw lignin. Panel (b) chars from the LMW lignin.....	89
Figure 6.7: Differences between the UV fluorescence intensities of the raw lignin chars and the calculated UV fluorescence intensities based on the percentages of the LMW portion in the raw lignin and their corresponding UV fluorescence intensities of chars produced at 100–300 °C.....	90
Figure 7.1: Char yield from the pyrolysis of lignin, cellulose and cellulose-lignin mixture at 100–350 °C.....	95
Figure 7.2: Glucose yields from pyrolysis of cellulose, lignin and cellulose-lignin mixture at 100–350 °C.....	96
Figure 7.3: FT-IR spectra of the chars from the pyrolysis of cellulose, lignin and cellulose-lignin mixture at 100–350 °C. Panel (a) cellulose and its chars: (1) cellulose; (2) 100 °C; (3) 150 °C; (4) 200 °C; (5) 250 °C; (6) 300 °C; (7) 350 °C. Panel (b) lignin and its chars: (1) raw lignin; (2) 100 °C; (3) 150 °C; (4) 200 °C; (5) 250 °C; (6) 300 °C; (7) 350 °C. Panel (c) cellulose-lignin mixture and its chars: (1) cellulose-lignin mixture; (2) 100 °C; (3) 150 °C; (4) 200 °C; (5) 250 °C; (6) 300 °C; (7) 350 °C.....	98
Figure 7.4: Differences between the experimental and calculated FT-IR absorbance intensities of chars for the pyrolysis of cellulose-lignin mixture at 100–350 °C.....	100
Figure 7.5: UV fluorescence spectra of the chars from the pyrolysis of lignin and cellulose-lignin mixture at 100–300 °C. Panel (a) lignin and its chars: (1) lignin; (2) 100 °C; (3) 150 °C; (4) 200 °C; (5) 250 °C; (6) 300 °C. Panel (b) cellulose-lignin mixture and its chars: (1) cellulose-lignin mixture; (2) 100 °C; (3) 150 °C; (4) 200 °C; (5) 250 °C; (6) 300 °C.....	101
Figure 7.6: Differences between the experimental and calculated UV fluorescence intensity of the chars for the pyrolysis of cellulose-lignin mixture at 100–300 °C..	102
Figure 7.7: <sup>13</sup> C CP/MAS NMR spectra of the chars from the pyrolysis of cellulose, lignin and cellulose-lignin mixture at 100–300 °C. (a) Cellulose and its chars; (b) lignin and its chars; (c) cellulose-lignin mixture and its chars.....	104

---

**List of Tables**

Table 3.1: Properties of the lignin used in this study.....	41
Table 3.2: Properties of the raw, LMW and HMW lignin samples used in this study. .....	42
Table 3.3: Properties of the raw cellulose, lignin and cellulose-lignin used in this study.....	42
Table 3.4: Gradient program for sugar analysis in HPAEC-PAD.....	49
Table 4.1: Properties of the pyrolytic lignin and its chars prepared at various temperatures.....	53
Table 4.2: Peak assignments for FT-IR spectra[35, 192].....	58
Table 4.3: Relative content analysis for <sup>13</sup> C CP/MAS NMR spectra.....	60
Table 5.1: Elemental compositions of the THF-soluble portion in the raw lignin and chars prepared from lignin fast pyrolysis at various temperatures.....	67
Table 5.2: Assignment of the main signals in the 2D <sup>1</sup> H- <sup>13</sup> C HSQC spectra [238-240] .....	70
Table 5.3: Elemental compositions of chars prepared from lignin fast pyrolysis at various temperatures.....	71
Table 5.4: Peak assignments for FT-IR spectra [35, 37, 172].....	71
Table 5.5: Relative content analysis for <sup>13</sup> C CP/MAS NMR spectra.....	76
Table 6.1: Peak assignments for FT-IR spectra [35, 37, 172].....	81
Table 6.2: Elemental compositions of the chars produced from the fast pyrolysis of the raw, LMW and HMW lignin at various temperatures.....	84
Table 7.1: Elemental compositions of the chars from the pyrolysis of cellulose, lignin and cellulose-lignin mixture at 100–350 °C.....	97
Table 7.2: Peak assignments for FT-IR spectra of lignin [35, 37, 172] and of cellulose samples [278-280].....	99

---

## Chapter 1 Introduction

### 1.1 Background and Motives

The global consumption of fossil fuels continues to increase, leading to various energy and environmental issues such as resource depletion, global warming and serious climate change [1, 2]. The use of alternative renewable energy sources, particularly biomass, can reduce our reliance on fossil uses, at least partly addressing those issues related to fossil fuels. It is estimated that the renewable energy generated from biomass contributes ~10% on the worldwide energy consumption in 2017 [3]. Therefore, it is critical to develop biomass processing technology for the production of bioenergy and biofuels [4].

Biomass is the most abundant organic carbonaceous materials on earth that stores solar energy into chemical energy [5]. However, there are some limitations of biomass for fuel production such as low volumetric energy density, high moisture content and high transportation costs [6, 7]. Therefore, biomass must undergo thermochemical processing to convert into biofuels. Various thermochemical technologies have been developed to utilise biomass for producing bioenergy and biofuels of low energy and carbon footprints such as combustion, gasification and pyrolysis [4, 8-10]. Combustion is a conventional process which involves the direct burning of biomass in the air for heat and energy production [10]. However, an efficient process required extensive biomass pretreatments to ensure the feedstocks contain very low moisture content and fine particle sizes [10, 11]. The gasification technology is primarily designed for the production gaseous fuels. The improved dual fluidized bed reactor configuration overcomes the ash melting issues, however the major challenges are the presence of undesired impurities in the gasifier and high capital and operating costs [9, 12, 13]. Recently, biomass fast pyrolysis is considered a promising technology to convert biomass to bio-oil and biochar that are more easily to transport for further processing in centralised centres [4, 14]. However, the quality of bio-oil produced from biomass fast pyrolysis is poor, such as low heating value, high acidity, high water content, high viscosity, poor stability [8, 15-18]. This largely

limits the direct use of bio-oil as a liquid fuel. Therefore, it is of critical importance to clearly understand the biomass pyrolysis mechanism to develop advanced biomass pyrolysis technologies.

Biomass consists of three major components, such as cellulose, hemicellulose and lignin. Cellulose has been widely used as a model compound to study the biomass pyrolysis mechanism. Significant advanced have been made on cellulose pyrolysis mechanism. It is known that the decomposition of cellulose structure leads to the formation of intermediates (i.e., active cellulose) from both crystalline and amorphous structures due to breakage of weak glycosidic bonds [19, 20]. The monomeric and oligomeric sugars formed within the intermediate phase, accelerated the dehydration and cross-linking reactions [21, 22]. The reactive oligomeric species may thermally ejected as aerosols [23] or polymerized to form solids [20, 24, 25]. Detailed reaction mechanisms of cellulose pyrolysis have been reported in literatures. However, the understanding of lignin pyrolysis mechanism is limited due to its complex structure.

The three main constituents in lignocellulosic biomass are cellulose, hemicellulose and lignin. Lignin, as the primary sources of aromatics in biomass [26, 27], however has been less developed and utilized for the production of bio-fuels and chemicals compared to cellulose and hemicellulose due to its complex aromatic polymer structure [27, 28]. Previous research on lignin pyrolysis mainly focused on the volatile products (gas and tar) released from lignin pyrolysis [29-35]. However, there are limited works towards understanding the structural characteristics of solid products (chars) from lignin pyrolysis, especially at low temperatures. It is reported that lignin undergo melting and softening starts from temperature as low as 140 °C [36], forming a “liquid intermediate” phase, similar to that have been observed in biomass chars [37-40]. Recent research showed that the wide range of molecular weight species that present in lignin affected the product distributions during depolymerisation [41], but the pyrolysis behaviors related to the intermediates formation at low temperature are rarely reported. Besides, it is well known that there are interactions between the three components in biomass during pyrolysis [42-47]. Since cellulose and lignin are both major components in biomass, it is important to understand the effect of cellulose species on the formation of such intermediates

during lignin pyrolysis. Therefore, a detailed study is essential to achieve better understanding on lignin and biomass pyrolysis at low temperatures for better biomass utilization in various applications.

## **1.2 Scope and Objectives**

This research study aims to provide better understanding on the mechanism of lignin pyrolysis. The detailed objectives of the study are as follow:

- To characterize the solid products produced from the thermal decomposition of lignin model compound (i.e., pyrolytic lignin) at low temperatures.
- To study the structural changes of chars produced from low temperature lignin pyrolysis.
- To investigate the pyrolysis behavior of different lignin components and their interactions during pyrolysis at low temperatures.
- To provide new insights into the understanding of cellulose-lignin interactions during co-pyrolysis of cellulose and lignin at low temperatures.

## **1.3 Thesis Outline**

This thesis comprised of 8 chapters including this chapter as outlined below, and the thesis structure is schematically shown in the thesis map presented in Figure 1.1.

Chapter 1 introduces the background and objectives of the current research study.

Chapter 2 reviews the existing knowledge in the literature on the pyrolysis of biomass-derived lignin compounds, thus leading to the identified research gaps and the specified objectives of the study.

Chapter 3 presents the methodology employed to achieve the research objectives and detailed description on the experimental instruments used.

Chapter 4 understands the char formation during the fast pyrolysis of lignin-derived model compound (i.e., pyrolytic lignin) at low temperatures.

Chapter 5 investigates the structural changes of chars produced from lignin pyrolysis at low temperatures, particularly the lignin of low molecular weight (i.e., the THF-soluble lignin).

Chapter 6 compares the pyrolysis behavior of the low- and high-molecular-weight portions of lignin and study their interactions at low temperatures.

Chapter 7 studies the cellulose-lignin interactions during the co-pyrolysis of cellulose and lignin, particularly at low temperatures.

Chapter 8 concludes the present study and lists recommendations for future research work.

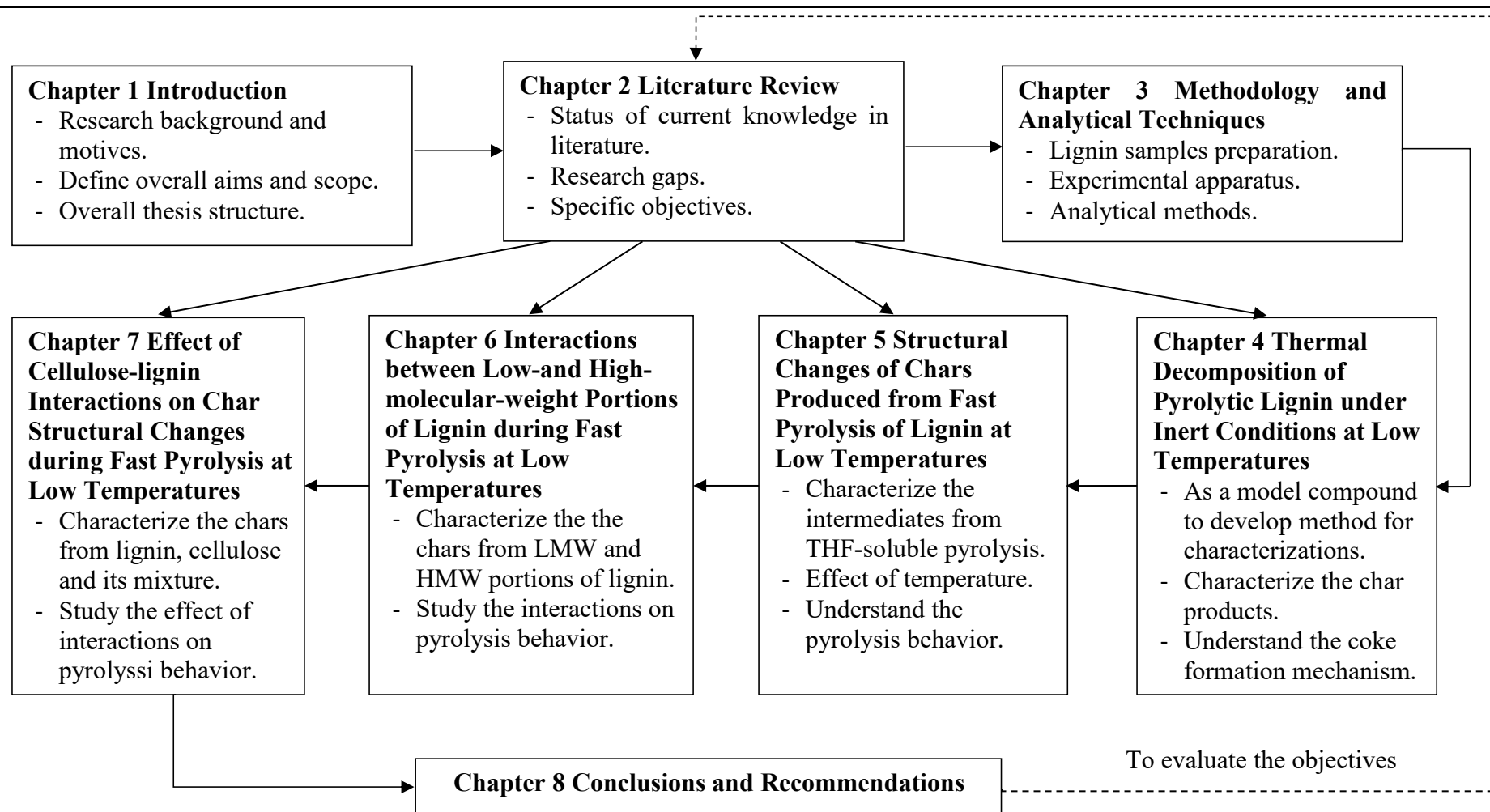


Figure 1.1: Thesis map



---

## Chapter 2 Literature Review

### 2.1 Introduction

Lignocellulosic biomass is considered as an important feedstock to produce renewable energy and fuels, due to its abundant availability worldwide. In the past few decades, pyrolysis process has been widely developed for thermal decomposition of lignocellulosic biomass into renewable liquid fuels. However, the produced pyrolysis liquid fuels (i.e., bio-oil) have poor quality, such as high water content, low heating value, high viscosity and low stability [8, 15-18]. It is of critical importance to clearly understand the fundamental pyrolysis mechanism of biomass, in order to develop advanced pyrolysis technologies for producing high-quality liquid fuels. However, the biomass pyrolysis mechanism is complicated due to its complex structures of three constituents (i.e., cellulose, hemicellulose and lignin). The objectives of this chapter are to review the existing knowledge on biomass pyrolysis, particularly lignin pyrolysis. This chapter first gives an introduction on biomass and its main constituents, followed by detailed pyrolysis mechanisms of three major constituents in biomass. Next, more attentions are paid on the pyrolysis of lignin and its derived products, as well as the co-pyrolysis of biomass constituents to understand the interactions of biomass constituents during pyrolysis. Lastly, the key research gaps are identified, which help to define the scope of the present study.

### 2.2 Lignocellulosic Biomass

Lignocellulosic biomass can be categorized into: agricultural wastes, wood residues and municipal wastes and energy crops [48]. As shown in Figure 2.1, lignocellulosic biomass consists of three major organic components: cellulose, hemicellulose and lignin, which are chemically bounded by intermolecular and covalent bonds. The plant cell fiber is formed by groups of parallel semi-crystalline rods (i.e., microfibrils) which consist of bounded cellulose polymers [49], and is often associated with hemicellulose and lignin [50]. Depending on the type of biomass, the macromolecular compounds vary in biomass. Generally, biomass is made up of approximately 40~60% cellulose, 15~30% hemicellulose, 10~25% lignin, as well as

some organic extractives and minerals [51]. The different components of the complex lignocellulosic biomass are outlined in Figure 2.2.

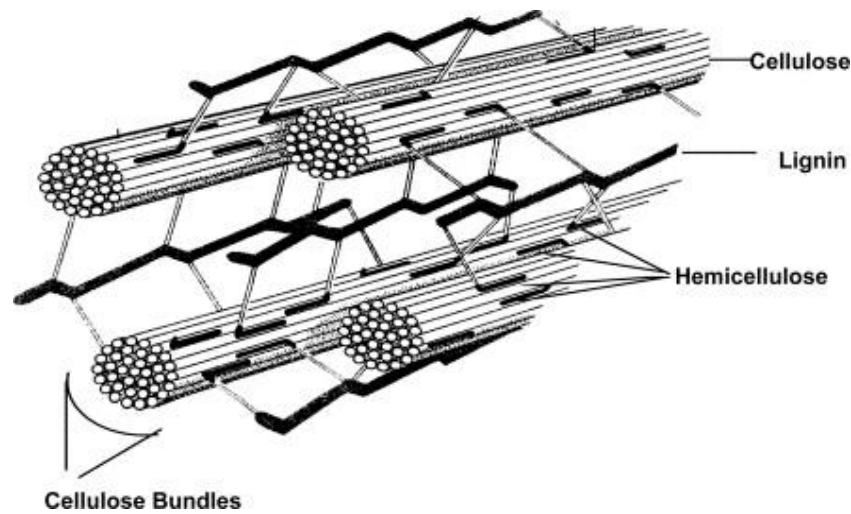


Figure 2.1: The schematic structure of typical biomass structure [52]

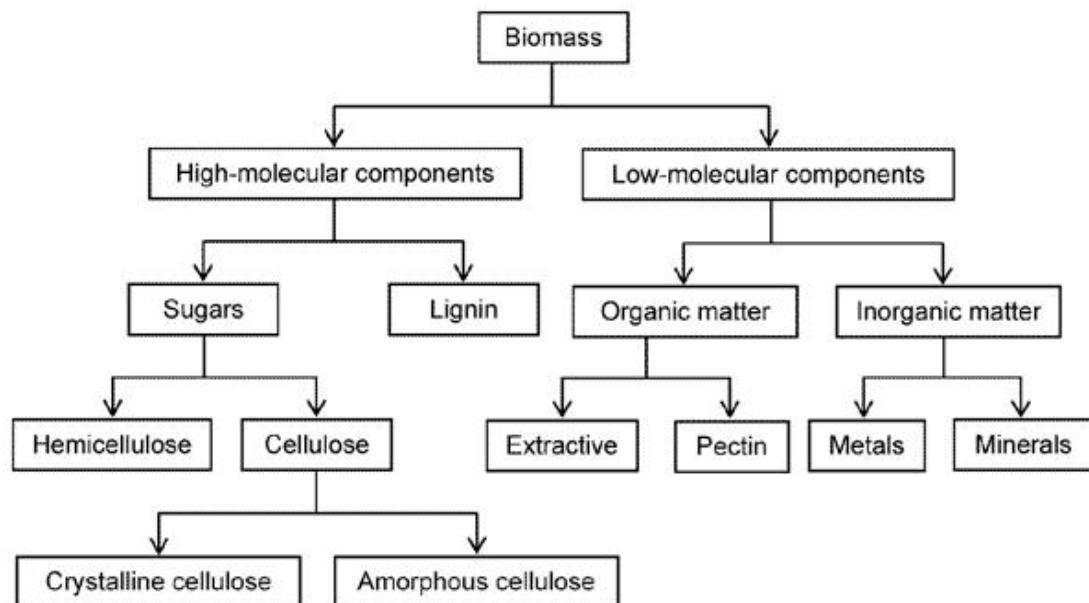


Figure 2.2: Main components in lignocellulosic biomass [53]

### 2.2.1 Cellulose

Cellulose is a linear organic polymer of repeating glucose monomer units that linked together by  $\beta$ -1,4 glycosidic bonds [54] (Figure 2.3). The basic repeating of two glucose units is known as a cellobiose unit. The degree of polymerization (DP) of cellulose varies depending on the biomass types, such as 7000~10,000 for wood and 15,000 for cotton [55]. It is known that cellulose is insoluble in water due to its

crystalline structure. However, this structure can be broken down into glucose upon acid hydrolysis [56].

The molecular structures of cellulose mainly include the crystalline cellulose that makes up the microfibrils with surrounded non-organized cellulose chains, called amorphous cellulose [48]. The high crystallinity of cellulose is due to the strong inter- and intra-molecular hydrogen bonds [54] (Figure 2.3), while weaker intermolecular hydrogen bonds are present in amorphous cellulose [57]. Thus, amorphous cellulose has higher accessibility and less thermal resistant than crystalline cellulose.

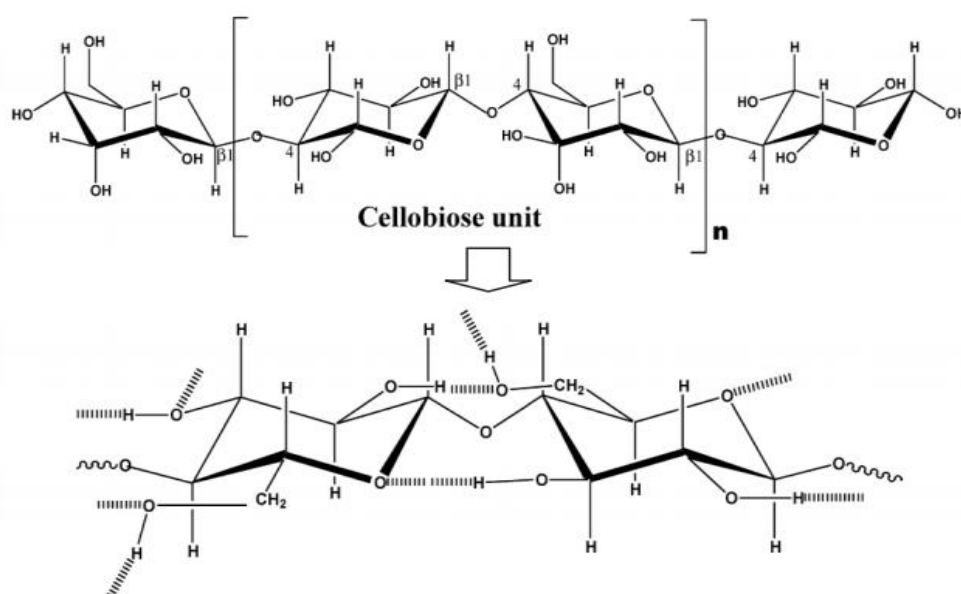


Figure 2.3: The atomic structure of cellulose with hydrogen bonding network [54]

### 2.2.2 Hemicellulose

In contrast to cellulose, hemicellulose comprises of various polymerized monosaccharides of pentose (C5) and hexose (C6) sugars such as xylose, arabinose, galactose, glucose and mannose as well as sugar-acids including galacturonic acid and 4-O-methyl glucuronic acid (Figure 2.4) [54, 58]. The sugars are linked to each other by  $\beta$ -1,4 or  $\beta$ -1,3-glycosidic bonds [48]. Hemicellulose consists of relatively lower DP ranging from 50 to 200 compared to cellulose. Hemicellulose also exhibits lower molecular weight than cellulose. Hence, it appears to be amorphous and short-chained in nature, which makes it hydrophilic and easily hydrolysed [8]. Xylan (i.e.,

polymer of xylose) is found to be the dominant saccharide monomers of hemicellulose in hardwood, whereas softwood is rich in galactoglucomannan [48, 54].

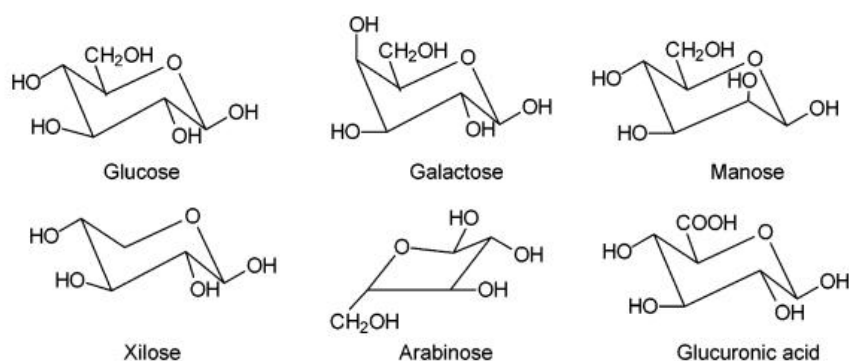


Figure 2.4: Main components in hemicellulose [54]

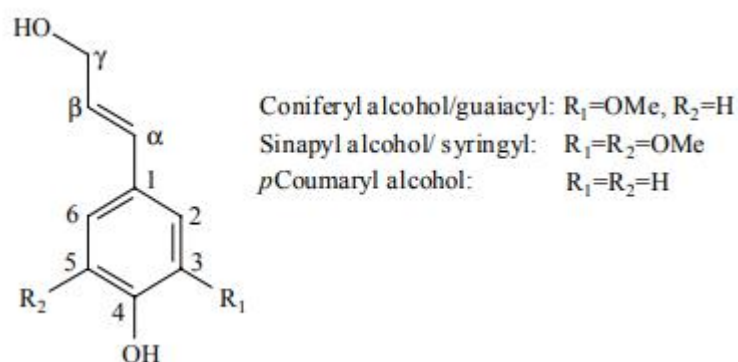


Figure 2.5: The three principal building blocks of lignin [59]

### 2.2.3 Lignin

Lignin is a three-dimensional polymer that is highly cross-linked with various hydroxyl- and methoxy- substituted phenylpropane monomeric units, including guaiacyl (G), syringyl (S) and *p*-hydroxyphenyl (H) [59, 60]. The three precursors of the monolignols that make up lignin by the enzymatic dehydrogenative polymerization are presented as coniferyl, sinapyl and *p*-coumaryl alcohol structures (Figure 2.5). In a woody biomass, lignin is found to be tightly connected to cellulose and hemicellulose via strong inter-chain covalent hydrogen bonds, forming a complex and rigid plant cells protection [61]. The naturally occurring amorphous structure of lignin is difficult to break down, thus making it difficult to access cellulose and hemicellulose for sugars extraction. Hence, biomass will need to undergo further pre-treatment process prior to bioconversion [59]. As seen in Figure

2.6, the common linkages between phenylpropane units of lignin includes  $\beta$ -O-4, 5-5,  $\beta$ -5, 4-O-5,  $\beta$ -1,  $\beta$ - $\beta$  and dibenzodioxocin, in which  $\beta$ -O-4 linkage is dominant in both hardwoods and softwoods lignin [59].

Lignin is also known as the major renewable aromatic resource in nature, abundantly sourced from the pulp and paper industry and biofuels production plants [26, 62, 63]. Presently, lignin is mainly utilized as a fuel in biomass boiler for heat and power [8]. The aromatic structure of lignin makes it a potential new feedstock for the production of aromatic chemicals and fuels [16, 62]. Lignin also exhibits widespread interests in the field of applications including: emulsifiers, dyes, synthetic floorings, sequestering, binding, thermosets, dispersal agents, paints and fuels to treatments for roadways [64, 65].

Lignin appeared in many varieties as reported in literatures, including kraft lignin, organosolv lignin, sulfonated lignin and pyrolytic lignin. All types of lignin are isolated using different techniques, hence they possess different chemical properties and characteristics due to their changes in structure and molecular weights [66].

- ***Kraft lignin.*** It is also known as alkali lignin, which is treated in NaOH or mixture with Na<sub>2</sub>SO<sub>4</sub> solution at 170 °C. The cleavage of bonds within the polysaccharides enables the dissolution of lignin fragments in the solution [67]. Some of the linkages in lignin except ether 5-5 are dislocated due to the chemical bleaching during the process [26, 68].
- ***Sulfonated lignin.*** The traditional sulphite pulping process employs sulfonic acid as solvent at 140 °C to extract the brown liquor as lignin [69, 70]. The process produced lignosulfonates, which have greater molecular weight than kraft lignin [26, 67].
- ***Organosolv lignin.*** Organic solvent such as ethanol or ethanol/water was used to dissolve lignin from the wood treatment under sulphur-free condition [26, 69, 71]. The organosolv lignin is suitable for the production of valuable chemicals due to its high purity and low molecular weight [71]. However, the disadvantage is the high recovery cost of solvent during the process [26].

- Pyrolytic lignin.** Pyrolytic lignin is extracted from the pyrolysis oil of lignocellulosic biomass pyrolysis via cold-water precipitation [54, 72, 73]. The water insoluble fraction from pyrolysis oil is composed of mainly lignin-derived phenolic compounds and much lower molecular weight compared to lignin [74]. The original structure of lignin is disrupted, thus forming a mainly alkylated aromatics structure with novel ether bonds [72, 75].

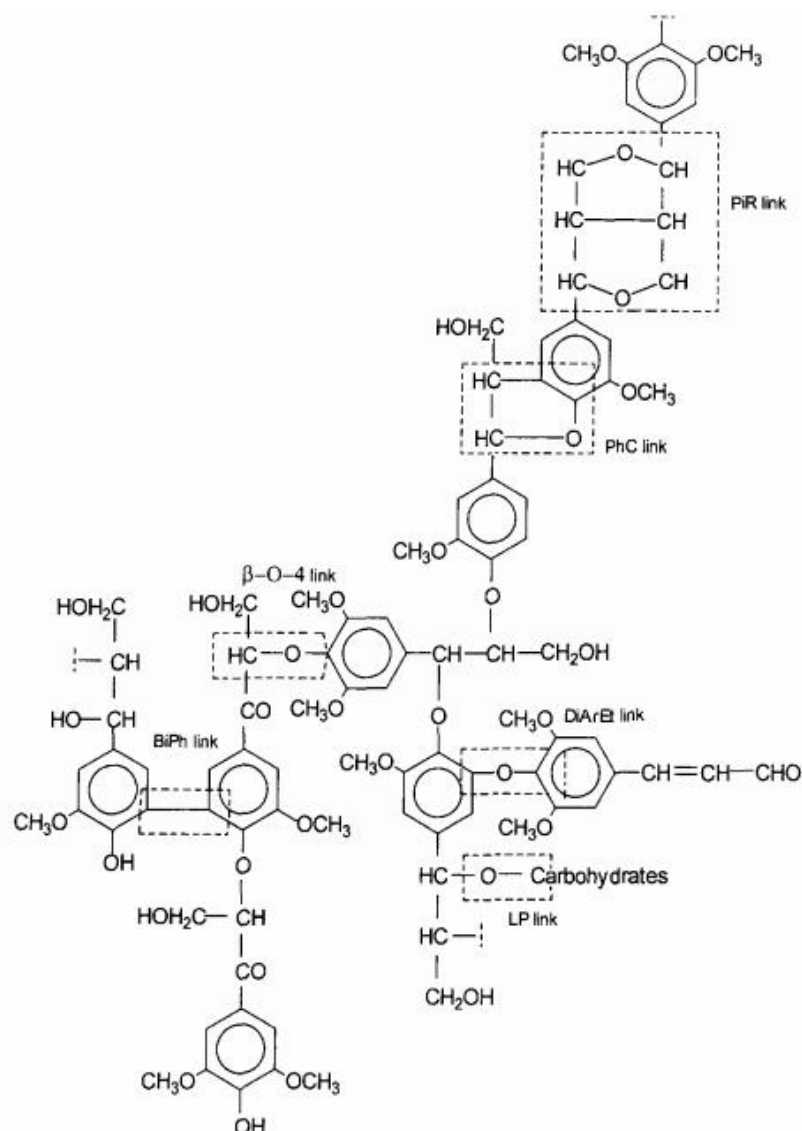


Figure 2.6: Schematic structure of hardwood lignin with various linkages as indicated in dashed line: PiR (pinoresinol), PhC (phenylcoumaran),  $\beta$ -O-4 (aryl glycerol-arylether), BiPh (biphenyl), DiArEt (diarylether) and LP (lignin-carbohydrate links) [76]

### 2.2.4 Other Components

Biomass also consists of a small amount of organic extractives, including waxes, fats, resins, glycosides, tannin, simple sugars, starches, pigment, proteins and pectins [77]. They can be extracted via polar solvents (e.g., water, methylene chloride, or alcohol) or non-polar solvents (e.g., toluene or hexane) [54]. Due to the nutrient uptake during the growth, biomass also contain little amount of inorganic matters such as alkali and alkaline earth metallic (AAEM) species (i.e., sodium, potassium, calcium and magnesium), silicon, aluminium, iron, phosphorus and chlorine [54].

### 2.3 Pyrolysis of Lignocellulosic Biomass

Biomass is increasingly recognized as an alternative and significant source of renewable energy for the production of biofuels and chemicals. The utilization of biomass as an alternative energy has received increasing attentions due to the abundant biomass resource worldwide and the environmental friendly nature. In fact, there are some limitations of biomass for fuel production such as low heating value and low energy density due to the high moisture and high oxygen content (40-45 wt%) as well as poor grindability and transportability [6, 7, 78]. However, these undesirable characteristics can be improved via pyrolysis. Pyrolysis is a process that thermally decomposes organic materials in the absence of oxygen to produce solid (bio-char), liquid (bio-oil) and non-condensable gaseous products [79]. Biomass pyrolysis can be classified into three main types: slow pyrolysis, fast pyrolysis and flash pyrolysis [80, 81]. Slow pyrolysis involves slow heating of the particles with long residence time (450-550 s) [79]. This reaction is usually applied for the production of bio-char, in which the low temperatures and low heating rates allow sufficient time for the secondary reactions (i.e., polymerization) to occur and hence maximise the solid yields. On the other hand, fast pyrolysis is defined by the high heating rates (10-200 K/s) and short vapour residence time (0.5-2.0 s) [79]. This favours the bio-oil production, with a bio-oil yield as high as 50-70 wt%, since the secondary reactions are limited due to the rapid heating rate [80, 82]. A higher bio-oil yields (75-80 wt%) can even achieved during the flash pyrolysis process, with higher heating rates ( $> 1000$  K/s) and shorter vapour residence times ( $< 0.5$  s) [79].

### 2.3.1 Properties of Pyrolysis Products

There are three main products produced from biomass pyrolysis: solid char, liquid bio-oil and gas. These products have different properties and vary depending on the feedstock type and pyrolysis conditions.

#### 2.3.1.1 Bio-char

The solid product generated from biomass pyrolysis is a carbon-rich organic residue, which is known as bio-char or charcoal. It is usually characterized by proximate analysis for its moisture, ash, volatile matter and fixed carbon content and ultimate analysis for carbon, hydrogen, nitrogen and oxygen content [83, 84]. A series of fast pyrolysis experiments using different feedstock in a tubular reactor were performed by Demirbas [85, 86] to investigate the yields and properties of bio-char at different pyrolysis temperatures and heating rates. The results showed that the solid yields ranged from ~90 to ~30 wt%, with the carbon content of ~53-96 % and the HHV of 20-36 MJ/kg when temperature increases from 470 K to 1050 K. Generally, chars with higher HHV values are preferred as coal substitution [17].

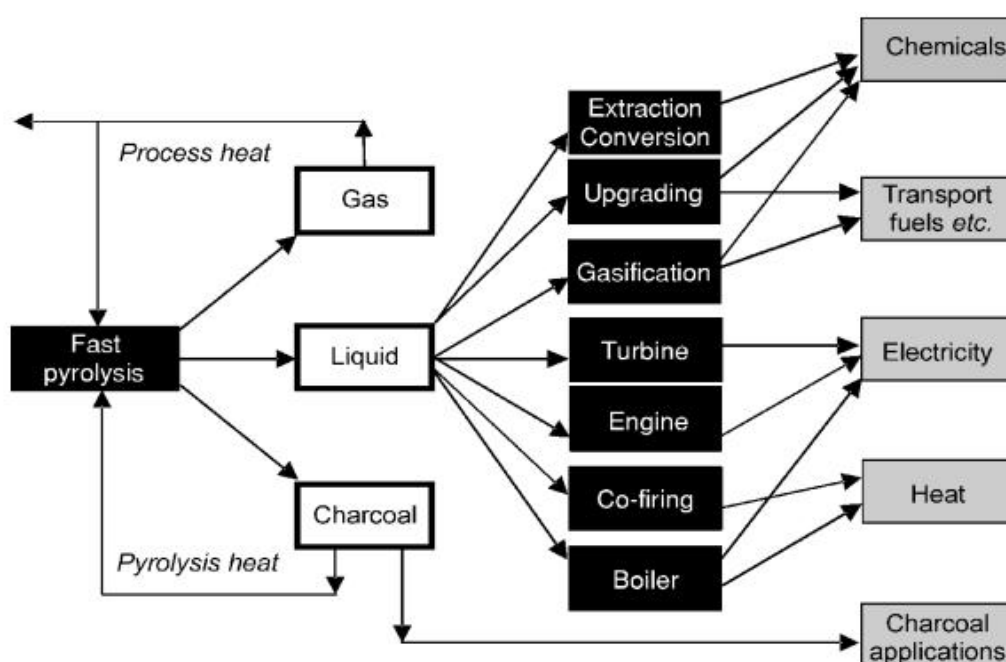


Figure 2.7: The applications of products from fast pyrolysis [87]

During the thermal decomposition of biomass, there are two different aromatic structures formed in bio-chars: amorphous phase aromatic rings and crystalline phase with condensed polyaromatic sheets [88]. The formation of bio-char begins from the



organized aromatic structure, followed by the structural rearrangement forming a larger aromatic system [89]. Depending on the size of the aromatic ring system, it is usually quantified by the aromaticity, which describes the total carbon proportion present in the aromatic structure of chars. It also can be characterized by the degree of aromatic condensation that corresponds only to the carbon proportion in a condensed structure [90]. According to McBeath et al. [89], the aromaticity of the bio-char produced from the wood pyrolysis increased significantly from 200 to 400 °C, and reached maximum around temperature between 600 and 700 °C. Their results indicate that the whole carbon content within the chars may be hold in the aromatic structure.

It is important to determine the ash content in the bio-char during the product characterization, because the amount and inorganics species type greatly affect their further applications. The ash content of bio-chars may originate from their parent biomass feedstocks. However, a large portion of the ash remains in the solid char structure during the biomass conversion. As the pyrolysis temperature increases, the continuous release of volatile matter and removal of water via dehydration reaction, leads to the increased ash content in the bio-char [88]. Apart from that, the properties of bio-chars may change during pyrolysis process due to the removal of functional groups such as hydroxyl –OH and changes in solid porosity for water absorption ability [88]. It is found out that the bio-chars appeared to be more hydrophobic with increasing pyrolysis temperature, as most of the polar functional groups are eliminated and increased aromaticity [91-93].

The products from pyrolysis process have achieved commercial success for the production of chemicals and fuels as well as other applications as illustrated in Figure 2.7. The solid product (bio-char) from biomass pyrolysis has been widely applied in carbon sequestration for soil management [94]. Biochars act as fertilizers or conditioners because they consist of various plant nutrients that are advantageous in improving the soil quality and also dedicated to alleviate atmospheric carbon [95]. Another beneficial feature is the great thermodynamic stability of biochar due to its highly aromatic configurations, which is valuable in metallurgical applications [88]. However, the high ash content in biochar is unfavourable in some applications [96].

### 2.3.1.2 Bio-oil

Bio-oil from the biomass pyrolysis is appeared to be a viscous and dark brown liquid which comprises of mostly oxygenated compounds [15, 97, 98]. Up-to-date, hundreds of compounds have been found in the biomass-derived pyrolysis oil, including water, acids, alcohols, sugars, aldehydes, ketones, esters, phenolic and aromatic compounds [8, 18, 98]. However, bio-oil suffers from high moisture and oxygen content, high acidity, low volatility, incompatible with conventional fuels and coking issues that significantly limiting its direct use as a fuel [8, 15, 18, 99]. From the literature, it is reported that the high heating value (HHV) of the bio-oil from biomass pyrolysis (15-20 MJ/kg) is only about 50% compared to the fossil fuels (42-45 MJ/kg). Apart from the low HHV, bio-oil has high oxygen content of 35-40 wt% on a dry basis due to its high moisture (15-30 wt%) [16, 100]. The high water content is originated from its biomass feedstock and also from the dehydration reactions during the pyrolysis process [15]. Due to the presence of the carboxylic acids, bio-oils exhibit high acidity with pH of 2 to 3.7 [17]. In addition, bio-oil is chemically unstable and undergoes slow changes with time even at room temperature, which is known as aging. Aging can increase the viscosity and water content and decrease the volatility due to the polymerization reactions [99]. These problems will lead to the difficulties in storage and for further applications or upgrading.

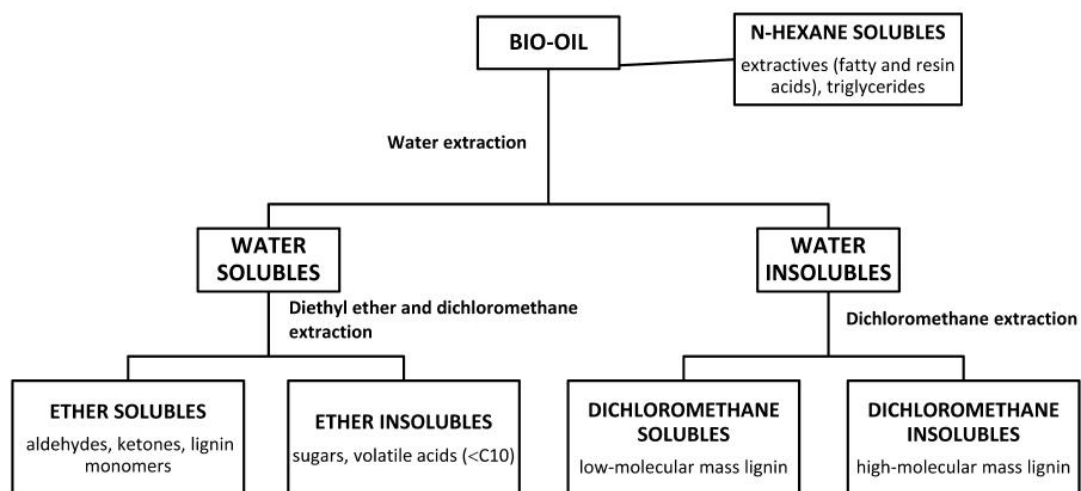


Figure 2.8: Solvent fractionation method of bio-oil [101, 102]

Due to the complex nature of bio-oil, the fractionation of bio-oil is essential for further bio-fuel or bio-chemical production. The separation of the different bio-oil constituents may simplify the downstream upgrading processes for chemicals and

fuels production. Since the pyrolysis oil is thermal unstable, traditional separation techniques such as distillation cannot effectively separate bio-oil into fractions [16, 103]. Bio-oil can be easily separated via solvent fractionation method as shown in Figure 2.8.

The simplest and cheapest way to separate bio-oil is by water addition, obtaining the two fractions with light and heavy compounds. The top aqueous layer, which is water soluble fraction is mostly comprises of carbohydrate-derived compounds. The water-soluble sugars can be easily separated and upgraded into chemicals or fuels (i.e., ethanol by fermentation) [8, 99, 104]. Whereas the water fractionation precipitated out mostly lignin-derived fragments, called pyrolytic lignin, as bottom layer [54, 73, 87]. In bio-oil, pyrolytic lignin is regarded as a major fraction that complicates the thermal treatment process and contributes the most to the viscosity of bio-oil compared to other constituents in lignocellulosic biomass [74]. Difficulty in decomposition and formation of high solid residue (i.e., coke) yield are the major challenges of pyrolytic lignin fraction in bio-oil [75, 105, 106]. The coking in bio-oil is due to the polymerization reaction among the lignin-derived particles in pyrolytic lignin [107, 108]. The presence of pyrolytic lignin exhibits negative impacts on the bio-oil properties and quality. For example, the chemical compositions from pyrolytic lignin will affect the reactivity and viscosity as well as deteriorate the thermal stability of bio-oil. Since pyrolytic lignin is difficult to decompose, it requires longer time during combustion compared to other components. This eventually leads to incomplete combustion and coking, which exhibits poor performance in the applications such as engines and boilers combustion [75, 107, 109]. Therefore, it is significant to extract the pyrolytic lignin from bio-oil for the upgrading and bio-refinery processes into useful chemicals or fuels. There are ongoing efforts performed from the literature on the conversion and depolymerization of pyrolytic lignin such as pyrolysis, catalytic hydrocracking, supercritical water or solvent treatment [72, 107, 109, 110]. Among these technologies, pyrolysis process is an attractive route that depolymerize the linkages in pyrolytic lignin to yield smaller compounds [105]. The pyrolysis of pyrolytic lignin fraction will decompose part of phenolic oligomers into monomers and also yields some aliphatic compounds [105, 107].

Bio-oil has been regarded as a potential energy source to replace the uses of fossil fuels for heat and energy generation in combustors, engines, boilers and furnaces [111]. The production of synthesis gas from bio-oil is also greatly applied and investigated. Panigrahi et al. [112] performed pyrolysis experiments on biomass-derived oil using tubular reactor and yields syngas products including  $\text{CH}_4$ ,  $\text{C}_2\text{H}_2$ ,  $\text{H}_2$ ,  $\text{CO}$ ,  $\text{CO}_2$  and hydrocarbons at  $800\text{ }^\circ\text{C}$  under atmospheric condition. Moreover, the bio-oil product contains various chemical compounds that are suitable for the production of phenols, resin, adhesives, fertilizers and pharmaceutical purposes [113]. Further upgrading of the bio-oil is necessary for the direct use as transportation fuels or applications in engines combustion [8]. The liquid fuels can be produced through upgrading techniques such as catalytic cracking, hydroprocessing, steam reforming and gasification [114-118].

### 2.3.1.3 Gaseous Products

The gaseous product from biomass pyrolysis is known as syngas or pyrogas, which mostly includes carbon dioxide ( $\text{CO}_2$ ), carbon monoxide ( $\text{CO}$ ), hydrogen ( $\text{H}_2$ ), nitrogen ( $\text{N}_2$ ) and methane ( $\text{CH}_4$ ). Some other gases also released in very small amount such as propane ( $\text{C}_3\text{H}_8$ ), ammonia ( $\text{NH}_3$ ), nitrogen oxides ( $\text{NO}_x$ ) and sulphur oxides ( $\text{SO}_x$ ) [17]. The gases species and concentrations are usually identified and quantified through gas chromatography (GC) and mass spectrometry (MS) [119-121]. The lower heating value (LHV) of the gas products is calculated from their respective gas composition, and is typically ranging between 10 and  $20\text{ MJ/Nm}^3$  [17]. Generally, the  $\text{CO}_2$  and  $\text{CO}$  gases are produced from the decomposition of carbonyl ( $\text{C=O}$ ) and carboxyl ( $\text{COO-}$ ) groups during primary reaction of biomass pyrolysis [121, 122]. The low hydrocarbon gases such as  $\text{CH}_4$  are released primarily due to the bond cleavage of methoxyl ( $\text{O-CH}_3$ ) and methylene ( $-\text{CH}_2-$ ) and some from the secondary decomposition of oxygenated compounds. It is also suggested that the  $\text{H}_2$  gas discharged from secondary decomposition of the aromatic  $\text{C=C}$  and  $\text{C-H}$  bonds at elevated pyrolysis temperature [33, 123].

The gaseous products (pyrogases) can be directly applied in the co-firing with coal and the production of electricity/heat, for examples gas combustion in compression engines [124]. The gas also can be used for the production of bio-syngas such as  $\text{CH}_4$ ,  $\text{H}_2$ ,  $\text{CO}_2$  and other gases [125]. In addition, the gas from the pyrolysis process can be

recovered and recycled to preheat the reactor or acts as a carrier gas [17]. Some other applications include the production of solvents such as acetone and methanol as well as hydrocarbons [87].

### 2.3.2 Parameters Influencing Biomass Pyrolysis

The pyrolysis mechanism as well as the quality and quantity of the pyrolysis products are significantly affected by several factors. These factors can be categorized as feedstock property, pyrolysis temperature, heating rate and the presence of inorganic species during biomass pyrolysis.

#### 2.3.2.1 Feedstock Property

In lignocellulosic biomass, the relative dry weight ratio of the main constituents (cellulose, hemicellulose and lignin) varies in different species type. Each of the constituents exhibits different structural stability as they undergo thermal decomposition, and subsequently influence the pyrolysis performance. For instance, cellulose and hemicellulose produces higher yield of bio-oil during the pyrolysis process, while lignin yields higher solid bio-char [126, 127]. Previous studies from Zanzi et al. [128] showed that agricultural residues such as olive waste and straw yield more char than wood, but lesser volatiles. They pointed out that the presence of higher ash content in agricultural residues favours the charring reactions. While the higher content in lignin produces a more viscous and higher molecular weight bio-oils but lower water concentration [129]. In addition, the reactivity of the biomass components is influenced by the existence of heteroatom and oxygen content. The higher the amount of heteroatom and oxygen in the biomass species, the more reactivity the biomass is during thermal decomposition. Figure 2.9 demonstrated the changes in weight loss for different biomass type with increasing temperature and under the same pyrolysis condition. It is observed that the conversion of the wood pellets from wood industry residues is less significant and more thermally stable than other biomass types such as pine wood, paper sludge, olive residue and hazelnut shell [130]. Moreover, most of the biomass experienced significant weight loss between 300 to 400 °C due to the primary devolatilization reaction [130]. The small amount of extractives in biomass may also affect the product distribution. This is supported by Wang et al. [131] that the presence of extractives promote the bio-oil yield but suppress the solid char and gas production during pyrolysis.

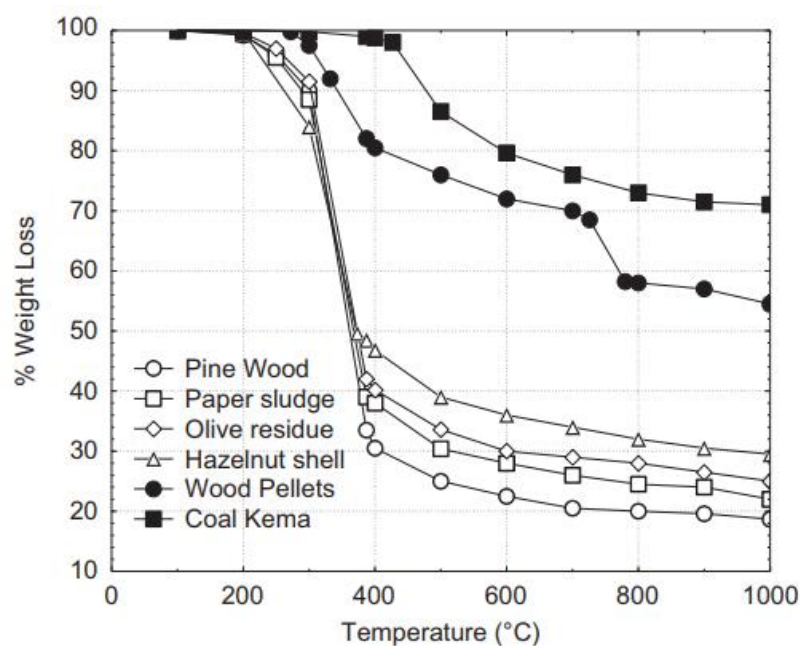


Figure 2.9: Weight loss (%) of different biomass feedstock with temperatures [130]

### 2.3.2.2 Pyrolysis Temperature

Pyrolysis temperature is one of the major determinants for the product distribution and their properties in thermal decomposition process. The changes in product yields distribution and physio-chemical properties of the products such as carbon content, aromatic rings, high heating value, surface area and conductivity produced from biomass pyrolysis at different pyrolysis temperature ranges were focused in the past [132-138]. Generally, the reaction begins with the release of more volatile gaseous product and the formation of char as the temperature increases above 150 °C [119]. Figure 2.10 shows the typical trends of the changes in products (bio-char, bio-oil and syngas) yield with increasing temperature between 425 to 625 °C under the same pyrolysis conditions [134]. Higher pyrolysis temperature releases more gaseous and liquid products but reduce the solid bio-char yield. However, the bio-oil production reached its maximum yield at temperature about 500 °C and decreases beyond the point [134]. It is also figured out that the bio-oil with its best caloric value and H/C ratio is obtained at high temperature of 500 °C [136]. Moreover, the yield of lignin-derived oligomers were observed to be the most at temperature around 450 to 500 °C [104]. The chars produced from higher pyrolysis temperature are with higher carbon content [139]. Beyond the temperature range of 550°C, the release of volatile gases from converted liquids become dominant due to secondary cracking reactions [135].

According to Luo et al. [140], the pyrolysis reaction released more CO and CH<sub>4</sub> gases compared to CO<sub>2</sub> at temperature above 450 °C, which will resulting in higher heating value pyrogases.

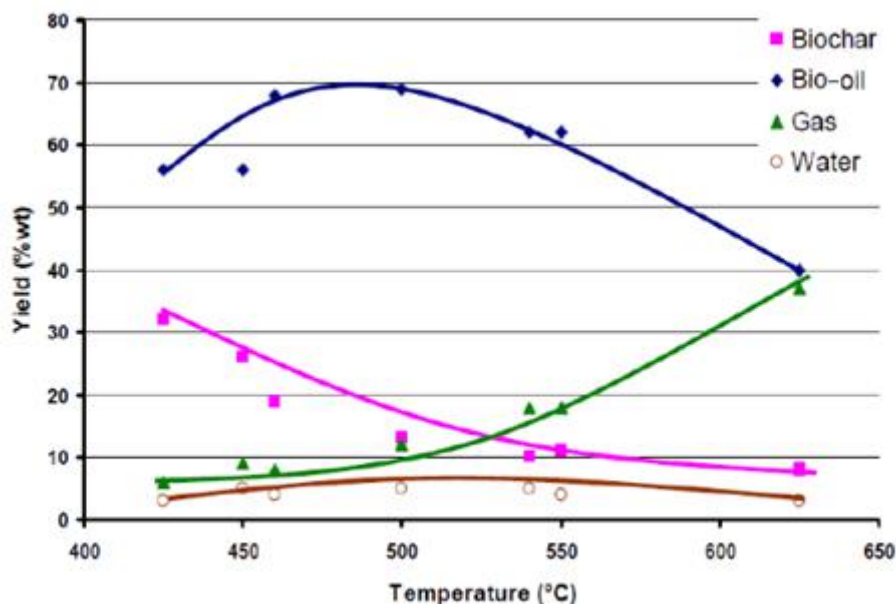


Figure 2.10: Typical yield of end products from biomass pyrolysis [134]

### 2.3.2.3 Heating Rate

Another key factor that affects the biomass pyrolysis and products distribution is the heating rate of the reaction. In fast pyrolysis process, the heating rate is generally higher than that of slow pyrolysis, thus increase the volatile products due to the enhanced decomposition of biomass components. Fast heating rate also minimizes the occurrence of secondary reactions such as polymerization and cracking reactions, leaving a lower char yield [126, 141]. Many studies have been carried out to investigate the effects of heating rate on the product yields and their properties. Ozbay et al. [142] observed an increase in the bio-oil yield from 26 wt% to 35 wt% when the heating rate increased from 5 °C/min to 300 °C/min for cottonseed cake pyrolysis. Similar results also obtained by Salehi et al. [143], oil yields increased from sawdust pyrolysis with increasing heating rate 500 °C/min to 700 °C/min. Shorter residence time favours bio-oil production due to the quick removal of organic vapours from reactors which minimises the secondary reactions [144]. For the pyrolysis of raw sorghum bagasse at 525 °C, Scott et al. [145] observed that an

increase in vapour residence time from 0.2 to 0.9 s resulted in a decrease in the bio-oil yields from 75% to 57%, while the char and gas yields increased.

#### 2.3.2.4 Inorganic Matters

As mentioned earlier in section 2.2.4, biomass consists of traces amount of inorganic species such as K, Na, Ca and Mg, which is categorized as pyrolysis ash. The presence of inorganic species is one of the important parameter for the pyrolysis mechanism and solid product reactivity. Generally, the presences of inorganic matters lower the liquid oil yields but favoured the solid and gaseous products yields, mainly due to the enhanced dehydration and charring reactions during the pyrolysis [146-148]. The different types and composition of the inorganic species influenced the products distribution of the biomass. The inorganic species especially the alkali (i.e., K and Na) and alkaline earth (i.e., Ca and Mg) metal ions significantly influenced the biomass pyrolysis mechanism and the products yield distributions [149, 150]. For example, high concentration of alkali metals such as K, Na and Ca reduced the formation of tars during the secondary reaction of pyrolysis [126]. The K metals in biomass also reported to enhanced the low molecular weight components formation and suppressed the levoglucosan formation from cellulose pyrolysis [146]. The alkaline metals also tends to promote the formation of alkali-oxygen surface cluster, through the reaction with carbonates and oxides groups [151]. Raveendran et al. [152] found out that the biomass types which comprise of higher concentration of lignin and potassium content clearly resulting higher char product and lower volatiles yields. The behaviour is explained by the secondary reactions such as tars cracking as well as the easier pathway for the tars diffuse into the mineral pores.

#### 2.3.3 Pyrolysis Mechanism of Biomass

The pyrolysis of biomass involves complex reaction mechanisms as the decomposition varies with different constituents in biomass as illustrated in Figure 2.11, which also depending on the operating conditions and reactor configuration. During the heating up of biomass, it involves different reactions which can be classified into primary reactions (i.e., depolymerization, fragmentation and char formation as illustrated in Figure 2.12) [153] and secondary reactions (i.e., cracking and polymerization) [154, 155]. Generally, biomass experiences major decomposition during primary reaction range from temperatures 200 to 400 °C,



yielding solid char as residue. Volatile products are also released due to the breaking of bonds linked between the monomers in the polymers. The depolymerization reaction results in the reduction of the DP of the carbon chain and those volatiles which are condensable can be recovered as liquid oil [156]. While some of the volatile compounds were unstable in the reactor and tend to undergo secondary reaction via cracking or polymerization [154, 157]. Cracking reactions involve the bond cleavage between the volatile compounds to form low molecular weight compounds. The polymerization reaction may take place among the polymers to form secondary char or deposited on the char surface [157, 158]. To gain better understanding on the biomass pyrolysis behaviour, it is important to first study the decomposition pathways of cellulose, hemicellulose and lignin components individually.

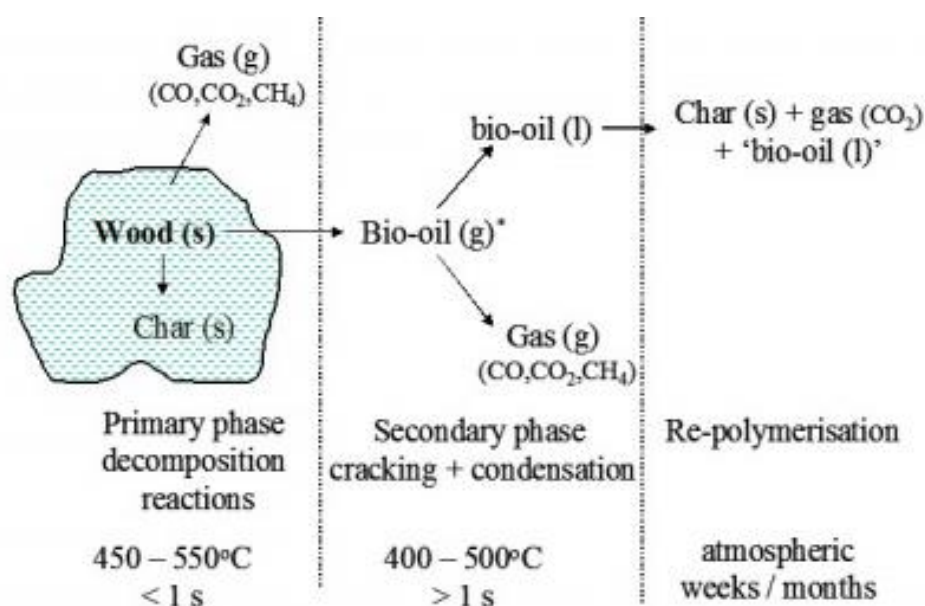


Figure 2.11: The proposed pathway of biomass pyrolysis [159, 160]

- 1. Cellulose.** It is well accepted that the thermal decomposition of cellulose has been widely investigated and achieve the best understanding compared to that of hemicellulose and lignin. From the TG analysis of cellulose component presented in Figure 2.13, the decomposition mainly takes place between temperatures 300 and 400 °C, and reaches it maximum around ~355 °C [45, 127, 161]. The minor weight loss of the cellulose during pyrolysis at  $T < 300$  °C is mainly due to the dehydration reaction, either in terms of intermolecular or

intramolecular, by releasing the H<sub>2</sub>O molecules as well as promoting the C=C bonds formation [45, 154]. After 300 °C, the depolymerisation reaction is responsible for the major weight loss and reduction in degree of polymerization (DP) of cellulose, which resulting from the breakage of glycosidic bonds [21, 45, 127]. It is reported that the depolymerisation of cellulose structure gives rise to the formation of active cellulose, also known as intermediates in liquid phase, which leads to the formation of anhydro-oligosaccharides and anhydro-saccharides (i.e., levoglucosan) [19, 20]. In the liquid phase, the intermediate species could react to produce smaller molecules that can be thermally ejected as aerosols [23] or undergo polymerization to form solid [20, 24, 25]. Some intermediates may turn into furans such as 5-HMF, furfural and furfuryl alcohol via dehydration reaction [21, 22]. Functional groups such as carbonyl and carboxyl are also formed during the primary depolymerisation reactions, however they are unstable and easily decompose to yield CO<sub>2</sub> and CO [45, 127, 162]. The proposed reaction mechanisms during the cellulose pyrolysis are illustrated as shown in Figure 2.14.

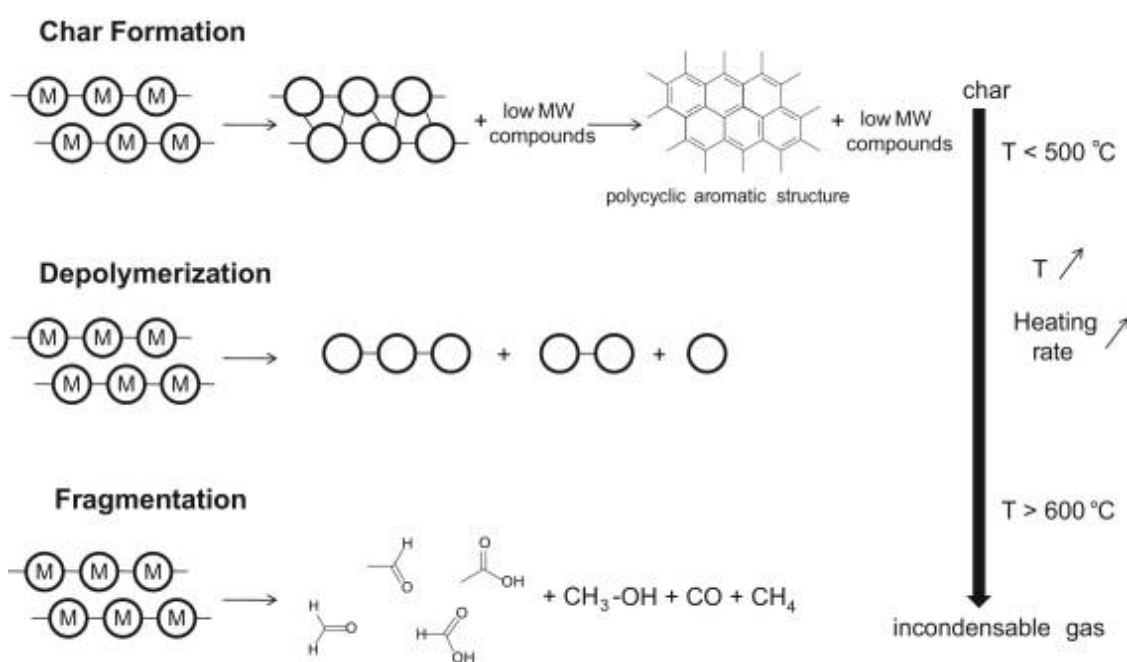


Figure 2.12: The three main primary reactions in biomass pyrolysis [153]

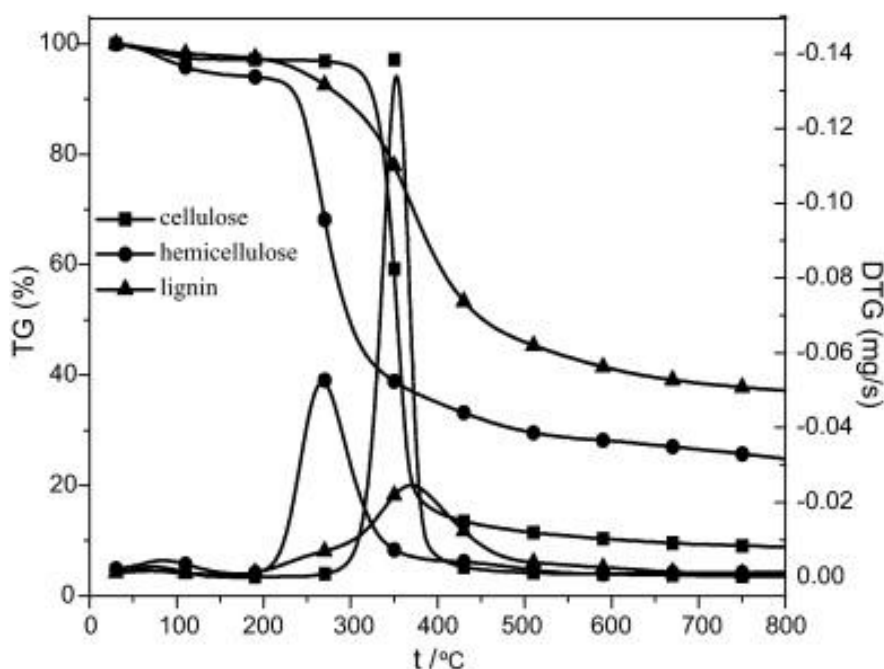


Figure 2.13: TG and DTG curves of cellulose, hemicellulose and lignin [44]

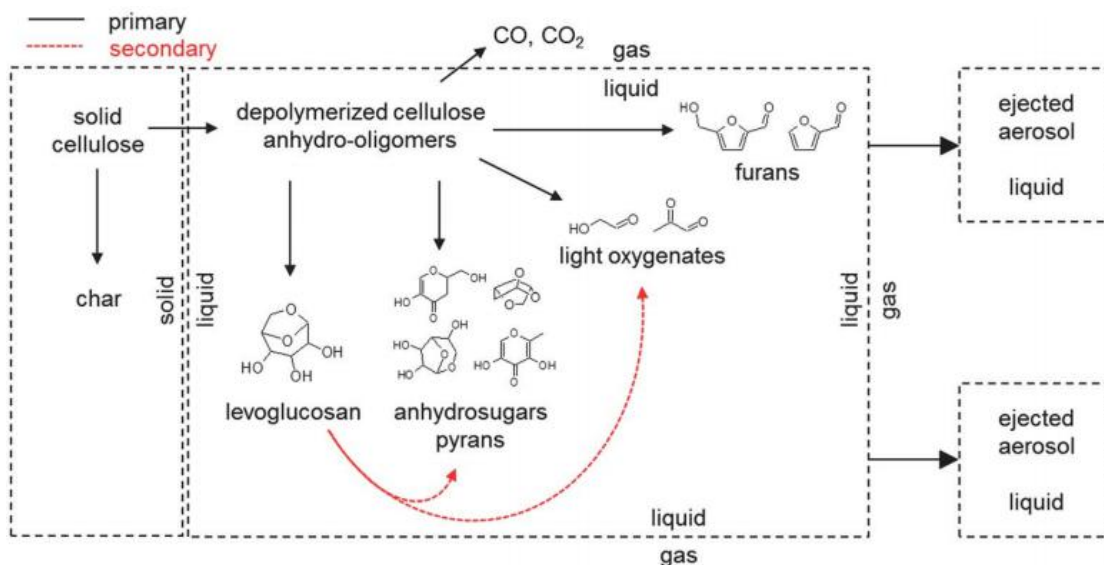


Figure 2.14: The proposed reaction mechanisms during cellulose pyrolysis [163]

- Hemicellulose.** Unlike the uniform structure of cellulose, hemicellulose composes of amorphous and random short chains structure with different saccharides (e.g., xylose, glucose, galactose, mannose, etc.) [54-56]. The thermal decomposition of hemicellulose may be complicated because each polysaccharides show different chemical properties and pyrolysis behaviours. Therefore, xylan has been long regarded as the model compound to represent hemicellulose for pyrolysis study in the literatures [122, 127, 164] since xylose

is the basic building block of hemicellulose. Compared to cellulose, hemicellulose can be easily decomposed at lower temperature range usually between 220 to 315 °C (Figure 2.13) [127, 161]. It was found out that the major products identified from the pyrolysis of hemicellulose are acids, furans, ketone and anhydro-sugars. Furans such as furfural can be formed through the C<sub>5</sub>-O bond breaking of xylose monomer, and then rearrange between carbon C<sub>2</sub> and C<sub>5</sub> in the form of ring structure via dehydration reaction [161, 165]. While the acids, mostly acetic acid produced from the removal of O-acetyl groups in the xylan and the scission carbon chain of uronic acid [166]. At elevated temperatures, the acetic acid may undergo secondary decomposition into gases such as CO and CO<sub>2</sub> [165]. In addition, the mono-sugar units in hemicellulose may undergo ring opening reactions to form ketones and some low molecular weight compounds. At temperature 300 °C, hemicellulose pyrolysis mostly yields acids and ketones. Lv and Wu [161] reported that approximately half percentage (~46%) of the pyrolysis products from hemicellulose pyrolysis are ketones group compounds, including 1-hydroxy-2-butanone, 1-hydroxy-2-propanone, 3-methyl-1,2-cyclopentanedione, acetone, cyclopentenone and etc. The decomposition of hemicellulose with more pentose and side chains is most likely to form higher char yield due to the enhanced polymerization between the large molecular radicals produced from the glycosidic bonds cleavage [167].

- 3. Lignin.** Among the three major components in biomass, lignin is the most complex and highly branched with mainly aromatic rings structure, which led to difficulties in fully understanding the knowledge of its pyrolysis behaviour. Yang et al. [127] carried out the research of lignin decomposition using a thermogravimetric analyser (TGA) and the results showed that lignin decompose slowly over a wide range of temperature from 160 to 900 °C, with ~46 wt% solid residue remaining. This is due to the activity of various chemical bonds, namely ether bonds and carbon-carbon bonds in lignin structure such as β-1, α-1, β-5, α-O-4, β-O-4, 4-O-5 and 5-5 [168-171], however each of the linkages exhibit different thermal stability. Upon thermal decomposition, the strengths of the ether bonds were reported following the descending order: 4-O-5 > β-O-4 > α-O-4 (Figure 2.15) [169]. The main decomposition of lignin was observed between temperature from 200 to 450 °C [34, 172]. The pyrolysis products of

lignin generally include monomeric phenols, heterocyclic compounds, hydrocarbon gases, H<sub>2</sub>O, CO and CO<sub>2</sub> [34, 105, 127, 161]. The presences of the lignin-derived molecules in lignocellulosic biomass or extracted lignin are seemed to easily melt and agglomerate upon heating [36, 108]. In order to achieve sustainable source of bio-fuels, it is important to investigate lignin pyrolysis in order to tackle the significant challenges in depolymerisation of lignin into smaller molecules for further upgrading purposes.

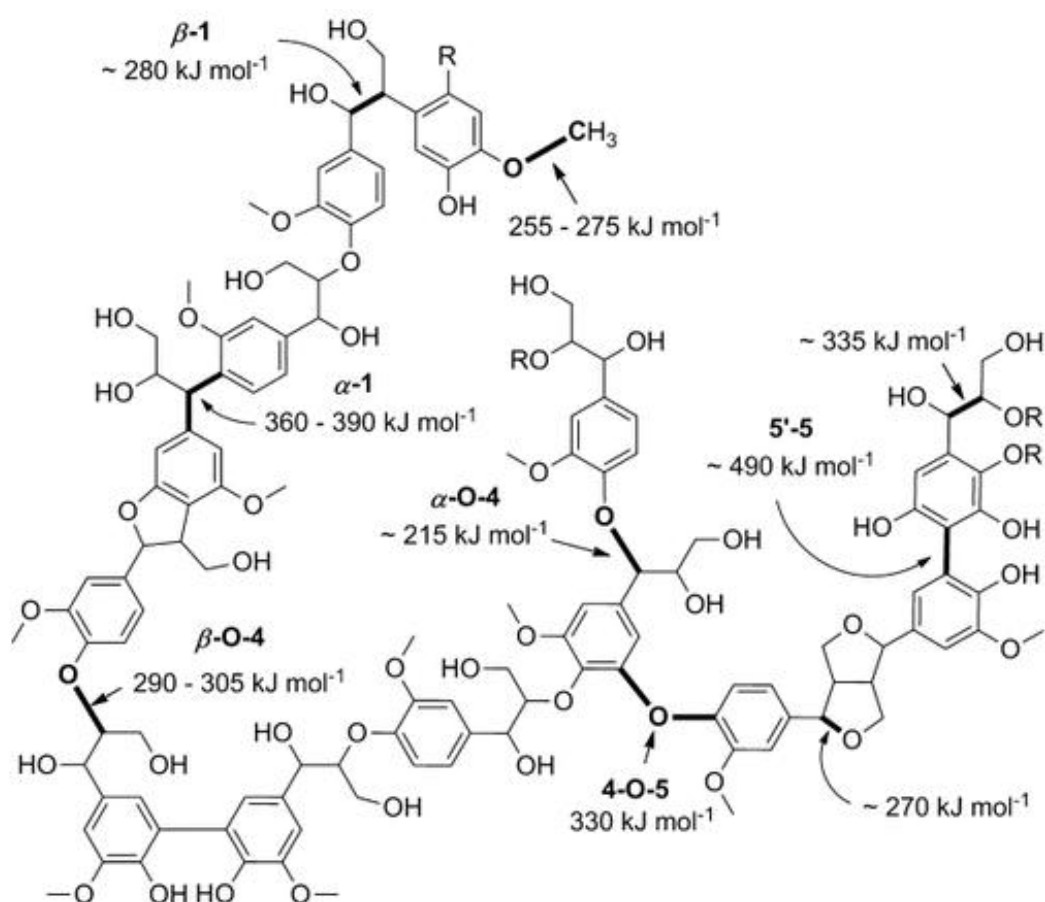


Figure 2.15: Types of linkages with their estimated bond dissociation enthalpies values that exist in lignin structure [169]

#### 2.4 Mechanisms of Lignin Pyrolysis

A good understanding on the chemical reactions involved in lignin decomposition is essential for process development and enhancement. It is well known that the abundant aromatic contents in lignin [26, 27] make it as a potential feedstock for high value chemicals and energy-densed bio-fuels [27, 28]. However, the complex

aromatic polymer structure in lignin [27, 28] leads to the difficulties on lignin conversion technologies in most bio-fuels refineries and industries. The depolymerization of lignin component into smaller compounds is the key challenge to produce high quality fuels and valuable chemicals from lignocellulosic biomass [26].

The lignin structure undergoes decomposition or transformation as the temperature increases during the pyrolysis process. At low temperature of 150 – 200 °C, the weight loss initiated is mainly due to dehydration reactions including the loss of moisture [29, 44, 153, 171]. The less thermally stable alkyl chains in the lignin polymer begin to rupture by the cleavage of ether linkages and carbon-carbon bonds at temperature between 200 to 420 °C [34, 173]. It is known that the weakest ether linkage in lignin,  $\alpha$ -O-4, which can easily break at temperature 200 °C [169, 171]. While the main linkages  $\beta$ -O-4 in lignin become unstable and started to rupture at a slightly higher temperature ~245 °C [169, 171]. Hence, most of the ether linkages that implied between the monomer units in lignin can be broken at temperature higher than 300 °C, releasing a significant amount of mono-phenols or oligomers compounds [33, 34, 174]. This is proven by the research studies by Lv et al. [161], who reported that ~48% of the lignin-derived phenolic compounds generated from the lignin pyrolysis process were due to the rupture of the linkages of the aliphatic chains. Majority of the phenols derived from guaiacyl and syringyl units in lignin structure (i.e., ~11% of 2-methoxy-4-vinylphenol and ~9% was 2,6-dimethoxyphenol) [161]. The reactions involving the depolymerization of aliphatic propyl side chains, breaking of linkages and C-C bonds mostly contributed to the maximum decomposition rate at low temperatures ( $T < 420$  °C). With increasing temperature, most of the connections between lignin monomers are broken except those with higher stability such as diaryl ether 4-O-5 and phenyl 5-5 may be still remained [171, 175].

Some researchers studied the pyrolysis behaviors of lignin using various lignin model compounds or lignin substructure such as dimers to provide better understanding on the overall lignin pyrolysis [170, 171, 176, 177]. Kawamoto et al. [170] reported the reactivity of different lignin model dimers with the main linkages (i.e.,  $\alpha$ -O-4,  $\beta$ -1,  $\beta$ -O-4 and biphenyl) in lignin structure on depolymerization and

condensation reactions during pyrolysis at 400 °C. The results suggested major depolymerization on  $\alpha$ -O-4 and  $\beta$ -O-4 types, whereas  $\beta$ -aryl and phenolic  $\beta$ -ether types contribute more to condensation or carbonization reactions in pyrolysis. Nakamura et al. [171] compared pyrolysis of milled wood lignin (MWL) with dimers and found out that phenolic linkage types are important for condensation reaction at low temperature of 250 °C, to form  $C_{\alpha}=C_{\beta}$  structures. The authors proposed a pyrolysis pathway based on the reactivity of linkage types and from that of MWL with increasing temperature, as summarized in Figure 2.16. The study on these model dimers derived from lignin may be useful to understand the reactions involved, but there is still some differences when apply to that in lignin pyrolysis due to the highly reactive types, particularly phenolic dimers [176].

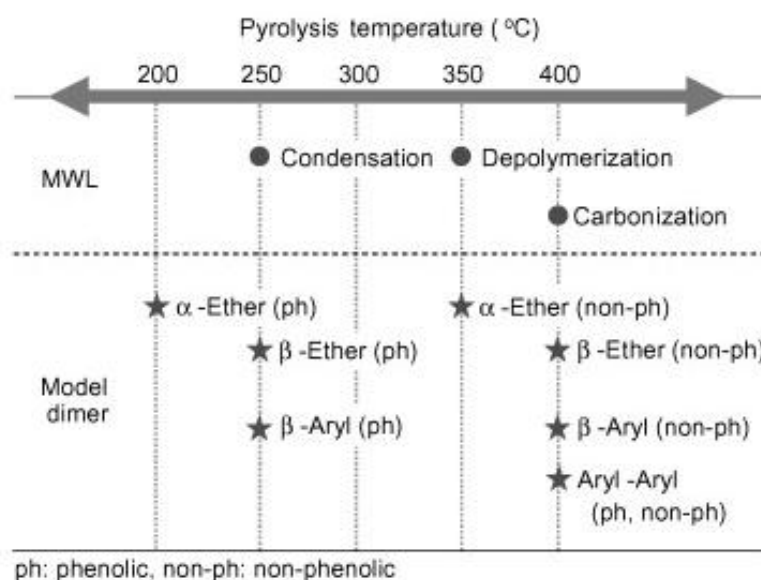


Figure 2.16: Proposed pyrolysis mechanism from MWL pyrolysis with various model dimers [171]

In the past few decades, great efforts have been done on the studies of volatile products (gas and tar) released from lignin pyrolysis [29-35]. The breaking of the ether bonds leads to the formation of low molecules gases such as CO, CO<sub>2</sub> and H<sub>2</sub>O as volatiles [29, 33, 34, 173]. In addition, some other small molecules such as acetic acid, acetaldehyde, methanol and CH<sub>4</sub> may also form from the reactions [33, 161]. Acetic acid can be produced from the bonds scission and reforming of the side propyl chains in lignin [161]. Methanol and light hydrocarbon such as CH<sub>4</sub> are

produced most likely due to the removal of the weakly bonded methoxyl groups ( $-\text{OCH}_3$ ) [33, 171, 173, 174]. The reactive chemical groups that attached to the  $\gamma$ -carbon of the side chains were responsible for the dehydration reactions and yield different gaseous products. For instance, when the hydroxyl group is joined to the  $\gamma$ -carbon in lignin, the bonds between  $\gamma$ -carbon and  $\beta$ -carbon fragmented and released formaldehyde compounds [33, 173]. Likewise, if the  $\gamma$ -carbon is attached to carbonyl or carboxyl groups, the C-C bonds will also undergo fragmentation but the reactions generated CO and  $\text{CO}_2$  gases [34, 173]. Various reactions occurred subsequently or simultaneously which leads to the release of volatile products with increasing temperature are summarized in Figure 2.17.

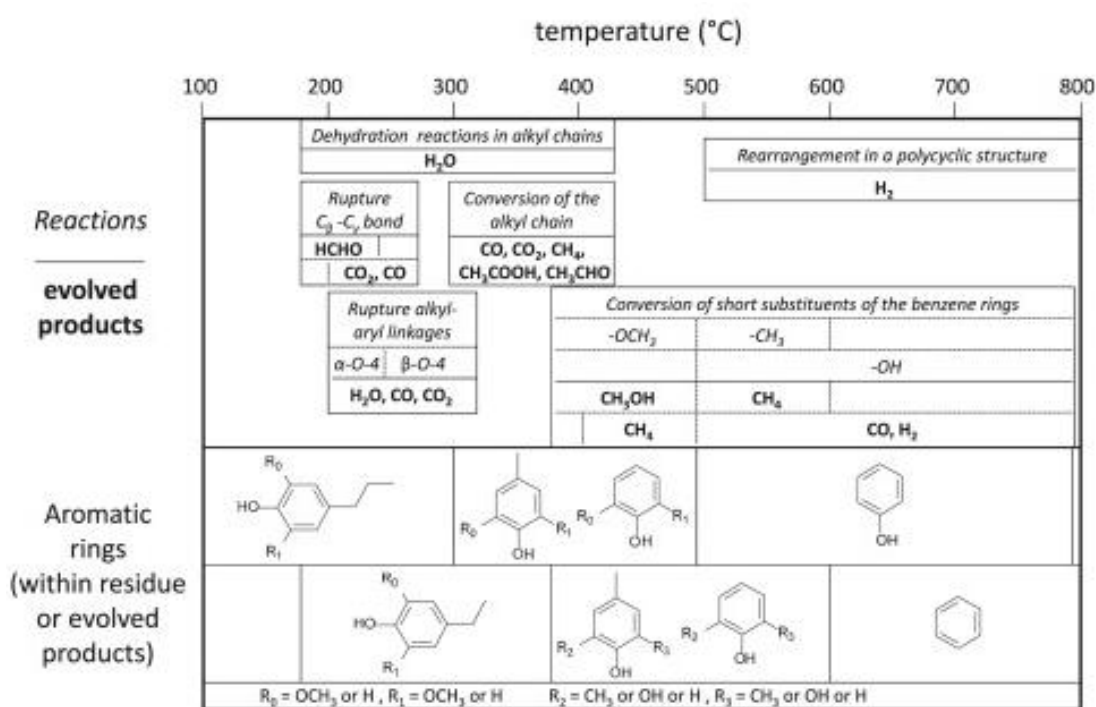


Figure 2.17: Types of reactions occurring over the temperature ranging from 100 to 800 °C [153]

Limited studies have been focused on the structural analysis of another major product from pyrolysis, which is the solid product (i.e., char), especially at low temperatures. Sharma et al. [37] characterized the chars produced from lignin pyrolysis from 250 to 750 °C in a tubular reactor. The results showed the decreased in char yield and the solid char from lignin pyrolysis becomes more condensed with higher aromatic structure as temperature increased due to the loss of aliphatic,



methoxyl and carboxyl groups. The results were supported by Foston et al. [178] in their findings using  $^{13}\text{C}$  NMR analysis to study the structural changes in solid char produced from lignin pyrolysis. The authors observed significant reduction in the number of aliphatic chains, methoxyl and oxygenated chemical moieties, nevertheless accompanied with increasing condensed carbons amount in aryl structure, which promote the char carbonization. Similar results were reported by Shrestha et al. [36], who observed the existence of aromatic clusters formation at temperature  $T > 400\text{ }^\circ\text{C}$ , which coincided with the release of maximum exothermic heat which corresponded to the cross-linking reactions between the aromatics to form char from DSC analysis.

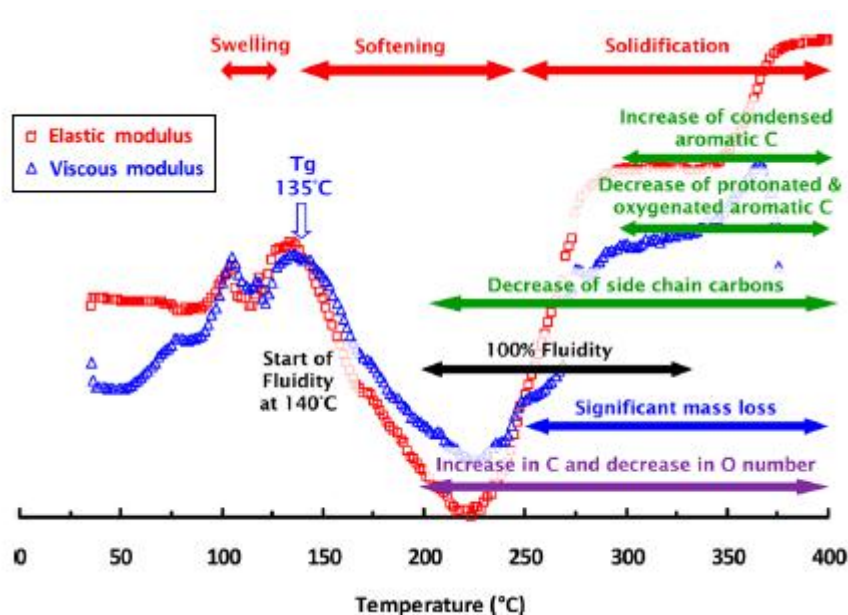


Figure 2.18: Rheological properties of lignin during thermal decomposition [36]

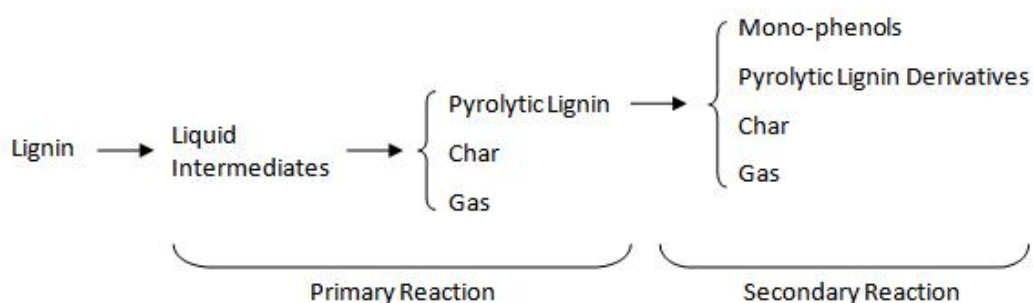


Figure 2.19: The proposed pyrolysis mechanism of lignin [38]

However, it was recently reported that the lignin softening leads to the formation of a “liquid intermediate” phase at very low temperature of  $\sim 150$  °C, which affected the pyrolysis product distributions [36, 37, 39]. Upon the thermal decomposition, the lignin structure was initially melts and undergo softening/shrinking at the temperatures ranging from 140 to 250 °C [36], as shown in Figure 2.18. The softening process of the lignin structure was evidenced by the formation of vesicles from the released volatiles that stimulate the soften surface on lignin char mainly occurred at temperature 250 °C via SEM analysis [37, 38]. Further elevating the temperature, the intermediates formed in the liquid phase may turn out to be unstable under pyrolysis temperature in reactors also react and undergo secondary reactions [179-181], similar to that of intermediates found in cellulose pyrolysis [19, 162, 182]. The liquid intermediates species produced from lignin pyrolysis in a wire mesh reactor at 300–650 °C observed by Zhou et al. [38] seems to responsible for the lignin oligomers production at early stage, but promoted the release of monomers at elevated temperature due to secondary reactions (see Figure 2.19).

Since it was revealed that the intermediates play important roles in cellulose pyrolysis, hence it must not be neglected in lignin pyrolysis. The information on the pyrolysis behaviour related to the intermediates formation at such low temperatures are still unclear. Therefore, the characterizations and structural analysis on solid products are the main focus of this study especially at low temperatures, as intermediates most likely to form at low temperature ranges and higher char yield can be obtained from lignin pyrolysis.

## 2.5 Interactions of Components during Biomass Pyrolysis

A significant finding from the pyrolysis of biomass is the existence of interactions between the three main constituents in biomass. Cellulose, hemicellulose and lignin interact with each other and influence the product distribution and pyrolysis behaviour [42, 44, 45, 183, 184]. For instance, a study from Greenhalf et al. [185] showed that the higher lignin content in hardwoods compared to straws and grasses, resulting in a lower decomposition rate at higher temperature range during pyrolysis. According to Qu et al. [122], the pyrolysis of peanut vine yields more carbohydrates in the bio-oil product because it contains higher cellulose content than rice straw and corn stalk. They pointed out that the bio-oil from corn stalk pyrolysis produced the

most aldehydes due to its higher hemicellulose content. From the results, it seems that the pyrolysis mechanism can be affected by the interactions between the biomass components. The interactions between cellulose-hemicellulose, hemicellulose-lignin and cellulose-lignin mixtures are further investigate respectively to better understand the pyrolysis mechanism during thermal processing.

### 2.5.1 Cellulose-Hemicellulose Pyrolysis

Compared to cellulose, the decomposition of hemicellulose occurred at a lower temperature range during pyrolysis as discussed earlier. Therefore, hemicellulose started to melt and soften while the cellulose was enclosed within the molten structure before it reacted [42]. The presence of hemicelluloses hindered the volatile formation from cellulose, thus decreased the product yields [42]. According to the TG-FTIR study on pyrolysis of biomass components mixture by Liu et al. [43], the results showed the reduction in the levoglucosan yield but increased the formation of hydroxyacetaldehyde from cellulose affected by hemicellulose. In contrast, cellulose promoted the volatilization of hemicelluloses-derived products such as acetic acid and furfural [44]. As seen from experimental results of cellulose-xylan/glucomannan pyrolysis at gasification temperature, Hosoya et al. [42] observed negligible changes in the char compared to calculated data, gas and tar production, with only slight increase of char (from 14.3 wt% to 13.7 wt%) and decreased of total tars (from 73.3 wt% to 72.3 wt%). It seemed that the interaction between the cellulose-hemicellulose during thermal decomposition is not strong.

### 2.5.2 Hemicellulose-Lignin Pyrolysis

During the pyrolysis of hemicellulose-lignin, most of the weight loss contributed by hemicellulose component below temperature  $\sim 320$  °C, while the solid residues are mainly generated from lignin [43]. The presence of hemicellulose will enhance the production of lignin phenols and its derivative products including 2,6-dimethoxyphenol, 2-methoxy-4-ethylphenol and 2-methoxy-4-vinylphenol [44]. In addition, negative effect is observed on the formation of hydrocarbon gases such as  $\text{CH}_4$ ,  $\text{C}_2\text{H}_4$  and  $\text{C}_2\text{H}_6$  during hemicellulose-lignin pyrolysis. In another way, lignin affected hemicellulose pyrolysis by reducing the formation of furfural and mostly C=O group containing compounds (aldehyde and ketone groups) [43]. The pyrolysis of hemicellulose-lignin mixture shows minor effect on the pyrolysis behaviour.

### 2.5.3 Cellulose-Lignin Pyrolysis

The interactions involved for the pyrolysis of cellulose-lignin are found to be more significant on the product formations and distributions. Hosoya et al. [42] proposed the mechanism during the co-pyrolysis of cellulose and lignin and their interactions as illustrated in Figure 2.20. The authors suggested the presence of cellulose suppressed the carbonization of lignin-derived molecule products, thus yielding a lower char formation. It is nevertheless enhanced the formation of lignin products such as guaiacol-derived compounds. It is supposed that the decomposition of cellulose and lignin structures released some reactive intermediates that affected the reactions, leading to higher formation of total tar but lower char yields [184]. In addition, the interactions between cellulose and lignin was explained to follow the reactions involving hydrogen transfer, in which the cellulose-derived compounds act as hydrogen donors and lignin-derived compounds as hydrogen acceptors [184]. The hydrogen transferred from cellulose-derived compounds stabilizes the radicals from lignin pyrolysis products and thus enhanced the formation of low molecular weight compounds in the tar [see Figure 2.21 (a)]. From Figure 2.21 (b), the char formation from the lignin pyrolysis is less favored, compared to the formation of phenolic-type compounds.

On the other hand, cellulose pyrolysis mainly produced anhydro-sugars especially levoglucosan during primary depolymerization reaction. At elevated temperature, the unstable active cellulose may undergo ring opening polymerization to form polysaccharide intermediates, which may then transform into char by polymerization reactions [186]. In cellulose-lignin pyrolysis, the lignin content inhibits the polymerization reaction of levoglucosan from cellulose, thus decreasing the char formation. The co-pyrolysis of cellulose and lignin also enhanced the formation of low molecular weight products such as furans, 5-HMF, glycoaldehyde, hydroxyacetone and acetic acid [47, 187]. A study on the pyrolysis of components mixture using a wire mesh reactor conducted by Yu et al. [46] reported that the solid residue decreased ~1 wt% than calculated value from cellulose-lignin mixture at 525 °C, while the light gaseous products increased from ~18 wt% to ~28 wt%, indicating more low molecular volatiles are released from the process. Similar results were reported by Hosoya et al. [184], who suggested the loss of hydrogen in cellulose-derived compounds enhanced the evaporation of volatile products into vapor phase.

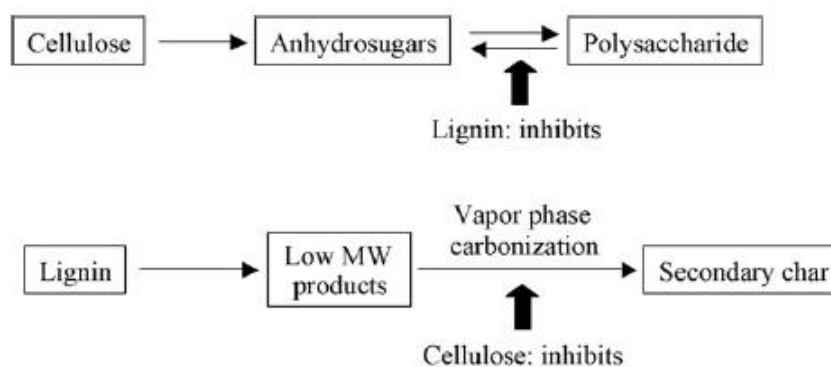


Figure 2.20: The proposed interactions between cellulose and lignin during pyrolysis [42]

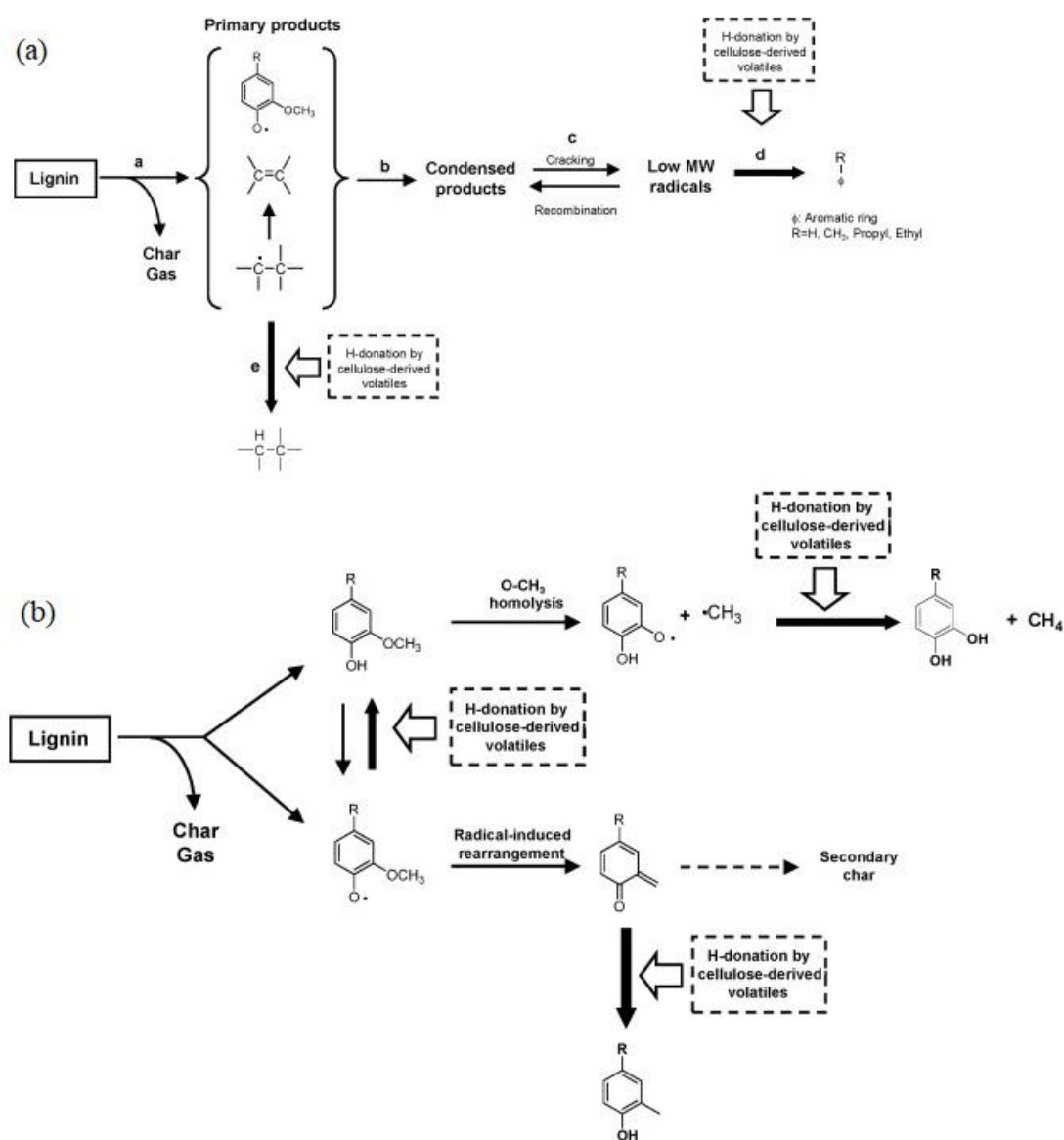


Figure 2.21: The proposed pyrolysis mechanism of the effect of cellulose-derived compounds on lignin pyrolysis of (a) tar formation; (b) char formation [184]

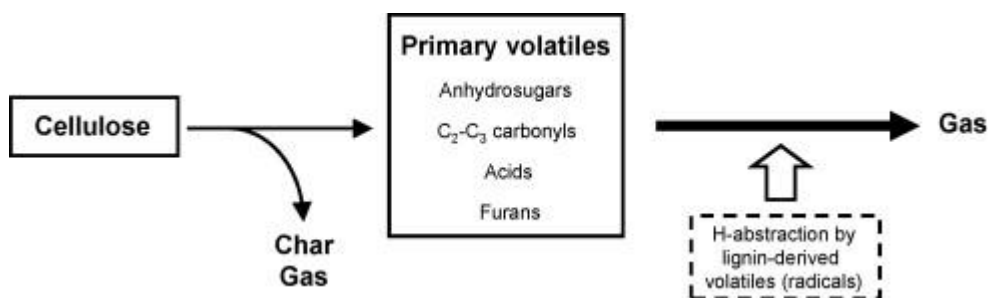


Figure 2.22: The proposed pyrolysis mechanism of the effect of lignin-derived compounds on cellulose pyrolysis [184]

## 2.6 Conclusions and Research Gaps

The abundant sources of lignocellulosic biomass materials have great potential for the production of energy, fuels and chemicals via pyrolysis technology. Lignin, as the main constituent in biomass, is difficult to be valorized due to its complicated and heterogeneous structure. The significant interactions between the main constituents in biomass also make biomass pyrolysis mechanism more complicated. Upon heating, the formation of liquid intermediates tends to promote the polymerization of phenolic compounds in lignin, leading to the formation of carbonaceous solid. This phenomenon leads to operation problems in some industry processes, such as the agglomeration in fluidised reactors. Therefore, the key challenge is to gain fundamental understanding of lignin pyrolysis mechanism, especially at low temperatures where the formation of liquid intermediates is significant.

Further research and development is required for the identified research gaps, including:

- Systematic study to achieve fundamental understanding on the detailed pyrolysis mechanisms of lignocellulosic biomass pyrolysis. The interactions between the three biomass components, particularly cellulose and lignin have to be clearly understood for efficient production of high-quality bio-oil. It is important to examine their effect on char structure, as the intermediates can be generated from both cellulose and lignin components during pyrolysis reactions.
- Systematic study to achieve fundamental understanding on the detailed pyrolysis mechanisms of lignin pyrolysis. The development of analytical method is required to characterize the pyrolysis products produced from the pyrolysis of lignin and its derived compounds, focusing more on the solid products. It is

important to clearly understand the structural changes of the chars during lignin pyrolysis, as lignin composed of a wide variety of aromatic compounds that decomposed over a wide pyrolysis temperature ranges. The characterization of solid products from lignin pyrolysis is important in facilitating the understanding of the intermediates formation from the reactions.

- Understanding the pyrolysis behavior of different portions of lignin during the pyrolysis, as both low- and high-molecular-weight species exist in lignin structure. The reactive species produced from low-molecular-weight lignin pyrolysis affects the pyrolysis reactions. Therefore, the changes in char structure need to be understood to discover their interactions during pyrolysis.
- Investigating the evolution of liquid intermediates formed from lignin pyrolysis. The intermediates are most likely to generate at low temperatures, but rapidly decomposed or reacted with other lignin-derived species via secondary reactions. Therefore, the study on the char structure is important to discover their effect on pyrolysis reactions.

## **2.7 Research Objectives**

To address the research gaps identified in the previous section, the scope of this study will focus on the systematic investigation on the formation and characterization of solid products from fast pyrolysis of lignin and its derived compounds, particularly at low temperatures. It is known that the intermediates are most likely to form at low temperature ranges. In addition, higher char yield can be obtained from lignin pyrolysis at low temperatures to ease the char collection for further structural analysis. The main objectives of this thesis are listed as below:

- To characterize the solid products produced from thermal decomposition of pyrolytic lignin at low temperatures;
- To study the structural changes of solid products from lignin pyrolysis at low temperatures;
- To examine the pyrolysis behavior of different portions (i.e., the low- and high-molecular-weight portions) of lignin and their interactions during pyrolysis at low temperatures;
- To provide better understanding on the cellulose-lignin interactions during the pyrolysis at low temperatures.

---

## Chapter 3 Research Methodology and Analytical Techniques

### 3.1 Introduction

This chapter provides the overall research methodology employed to achieve the thesis objectives outlined in Chapter 2. The detailed experimental setups and analytical techniques used will be describes in this chapter.

### 3.2 Methodology

In this study, a series of experiment procedures had been performed to achieve the research aims. The procedures include the preparation of samples: cellulose, lignin and its derived compounds including sieving (particle size 75-106  $\mu\text{m}$ ), washing, drying and solvent extracted into different fractions. Pyrolysis of different samples (cellulose, lignin-cellulose, lignin and its derived compounds) were then carried out in a pulse-feeding drop-tube/fixed bed quartz reactor for the char production at various temperatures for 15 minutes. The samples and solid products from pyrolysis were analyzed and characterized via a series of analytical instruments, such as elemental analysis, Fourier transform infrared (FTIR) and UV fluorescence spectroscopy, thermogravimetric analysis (TGA),  $^{13}\text{C}$  cross-polarization magic angle spinning nuclear magnetic resonance (CP/MAS NMR) spectroscopy, 2D  $^1\text{H}$ - $^{13}\text{C}$  heteronuclear single-quantum correlation nuclear magnetic resonance (HSQC-NMR) and high performance anion exchange chromatography with pulsed amperometric detection (HPAEC-PAD). All the experiments were performed at least in duplicates in order to ensure the repeatability of the results for this research study. Figure 3.1 illustrated the overall research methodology to achieve the objectives in section 2.7.



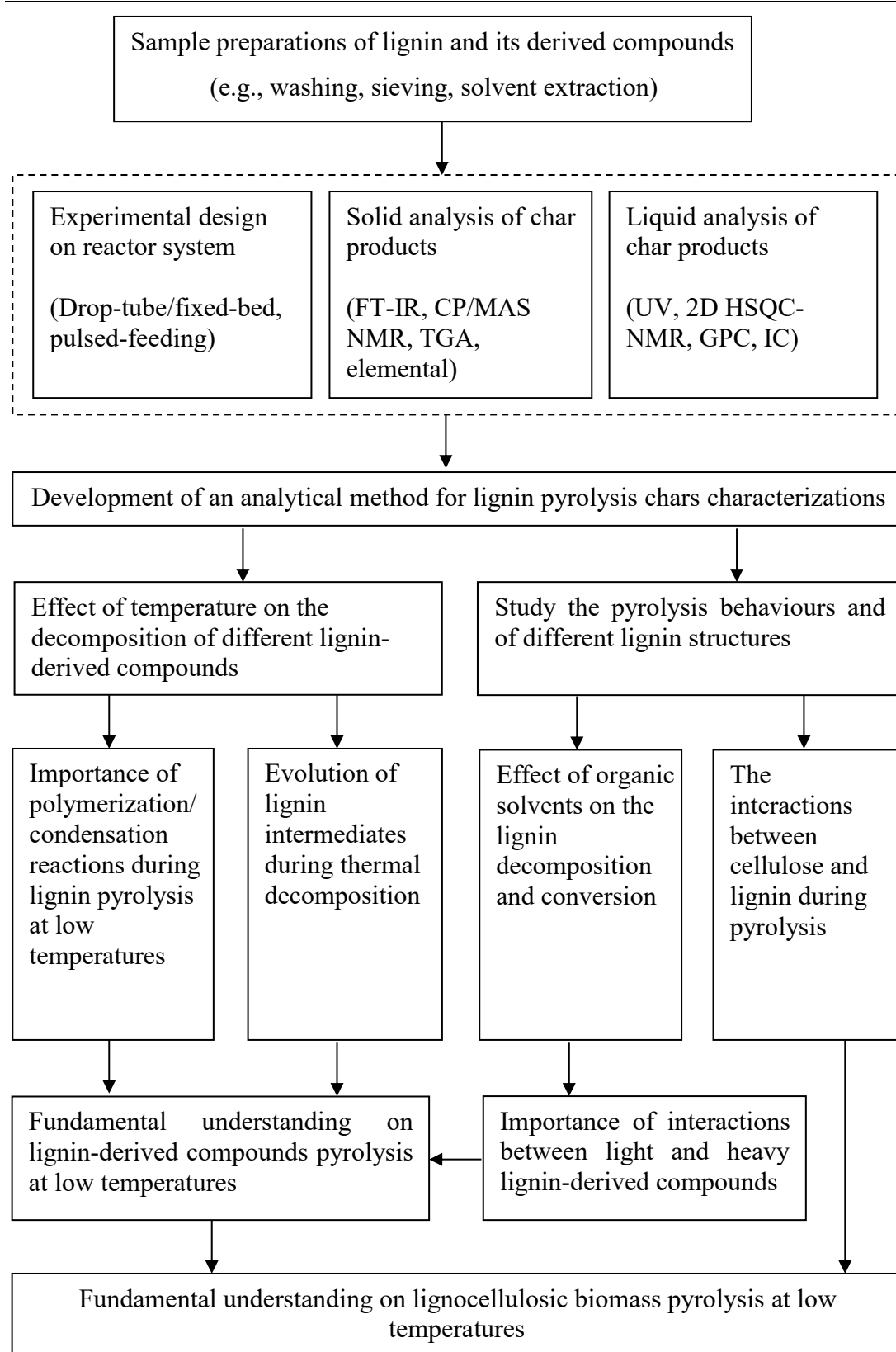


Figure 3.1: Research methodology

### **3.2.1 Thermal Decomposition of Pyrolytic Lignin under Inert Conditions at Low Temperatures**

In this study, the pyrolytic lignin, extracted from bio-oil via cold-water precipitation, consists of mostly lignin-derived oligomers compounds, was used as a model compound of lignin. The pyrolytic lignin sample was pyrolyzed in a drop-tube/fixed bed reactor with a pulse feeder under inert condition from 100–350 °C. The char products were then extracted using CH<sub>2</sub>Cl<sub>2</sub> into light and heavy aromatic oligomers to study the product distributions after the fast pyrolysis. The chars were further characterized via FT-IR, UV fluorescence, <sup>13</sup>C CP/MAS NMR and elemental analysis. Through these analyses, the structural change of the chars was investigated.

### **3.2.2 Structural Changes of Chars Produced from Fast Pyrolysis of Lignin at Low Temperatures**

In order to gain better understanding on the structural changes of the chars produced from lignin fast pyrolysis at 100–300 °C, focusing more on the low-molecular-weight portion (i.e., the THF-soluble portion) of lignin. The solid products produced from the THF-soluble portion and raw lignin were characterized and examined the structural changes of char via analysis including TGA, UV, FT-IR, GPC and <sup>13</sup>C CP/MAS NMR. The transformation of lower molecular weight lignin-derived compounds to a more condensed structure was further investigated in this study.

### **3.2.3 Interactions between Low- and High-molecular-weight Portions of Lignin during Fast Pyrolysis at Low Temperatures**

To investigate the interactions between the lignin-derived compounds during pyrolysis, the raw lignin sample was separated into low-molecular-weight and high-molecular-weight of lignin via THF solvent extraction. The raw lignin and its portions were pyrolyzed individually in a pulse-feeding drop-tube/fixed bed reactor under inert condition from 100–300 °C for comparison and further evaluation. The solid product obtained from pyrolysis of lignin and its derived portions were determined and characterized by a series of analysis such as elemental analysis, FT-IR and UV fluorescence to reveal the interactions occurred between different molecular weight.

### 3.2.4 Effect of Cellulose-lignin Interactions on Char Structural Changes during Fast Pyrolysis at Low Temperatures

In this study, the homogeneous mixture of cellulose and lignin were prepared by wet-impregnation method and pyrolyzed in a pulse-feeding drop-tube/fixed bed reactor at low temperatures from 100–350 °C. To study the influence of interactions between the components on the pyrolysis mechanism, both cellulose and lignin samples were pyrolyzed individually under the same pyrolysis conditions. The solid products from cellulose, lignin and cellulose-lignin pyrolysis were analysed by HPAEC-PAD to determine the changes in glucose amount after the post-hydrolysis. Other analysis also carried out such as FT-IR, UV fluorescence, <sup>13</sup>C CP/MAS NMR and elemental analysis to study the structural changes of char. The interactions between cellulose and lignin during the co-pyrolysis were discussed in detailed in Chapter 7.

## 3.3 Experimental

### 3.3.1 Raw Materials

The bio-oil sample used in this study was produced from fast pyrolysis of pine wood using a fluidised-bed reactor at 500 °C. The THF solvent (HPLC grade, purity ≥ 99.9 %), kraft lignin (alkali) and cellulose (Avicel PH-101) samples used were purchased from Sigma-Aldrich. Before further experiments, all the solid samples were sieved to a size fraction of 75-106 μm to ensure homogenous samples and stored in a freezer at around -10 °C prior to experiment.

### 3.3.2 Samples Preparation

In Chapter 4, the pyrolytic lignin sample was prepared from bio-oil by cold-water extraction [101]. The pyrolytic lignin sample was further separated into the CH<sub>2</sub>Cl<sub>2</sub>-soluble and CH<sub>2</sub>Cl<sub>2</sub>-insoluble fractions via CH<sub>2</sub>Cl<sub>2</sub> extraction. Generally, the CH<sub>2</sub>Cl<sub>2</sub>-soluble and CH<sub>2</sub>Cl<sub>2</sub>-insoluble fractions represent the light and heavy aromatic oligomers in the pyrolytic lignin [188, 189], respectively. The solvent in all samples was removed using rotary evaporator at 40 °C, and the dry residues were stored in a freezer for subsequent experiments.

In Chapter 5, the lignin was sieved to a size fraction of 75-106 μm (referred to as “raw lignin”) for subsequent experiments. Table 3.1 lists the properties of the raw lignin which contains 62.62% of C, 5.51% of H, 0.60% N and 31.23% of O (by

difference) on a dry ash free basis. It is known that THF is a good solvent for lignin dissolution [190]. The raw lignin sample was also extracted by THF to quantify the content of the THF-soluble portion, and the THF-soluble lignin was also recovered for further structural analysis.

Table 3.1: Properties of the lignin used in this study

sample	raw lignin
proximate analysis	
moisture (wt%, ar <sup>a</sup> )	2.9
ash (wt%, db <sup>b</sup> )	3.8
volatile matter (wt%, db <sup>b</sup> )	60.8
fixed carbon (wt%, db <sup>b</sup> )	35.4
ultimate analysis (wt%, daf <sup>c</sup> )	
C	62.62
H	5.51
N	0.60
O <sup>d</sup>	31.27
inorganic species (wt%, db <sup>b</sup> )	
Na	1.142
K	0.200
Mg	0.020
Ca	0.024

<sup>a</sup>ar = air-dried (as received). <sup>b</sup>db = dry basis. <sup>c</sup>daf = dry ash free. <sup>d</sup>By difference.

In Chapter 6, prior to the solvent extraction, the inorganic species in the raw lignin were removed by leaching in ultrapure water under agitation to eliminate their effect on lignin pyrolysis. The leaching of lignin was repeated for several times until no further inorganic species were released. The lignin sample after leaching (hereby referred to as the raw lignin) was then recovered and separated into the THF-soluble and THF-insoluble portions via THF extraction. Table 3.2 lists the properties of the lignin samples used in this study on a dry ash free basis. It is known that the THF-soluble and -insoluble fractions portion represents LMW and HMW portions of lignin (hereby referred to as the LMW and HMW lignin), respectively. After the extraction, the THF in both portions was removed via rotary evaporator under vacuum condition at 40 °C to recover the LMW and HMW lignin samples. Both lignin samples were sieved to a size fraction of 75-106  $\mu\text{m}$  and stored in a freezer for experiment use.

Table 3.2: Properties of the raw, LMW and HMW lignin samples used in this study.

Sample	Moisture (wt%, ar <sup>a</sup> )	Proximate (wt%, db <sup>b</sup> )			Ultimate (wt%, daf <sup>c</sup> )			
		Ash	VM <sup>c</sup>	FC <sup>d</sup>	C	H	N	O <sup>f</sup>
Raw lignin	3.0	0.83	58.8	40.4	63.33	6.08	0.37	30.22
LMW lignin	1.3	0.55	62.5	37.0	65.11	6.14	0.17	28.57
HMW lignin	2.1	1.55	57.0	41.5	62.87	6.05	0.47	30.61

<sup>a</sup>ar = air-dried (as received). <sup>b</sup>db = dry basis. <sup>c</sup>VM = volatile matter. <sup>d</sup>FC = fixed carbon. <sup>e</sup>daf = dry ash free. <sup>f</sup>By difference.

In Chapter 7, both cellulose and lignin samples were leached in ultrapure water under agitation to remove the water-soluble compounds and the inorganic species. The leaching of both samples was repeated for several times until no further water-soluble compounds or inorganic species could be detected in the washing solution. The cellulose-lignin mixture sample (with a mass ratio of 1:1) was then prepared by wet mixing method to obtain a more homogeneous mixture compared to dry mixing. Table 1 lists the properties of the cellulose, lignin and cellulose-lignin mixture samples used in this study. All samples were dried at 40 °C in oven to remove excessive moisture for experiment use.

Table 3.3: Properties of the raw cellulose, lignin and cellulose-lignin mixture used in this study.

Sample	Moisture (wt%, ar <sup>a</sup> )	Proximate (wt%, db <sup>b</sup> )			Ultimate (wt%, daf <sup>c</sup> )			
		Ash	VM <sup>c</sup>	FC <sup>d</sup>	C	H	N	O <sup>f</sup>
Cellulose	2.4	0.02	91.5	8.5	42.7	6.2	-	51.1
Lignin	3.0	0.83	56.3	42.9	63.3	6.1	0.4	30.2
Cellulose-lignin	2.3	0.34	71.9	27.8	52.8	6.1	0.1	40.9

<sup>a</sup>ar = air-dried (as received). <sup>b</sup>db = dry basis. <sup>c</sup>VM = volatile matter. <sup>d</sup>FC = fixed carbon. <sup>e</sup>daf = dry ash free. <sup>f</sup>by difference.

### 3.3.3 Reactor System

A series of pyrolysis experiments were carried out using a drop-tube/fixed-bed quartz reactor system with pulsed-feeding. The reactor configuration was employed to achieve fast heating of pyrolysis on lignin and its derived compounds in this study.

#### Pulsed-feeding System

A schematic of the designed pulsed-feeding system for the reactor is shown in Figure 3.2. The sample was first weighed and loaded into the ball valve of the sample holder.

A stream of argon gas (ultra-high-purity,  $\sim 1.1$  L/min) was purged from the inlet line. After 15 min of purging, the gate valve 1 near the inlet line closed, followed by the opening of gate valve 2 for complete degassing of all tubing lines for 5 min. The degassing line was then blocked until the pressure reached  $\sim 30$  kPa within the system to enable the feeding in one shot into the reactor, with residence time of  $\sim 0.1$  sec. The weight of the sample holder before and after were weighed and recorded to determine the sample added to the system.

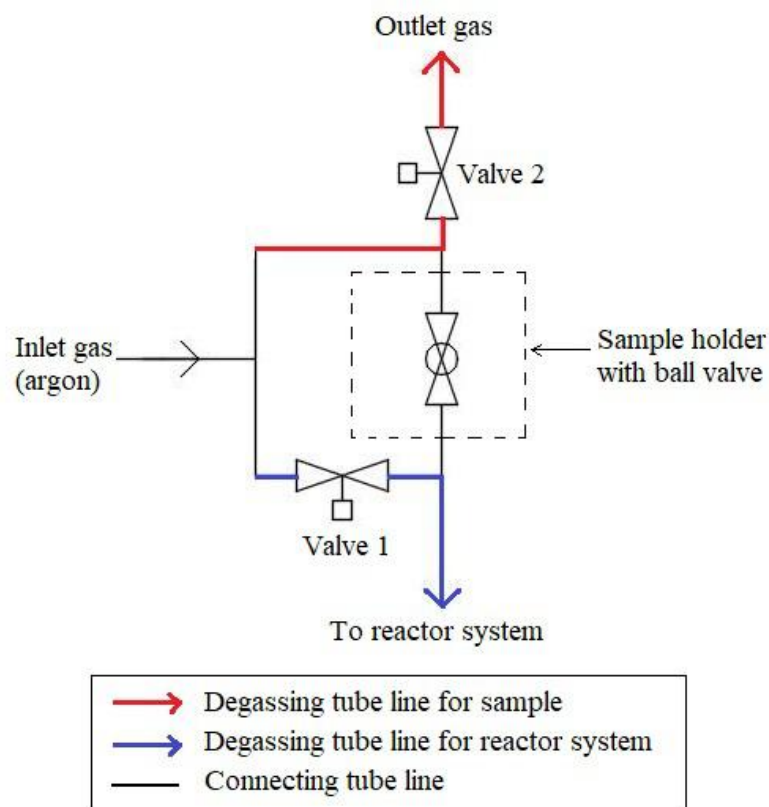


Figure 3.2: Schematic of pulsed-feeding system

### **Drop-tube/Fixed-bed Reactor**

The reactor system consists of a drop-tube reactor connecting with a fixed-bed reactor with internal diameter of  $\sim 30$  mm in quartz material as demonstrated in Figure 3.3. Briefly, the reactor was preheated in a furnace with a stream of argon as carrier gas to provide inert atmosphere. The temperature of the reactor was monitored by mounting a thermocouple just above the quartz frit. Once the reactor reached the desired temperature, approximately 0.4 g of the sample was fed into the reactor in one shot. The particles of the sample experienced fast pyrolysis in the drop-tube reactor section, with the volatiles subsequently passing through (but the

char particles remaining on) the quartz frit of the connected fixed-bed reactor section. The reactor was then held at reaction temperature for 15 min. After the experiment was completed, the reactor was immediately lifted out of furnace and allowed to cool to room temperature, with the inert carrier gas continuously flowing through the reactor. The condensed tar on the reactor outlet was burned off and the char yield was calculated by the weight difference of the reactor before and after the experiment. It should be noted that the char in this study is defined as the remaining solid residue after fast pyrolysis experiment. The above pyrolysis experiments were repeated to obtain the required amount of chars for further analysis.

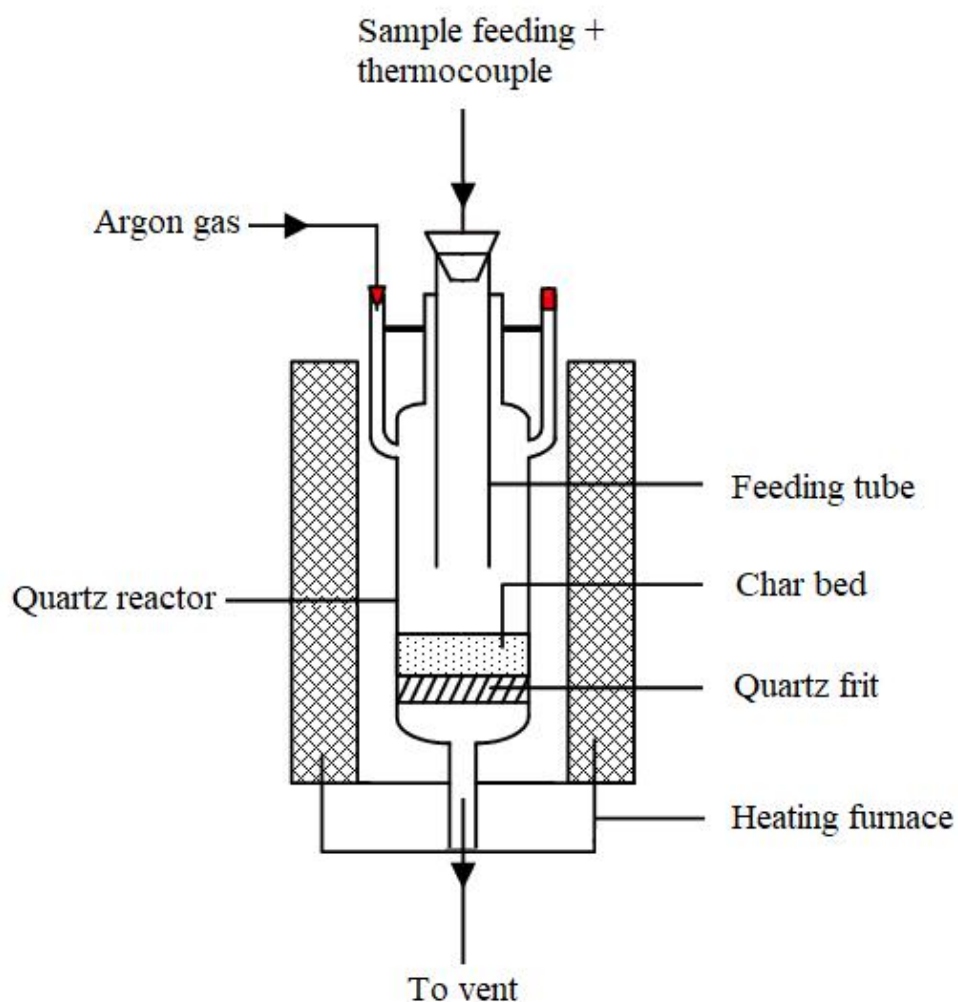


Figure 3.3: Schematic of drop-tube/fixed-bed reactor system for pyrolysis process

### **3.4 Instrument and Analytic Techniques**

#### **3.4.1 Analysis of Solid Products**

##### **3.4.1.1 Proximate and Ultimate Analysis**

The proximate analysis of lignin and its chars were obtained from a thermogravimetric analyser (TGA METTLER) according to method following ASTM E870-82 [191]. The ultimate analysis of all samples was determined using a CHN/O elemental analyser (Perkin Elmer 2400 Series II). The contents of carbon, hydrogen and nitrogen were obtained directly from the analyser, while the oxygen content was calculated by difference on dry ash-free basis (daf).

##### **3.4.1.2 Thermogravimetric (TGA) analysis**

The decomposition curves of the samples were obtained from a thermogravimetric analyser (TGA METTLER). In each experiment, ~10 mg of the sample was loaded in an alumina crucible and analyzed at a heating rate of 5 °C/min from 30 °C to 600 °C and hold for 10 min. A stream of argon gas flowing at 60 mL/min acts as a carrier gas throughout the analysis. The weight loss results were obtained from the TGA while the DTG curve was calculated to study the maximum rate of decomposition.

##### **3.4.1.3 <sup>13</sup>C Cross-Polarization Magic Angle Spinning (CP/MAS) NMR Analysis**

The solid state <sup>13</sup>C CP/MAS NMR spectra of solid samples were acquired to study the changes of carbon structures in the lignin char samples, via a Varian 400 MHz NMR spectrometer equipped with a 4 mm CP/MAS probe. A high power decoupling sequence with a MAS spinning speed of ~7000 Hz was employed to produce high resolution <sup>13</sup>C solid NMR spectra. The rotor loaded with a sample was spun at 25 °C with a 90° pulse, 0.04 s acquisition time and 4 s relaxation delay. Adamantane was used as an external standard for chemical shift calibration. The acquired spectra were processed using the software MestRenova.

##### **3.4.1.4 Fourier Transform Infrared (FT-IR) Spectroscopy**

The functional groups of lignin and char samples were analyzed using a FTIR spectrometer (Bruker IFS 66) with a potassium bromide (KBr) pellet method [192]. Briefly, 2 mg of the sample was ground with 150 mg of KBr for 3 min grinding time and the resulting mixture was pressed into a pellet via a hydraulic pellet press under 7 tons pressure for 5 min. The final pellet sample was obtained at a diameter of 10



mm and 0.43 mm thickness. The FTIR spectra were acquired at a resolution of  $4\text{ cm}^{-1}$ , and 32 scans were taken to produce an absorbance spectrum for each sample. All spectra were corrected for background (e.g., water vapour and  $\text{CO}_2$  contributions) and baseline then normalized to the unit mass (per gram on a dry basis) of the pyrolytic lignin.

It is important to point out that the FT-IR analysis was undertaken under the conditions that the absorbance intensities linearly change with the char concentration in the KBr pellet (see Figures 3.4 and 3.5). Therefore, the absorbance intensities of the char can be directly compared for understanding the changes in functional groups during the pyrolysis.

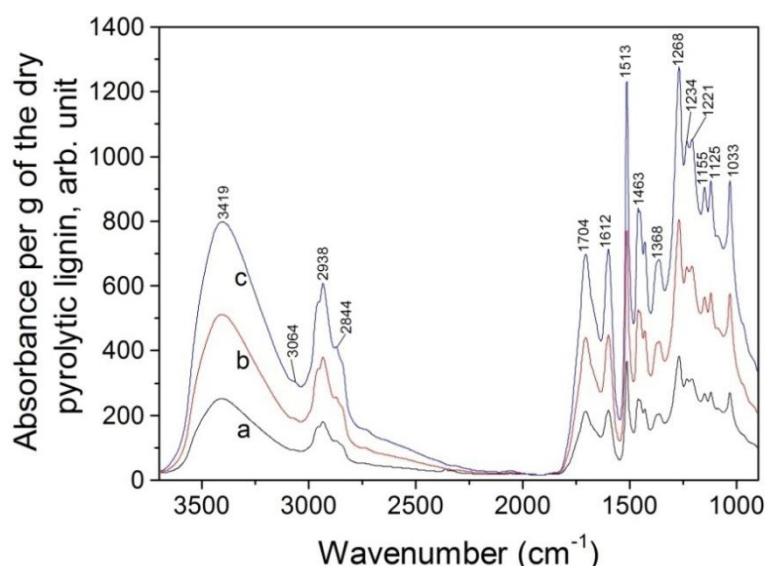


Figure 3.4: Absorbance changes of the functional groups with different samples concentration for FT-IR analysis. (a) 1 mg of pyrolytic lignin ground with 150 mg KBr; (b) 2 mg of pyrolytic lignin ground with 150 mg KBr; (c) 3 mg of pyrolytic lignin ground with 150 mg KBr.

### 3.4.2 Analysis of Liquid Products

#### 3.4.2.1 Two Dimensional (2D) $^1\text{H}$ - $^{13}\text{C}$ Heteronuclear Single Quantum Correlation Nuclear Magnetic Resonance (HSQC NMR)

The lignin and char samples were also analyzed by liquid state 2D HSQC NMR technique via a Bruker Advance IIIHD 500 MHz spectrometer. The frequencies of  $^1\text{H}$  and  $^{13}\text{C}$  for the Bruker AV500 NMR spectrometer are 500.132 and 125.771 MHz, respectively. For each NMR analysis,  $\sim 100$  mg of sample was dissolved in  $\sim 600\ \mu\text{L}$

of dimethyl sulfoxide (DMSO)-d<sub>6</sub>, which acts as a solvent for chemical shift calibration. The solution was filtered before added into the NMR tube for analysis. The HSQC NMR spectrometric data (1024 points for <sup>1</sup>H or 256 points for <sup>13</sup>C) were recorded for at 90° pulse angle, 1.5 s relaxation delay, and 0.08 acquisition time for a total of 48 scans. The acquired spectra were processed using the software MestRenova.

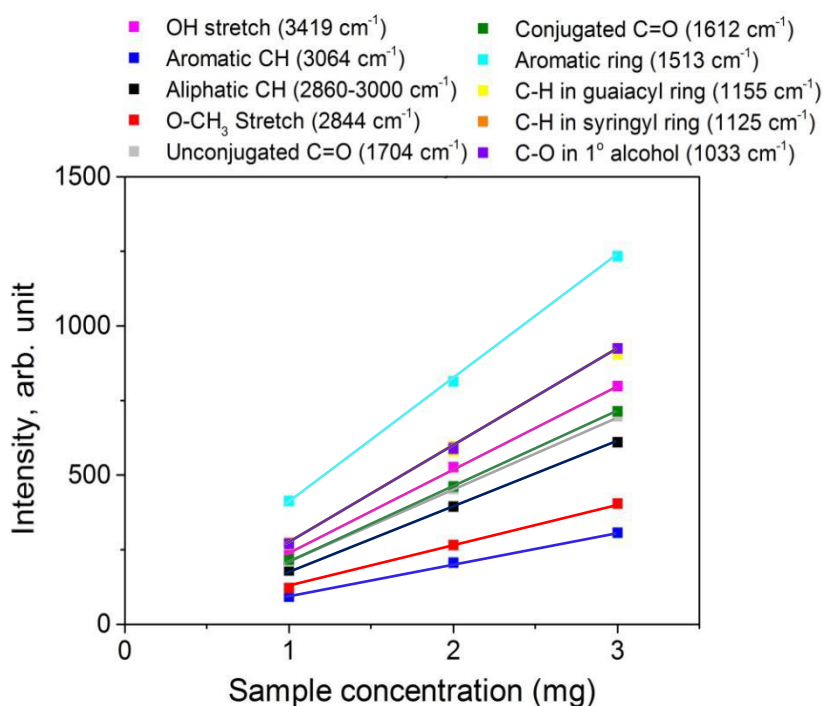


Figure 3.5: Linear relationship of the functional groups with different samples concentration for FT-IR analysis.

### 3.4.2.2 UV Fluorescence Spectroscopy

The UV fluorescence spectra of solid samples were obtained using a fluorescence spectrometer (Perkin-Elmer LS 55), following a method detailed elsewhere [104], to determine the size and concentration of aromatics in the samples. It is noted that the solvent used to dissolve pyrolytic lignin was mixture of chloroform-methanol solvent mixture (4:1 v/v) in Chapter 4, while THF solvent for lignin samples in Chapter 5, 6 and 7, for their best dissolution in different lignin structure. Briefly, the sample was dissolved in solvent, and the dissolved solution after filtration was diluted to a final concentration of 4 ppm for analysis. The spectra were recorded at the excitation wavelength range of 200–550 nm with a constant energy difference of  $-2800\text{ cm}^{-1}$ .

### 3.4.2.3 Gel Permeation Chromatography (GPC)

The molecular weight distributions of the lignin and chars samples were analyzed by gel permeation chromatography (GPC) using a Varian ProStar, equipped with an ultraviolet (UV) detector. A set of two Agilent PLgel 5  $\mu\text{m}$  ( $10^3$  A,  $300 \times 7.5$  mm) columns was used in this GPC analysis, following a method detailed elsewhere [193]. Briefly, THF solvent was used as a mobile phase at a flowing rate of 1.0 mL/min. All the samples were diluted to 1000 ppm in THF solvent and then filtered with 0.45  $\mu\text{m}$  polyvinylidene fluoride (PVDF) syringe filter before the analysis. Polystyrenes with molecular weight range from 800 to 35000 Da were used as standards for the calibration curve. In order to investigate the structural difference in solvent-extracted lignin fraction for Chapter 5 and 6, acetylation of lignin was carried out by dissolving the lignin in acetic anhydride/pyridine (1:1 v/v) mixture at 70 °C for 6 hours. The residue from the acetylation process was solvent evaporated via rotary evaporator.

### 3.4.2.4 High-Performance Anion Exchange Chromatography with Pulsed Amperometric Detection (HPAEC-PAD)

Before the sugar analysis, the samples were first subjected to acid hydrolysis experiments to determine total sugar content (i.e., glucose monomer), following the NREL method [194]. In brief, ~100 mg of sample was added into a pressure tube with 72% sulfuric acid in a water bath at 30 °C for 1 hour. Before the solution was treated in autoclave at 121 °C for 1 hour, the final concentration of acid was altered to 4% by addition of ultrapure water. The post hydrolysis was accompanied by a glucose standard in the same batch with samples for the sugar recovery calculation. After the post hydrolysis, the contents with sugar monomers were diluted and quantified using a HPAEC-PAD via a Dionex ICS-3000 ion chromatography (IC) system equipped with CarboPac PA20 analytical and guard columns. Post-column addition of NaOH was introduced via an HPLC pump for adequate linear detector response. A special gradient program developed in our previous work [195] was used for achieving a good separation of the sugars of interest as summarized in Table 3.4. The eluent A, B and C used in the analysis were 0.3 M NaAc in 0.1 M NaOH, 0.3 M NaOH and water respectively, with a total flow rate of 0.5 mL/min. To validate the results obtained from HPAEC-PAD, the calibration curve for the glucose standard based on peak height is shown in Figure 3.6.

Table 3.4: Gradient program for sugar analysis in HPAEC-PAD

Time (min)	Eluent A (%)	Eluent B (%)	Eluent C (%)
0.0	0	0	100
20.0	0	0	100
20.5	100	0	0
23.0	100	0	0
23.5	0	100	0
29.5	0	100	0
30.0	0	0	100
40.0	0	0	100

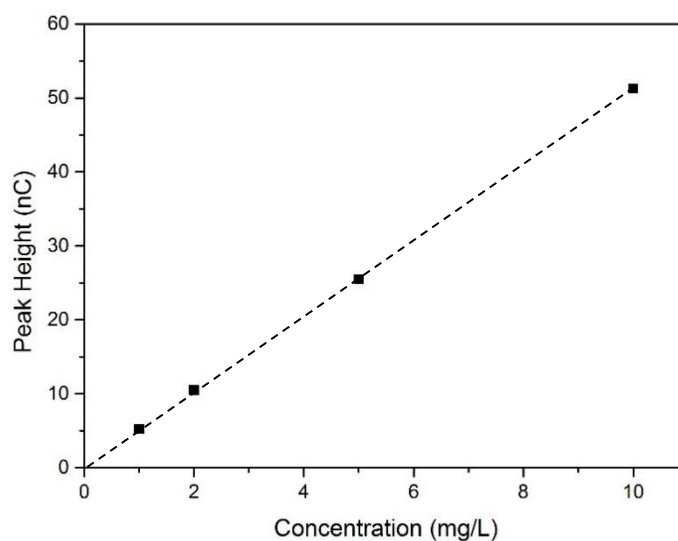


Figure 3.6: Calibration curve for glucose standard by HPAEC-PAD.

### 3.4.3 Inorganic Species Analysis

The content of AAEM species in the lignin and char solid samples such as Na, K, Mg and Ca were analyzed and quantified following a method detailed elsewhere [196]. In brief, ~10 mg of sample was loaded in a platinum crucible, and then undergo ashing heating program as shown in Figure 3.7. The ash residue was digested with mixture of concentrated acids of HF and HNO<sub>3</sub> for 24 hours. After the acid solution was evaporated, the leftover residue was dissolved in 0.02 M methanesulfonic acid (MSA). To quantify the AAEM species, the solution was then injected into an ion chromatography (Dionex ICS-3000) that equipped with IonPac CS12A 4x250 mm column and IonPac CS12AG 4x50 mm guard column.

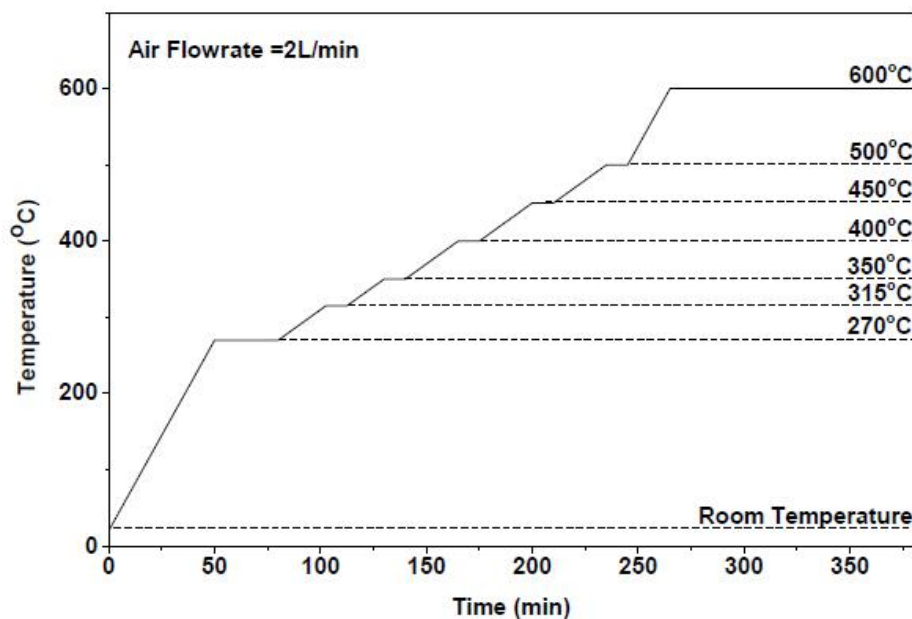


Figure 3.7: Ashing temperature program for AAEM species analysis

### 3.5 Summary

All samples of lignin and its derived components were extracted and prepared in uniform size fraction of 75-106  $\mu\text{m}$  for experiments use. The lignin sample was pre-treated and extracted into different portions for further investigation on the pyrolysis mechanism, particularly at low temperatures. The lignin pyrolysis experiments were conducted in a drop-tube/fixed-bed reactor with pulsed-feeding system to achieve fast heating reaction with minimum residence time. The solid product was then collected and subjected to a series of analysis to examine their structural changes. The analytical techniques including: elemental, FT-IR, UV fluorescence, solid and liquid state NMR for char structural change analysis; TGA for decomposition behaviour analysis; GPC for molecular weight distributions; HPAEC-PAD for glucose monomers quantification; and AAEM species quantification.

---

## Chapter 4 Thermal Decomposition of Pyrolytic Lignin under Inert Conditions at Low Temperatures

### 4.1 Introduction

Bio-oil from biomass fast pyrolysis is considered as an important feedstock that may be further refined into liquid transportation fuels in existing petroleum refineries [8, 14]. However, bio-oil is of low quality (e.g., high acidity, low heating value, high viscosity, poor stability, and immiscibility with petroleum fuels) and needs to be upgraded before it can be processed in existing petroleum refinery infrastructure [14, 102, 111, 113]. There may be various technologies for bio-oil upgrading, such as catalytic hydrotreating, steam reforming, cracking, and esterification [97, 115, 116, 197-200]. One of the key problems associated with bio-oil upgrading is related to the poor thermal stability of bio-oil [8]. The reactive functional groups in bio-oil, i.e., organic acids, carbonyl groups, sugars and aldehydes [188], have the tendency for decomposition, polymerization and/or condensation upon heating, resulting in coke formation during upgrading [106, 201, 202]. Coke formation causes significant operation problems (e.g., catalyst deactivation and reactor plugging) during bio-oil upgrading [203, 204].

Bio-oil has very complex chemical composition and consists of compounds with a wide range of different functional groups and molecular weights [72]. Due to the large molecular weight, the lignin-derived oligomers (so-called pyrolytic lignin) in bio-oil can easily polymerize upon heating, contributing significantly to coke formation [105, 107, 201]. Pyrolytic lignin can be isolated from bio-oil as the water-insoluble fraction via cold-water extraction [73, 205]. Previous studies were devoted to characterize the physical and chemical properties of pyrolytic lignin [72-74, 192, 205]. However, the knowledge on the thermal decomposition of pyrolytic lignin is still scarce, especially the fundamental mechanisms responsible for coke formation. A previous TG-FTIR study [206] reported that pyrolytic lignin is thermally unstable and can even start to decompose at temperatures as low as 160 °C. Therefore, it is of critical importance to understand the fundamental reaction mechanisms during the

thermal decomposition of pyrolytic lignin at low temperatures. Consequently, this is the main objective of this study that carries out a systematic investigation into the formation and characteristics of chars during thermal decomposition of the pyrolytic lignin at 100–350 °C.

#### 4.2 Yields and Elemental Compositions of Chars Produced from Thermal Decomposition of the Pyrolytic Lignin

Figure 4.1 shows that char yield from thermal decomposition of the pyrolytic lignin decreases with increasing pyrolysis temperature, from ~82% at 100 °C to ~23% at 350 °C. It is interesting to note that a large weight loss even takes place at a temperature as low as 100 °C. This can be attributed to the presence of some light aromatic compounds in the pyrolytic lignin as these light aromatic compounds can easily evaporate at low temperatures [206]. The pyrolytic lignin and char samples were further extracted with CH<sub>2</sub>Cl<sub>2</sub> to obtain the distribution of the CH<sub>2</sub>Cl<sub>2</sub>-soluble and CH<sub>2</sub>Cl<sub>2</sub>-insoluble fractions in the char samples (see Figure 4.1). It has been proven that the CH<sub>2</sub>Cl<sub>2</sub>-soluble fraction of the pyrolytic lignin mainly consists of low molar mass aromatic oligomers, while the CH<sub>2</sub>Cl<sub>2</sub>-insoluble fraction is composed of relatively high molar mass aromatic oligomers [188, 189]. The pyrolytic lignin contains ~70% of the CH<sub>2</sub>Cl<sub>2</sub>-soluble fraction, indicating that the pyrolytic lignin mainly consists of light aromatic oligomers. During thermal decomposition, an increase in pyrolysis temperature leads to a substantial reduction in the CH<sub>2</sub>Cl<sub>2</sub>-soluble fraction remained in the pyrolytic lignin char, from ~50% at 100 °C to ~2% at 350 °C. In contrast, there is only a small reduction in the CH<sub>2</sub>Cl<sub>2</sub>-insoluble fraction remained in the char, from ~30% at 100 °C to ~21% at 350 °C. It seems that majority of the weight loss during thermal decomposition of the pyrolytic lignin is due to the release of light aromatic oligomers that are less thermally stable. As a result, the structure of the pyrolytic lignin char becomes more condensed as temperature increases. Table 4.1 further lists the elemental compositions of the pyrolytic lignin and its derived chars. It can be seen that as the temperature increases from 100 to 350 °C, the carbon content in the char slightly increases from ~66.1 to ~68.5%, together with a significant decrease in hydrogen content from ~6.4 to ~4.6%. This is translated into a significant reduction in the atomic H/C ratio progressively from 1.17 at 100 °C to 0.82 at 350 °C, in contrast to only a slight reduction in the atomic O/C

ratio from 0.31 at 100 °C to 0.29 at 350 °C. Therefore, the continuous decrease in the atomic H/C ratio clearly indicates that the char structure becomes more condensed as temperature increases.

Table 4.1: Properties of the pyrolytic lignin and its chars prepared at various temperatures.

	Pyrolytic lignin	Chars prepared at various temperatures					
		100°C	150°C	200°C	250°C	300°C	350°C
C (%)	66.07	66.16	65.66	66.52	67.05	68.44	68.52
H (%)	6.41	6.41	6.01	5.64	5.54	5.25	4.63
N (%)	0.1	0.18	0.16	0.18	0.17	0.18	0.20
O (%)	27.32	27.26	28.17	27.66	27.24	26.53	26.65
atomic H/C	1.19	1.17	1.10	1.02	0.99	0.93	0.82
atomic O/C	0.31	0.31	0.32	0.31	0.30	0.29	0.29

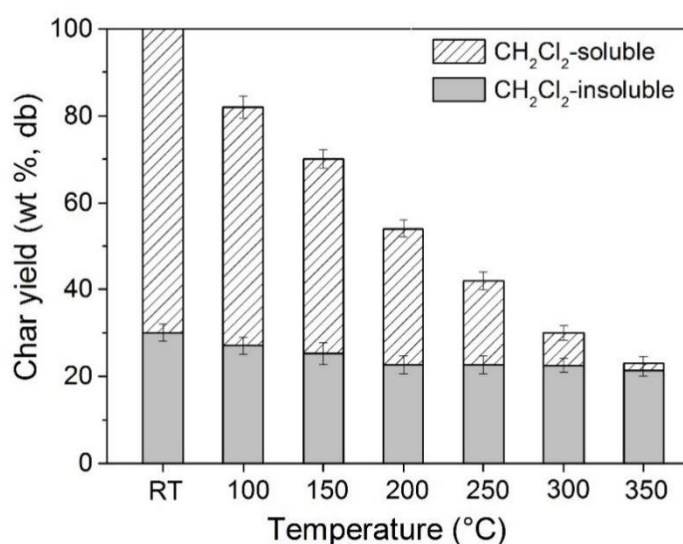


Figure 4.1: Char yield from thermal decomposition of the pyrolytic lignin at 100–350 °C and the distribution of the CH<sub>2</sub>Cl<sub>2</sub>-soluble and CH<sub>2</sub>Cl<sub>2</sub>-insoluble fractions in the char samples.

### 4.3 Char Yields of Thermal Decomposition of the Light and Heavy Aromatic Oligomers in the Pyrolytic Lignin

To gain insights into the thermal decomposition of the light and heavy aromatic oligomers in the pyrolytic lignin, the CH<sub>2</sub>Cl<sub>2</sub>-soluble and CH<sub>2</sub>Cl<sub>2</sub>-insoluble fractions were separated from the pyrolytic lignin. Each individual fraction was then subject to thermal decomposition experiments under similar conditions. Figure 4.2 presents the



data on char yields from thermal decomposition of the  $\text{CH}_2\text{Cl}_2$ -soluble and the  $\text{CH}_2\text{Cl}_2$ -insoluble fractions at different temperatures, along with those from the pyrolytic lignin. As temperature increases, there is a significant reduction in char yield for the  $\text{CH}_2\text{Cl}_2$ -soluble fraction from  $\sim 64\%$  at  $100\text{ }^\circ\text{C}$  to  $\sim 7\%$  at  $350\text{ }^\circ\text{C}$ . It is noted that over 35% of light aromatic oligomers are lost even at  $100\text{ }^\circ\text{C}$ . This can be mainly attributed to the evaporation of volatile compounds in the  $\text{CH}_2\text{Cl}_2$ -soluble fraction. Surprisingly, there is also a significant reduction in char yield for the  $\text{CH}_2\text{Cl}_2$ -insoluble fraction from  $\sim 97\%$  at  $100\text{ }^\circ\text{C}$  to  $\sim 34\%$  at  $350\text{ }^\circ\text{C}$ . There is little weight loss during thermal decomposition of heavy aromatic oligomers at  $100\text{ }^\circ\text{C}$  but the weight loss becomes appreciable ( $\sim 10\%$ ) at  $150\text{ }^\circ\text{C}$ . The results clearly demonstrate that both the light and heavy aromatic oligomers in the pyrolytic lignin experience substantial weight loss during thermal decomposition at  $100\text{--}350\text{ }^\circ\text{C}$ , although the light aromatic oligomers are less thermally stable. A larger weight loss for the light aromatic oligomers is expected because this fraction can easily evaporate and/or decompose as volatiles at lower temperatures. Although the weight loss for the heavy aromatic oligomers is less but it is still over 65% at  $350\text{ }^\circ\text{C}$ . Clearly, significant decomposition reactions take place during the pyrolysis of the heavy aromatic oligomers at elevated temperatures (e.g.,  $350\text{ }^\circ\text{C}$ ).

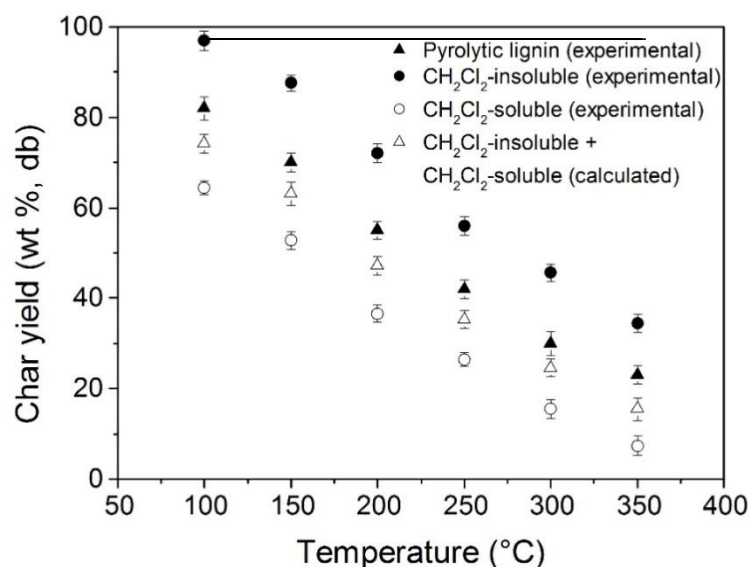


Figure 4.2: Char yields from thermal decomposition of the pyrolytic lignin and its  $\text{CH}_2\text{Cl}_2$ -soluble and  $\text{CH}_2\text{Cl}_2$ -insoluble fractions at  $100\text{--}350\text{ }^\circ\text{C}$

Figure 4.2 also presents the char yields of the pyrolytic lignin at different temperatures, along with those calculated based on the initial percentages of the  $\text{CH}_2\text{Cl}_2$ -soluble and  $\text{CH}_2\text{Cl}_2$ -insoluble fractions in the pyrolytic lignin, assuming that the thermal decomposition of the individual fractions proceed independently. Figure 4.2 shows an increase of ~8% in char yield for the experimental results in comparison to the calculated results. The results clearly demonstrate that there are strong interactions between the light and heavy aromatic oligomers during thermal decomposition of the pyrolytic lignin. It appears that the polymerization reactions of light aromatic oligomers into heavy aromatic oligomers are enhanced during thermal decomposition of the pyrolytic lignin.

#### 4.4 Structural Changes of Chars Produced from Thermal Decomposition of the Pyrolytic Lignin

##### 4.4.1 FT-IR Analysis

Figure 4.3a presents the FT-IR spectra of the pyrolytic lignin and char samples, with the absorbance intensities expressed on a basis of per gram of the pyrolytic lignin. The assignments of FT-IR peaks to functional groups are based on those reported in the literature [35, 192] and summarized in Table 4.2. It is important to note that the FT-IR analysis was undertaken under the conditions that the absorbance intensities linearly change with the char concentration in the KBr pellet. Therefore, the absorbance intensities in Figure 4.3a can be directly compared for understanding the changes in functional groups during thermal decomposition of the pyrolytic lignin. Furthermore, the reduction in each functional group in char is also calculated as the percentages of its initial intensity in the pyrolytic lignin and the results are presented in Figure 4.3b. It can be clearly seen in Figure 4.3a and b that the absorbance intensities of all functional groups decrease with increasing the temperature. The –OH stretch at  $3419\text{ cm}^{-1}$  decreases rapidly with increasing temperature, indicating the removal of hydroxyl groups. This is not surprising because it was reported that the predominant reactions during the pyrolysis of the pyrolytic lignin at 200–450 °C are the removal of hydroxyl groups in alkyl side chains and the release of some phenolic monomers due to the unstable ether linkages (e.g.,  $\alpha$ -O-4,  $\beta$ -1 and  $\beta$ -O-4) [35]. The removal of aliphatic C–H can be seen from the decreased intensity of band at region  $2860\text{--}3000\text{ cm}^{-1}$ , mostly due to the release of instable propyl chains in the pyrolytic

lignin. At 200 °C, the aliphatic  $-\text{CH}_2\text{OH}$  groups of the alkyl side chains in the pyrolytic lignin tend to release as volatile products [172], probably via C–C fragmentation of phenylpropane chains [207]. From the spectra, the aromatic C–H stretch at  $3064\text{ cm}^{-1}$  and C–H stretch of methoxyl group at  $2844\text{ cm}^{-1}$  start to reduce at 150 °C.

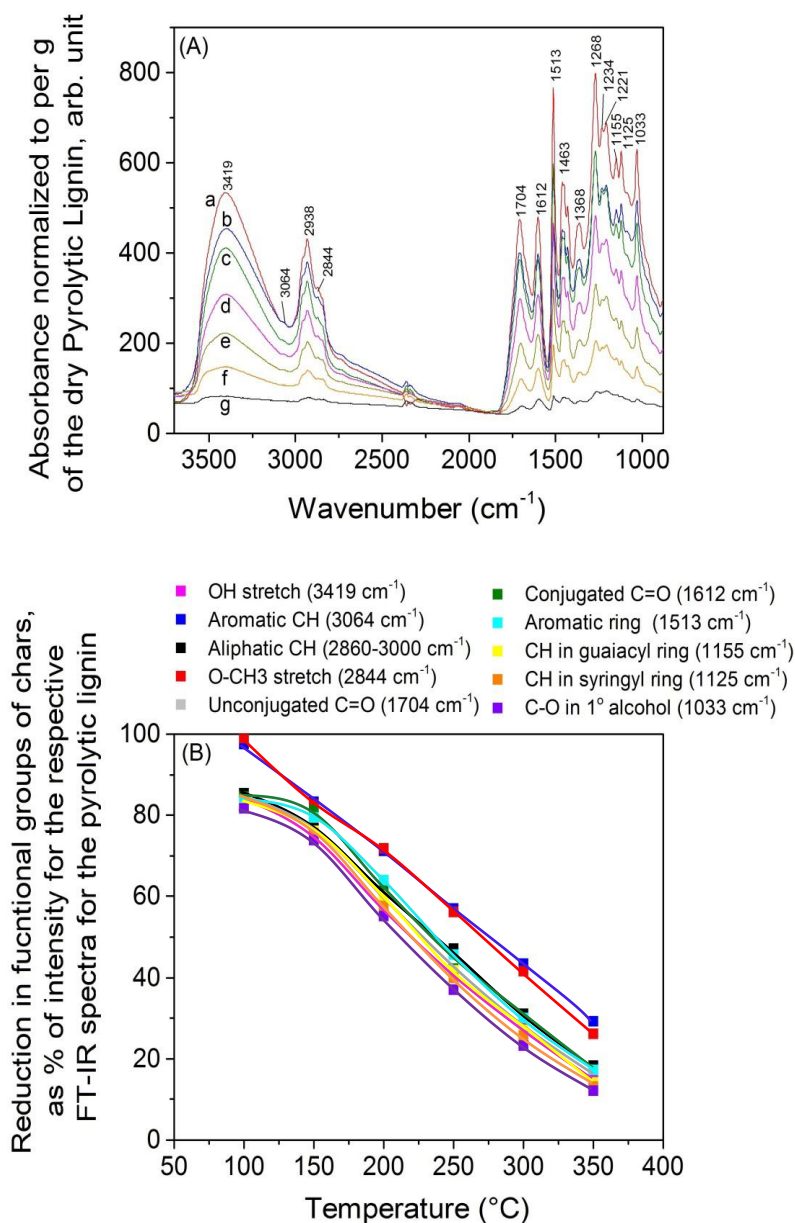


Figure 4.3: Panel (A) FT-IR spectra of the pyrolytic lignin and its chars prepared at 100–350 °C; legends: (a) pyrolytic lignin; (b) char prepared at 100 °C; (c) char prepared at 150 °C; (d) char prepared at 200 °C; (e) char prepared at 250 °C; (f) char prepared at 300 °C; and (g) char prepared at 350 °C. Panel (B) % Functional groups

in chars prepared at 100–350 °C, expressed as % the intensity of respective FT-IR spectra for the pyrolytic lignin.

It is known that the most common bond linkages in the pyrolytic lignin such as  $\alpha$ -O-4,  $\beta$ -1 and  $\beta$ -O-4 can be easily broken at low temperatures of  $\sim$ 200 °C [171]. The bond cleavage between the monomers in the pyrolytic lignin leads to the formation of volatile phenolic monomers or oligomers that linked to a methoxy substituents or alkyl chain with 2–3 carbon structures [153]. The intensities of unconjugated C=O stretching at 1704  $\text{cm}^{-1}$  and conjugated C=O with aromatic ring at 1612  $\text{cm}^{-1}$ , also decrease with increasing temperature. The existence of unconjugated C=O bands in the pyrolytic lignin can be attributed to the breakage of ether bonds that are known to be abundant in the pyrolytic lignin structure [181], suggesting the elimination of the carbonyl group or carboxylic acids in the pyrolytic lignin structure. It is also observed that at higher temperatures (i.e., 350 °C), some of the conjugated C=O bands still remains while unconjugated C=O bands almost disappear in the char. This can be due to the fact that the conjugated C=O groups with aromatic structures have better thermal stability than the unconjugated C=O groups [35]. The decrease of main aromatic ring stretches intensity at 1513  $\text{cm}^{-1}$  is due to the release of phenolic compounds. The bands at 1155  $\text{cm}^{-1}$  and 1125  $\text{cm}^{-1}$  indicate the presence of guaiacyl and syringyl units in the pyrolytic lignin. The aromatic structures in the pyrolytic lignin usually consist of the phenols such as guaiacol and syringol [35], and can be easily released as volatiles at above 160 °C [206]. The peak at 1033  $\text{cm}^{-1}$  shows the presence of hydroxyl groups of primary alcohol. A decrease in its intensity is attributed to the dehydration of terminal hydroxyl groups in propane side chains of the pyrolytic lignin structures. It is also noted that the band from region 1000 to 1100  $\text{cm}^{-1}$  indicates the presence of sugars in the samples [37]. This is consistent with the findings from our previous work proving that the sugar structure bonded to the water-insoluble fraction of pyrolysis oil [208].

#### 4.4.2 $^{13}\text{C}$ CP/MAS NMR Analysis

FT-IR is unable to detect larger aromatic ring systems, which may be present in the chars especially those prepared at temperatures above 300 °C while the changes in these carbon structures are important for coke formation during thermal

decomposition. Therefore,  $^{13}\text{C}$  CP/MAS NMR spectra were further acquired for the pyrolytic lignin and the char samples and the results are presented in Figure 4.4. The typical carbon structures are assigned based on literatures [72, 209, 210]. The signals at 10–50 ppm are assigned to aliphatic carbons including lignin propyl side chains. The signals between 50–90 ppm correspond to oxygenated alkyl carbons, such as methoxy groups, alkyl-O-aryl ether (i.e.,  $\beta$ -O-4,  $\alpha$ -O-4) structures. The region between 102–155 ppm indicates the presence of aromatics structures, such as syringyl and guaiacyl units. The signals at 160–200 ppm correspond to carbonyl groups. The spectra presented in Figure 4.4 clearly show that the char contains more structures of aromatic characteristics as temperature increases.

Table 4.2: Peak assignments for FT-IR spectra [35, 192]

Wavenumbers ( $\text{cm}^{-1}$ )	Assignments
3419	O–H stretch
3064	Aromatic C–H stretch
2860-3000	Aliphatic C–H stretch
2844	$\text{CH}_3$ stretch of methoxyl group
1704	C=O stretch unconjugated to ketones, carbonyl and ester groups
1612	C=O stretch conjugated to aromatic ring
1513	Aromatic ring stretch
1463	$\text{CH}_3$ , $\text{CH}_2$ deformations
1368	Syringyl ring breathing with C–O stretching
1268	Guaiacyl ring breathing with C–O stretching
1221-1234	C–C plus C–O
1155	Aromatic C–H deformations of guaiacyl ring
1125	Aromatic C–H deformations of syringyl ring
1033	C–O stretch in primary alcohol

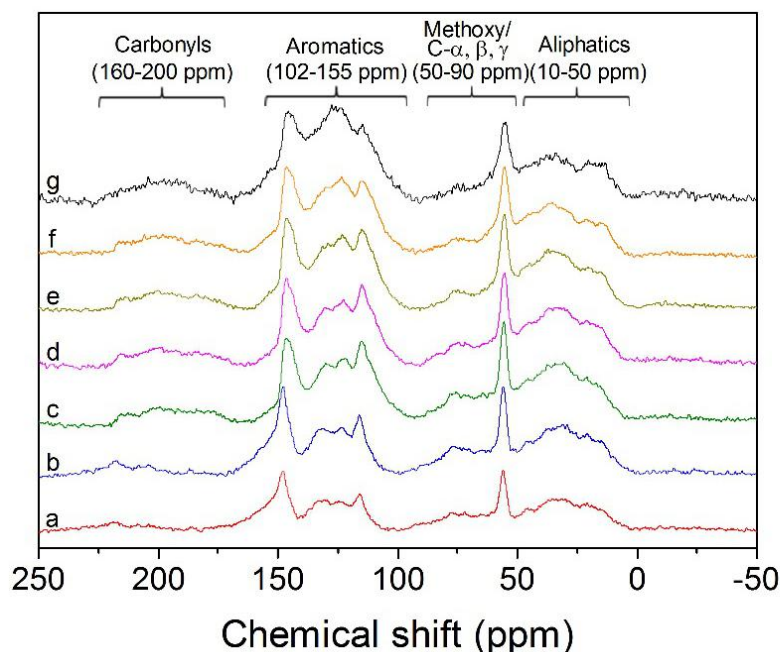


Figure 4.4: Solid  $^{13}\text{C}$  CP/MAS NMR spectra of the pyrolytic lignin and its chars prepared at 100–350 °C. Legends: (a) pyrolytic lignin; (b) char prepared at 100 °C; (c) char prepared at 150 °C; (d) char prepared at 200 °C; (e) char prepared at 250 °C; (f) char prepared at 300 °C; and (g) char prepared at 350 °C.

To obtain some semi-quantitative changes of different carbon structures, the contribution of each carbon structure was calculated based on the integrated intensity of each carbon structure normalized to the total intensity of the sample. The results are listed in Table 4.3 which summarizes the contribution of each carbon structure for the pyrolytic lignin and char samples at 100–350 °C. The aromaticity was also calculated based on the ratio of aromatic carbon to the total aliphatic and aromatic carbons in the sample (following a definition previously [211]). The aliphatic carbons at 10–50 ppm and oxygenated aliphatic carbons including methoxyl groups at 50–90 ppm decrease gradually with increasing temperature, indicating the increased decomposition of propyl side chains and methoxyl substituents of aromatic ring due to the breakage of less stable ether bonds. The aromatic carbons at 102–155 ppm increase at temperatures above 250 °C, leading to the increase in the aromaticity of char from ~61% for the pyrolytic lignin to ~72% for the char at 350 °C. This indicates that the char structures at high temperatures become more condensed, in consistent with the decreased H/C ratio at increased temperatures.

### 4.4.3 UV Fluorescence Analysis

The pyrolytic lignin and char samples were also extracted using chloroform-methanol solvent mixture (4:1 v/v), which is known to be a good candidate for dissolution of pyrolytic lignin [212, 213]. It is noted that while ~85% of pyrolytic lignin is soluble in the solvent, the solubility of char decreases with pyrolysis temperature, from ~80% for the char prepared at 100 °C, to ~70% for the char prepared at 200 °C then to only ~30% for the char prepared at 350 °C. The solutions were then characterized via UV fluorescence analysis, with the results presented in Figure 4.5. To enable comparison among the samples, the UV fluorescence intensities were normalized to the mass of the pyrolytic lignin (i.e., on a basis of per gram of the pyrolytic lignin). The wavelength of the UV spectrum indicates the size of the fused rings in the aromatic structures, e.g., wavelength < 290 nm represents mono-ring, 290–340 nm represents 2–3 fused rings and 340–390 nm represents 3–5 fused rings [214]. The results in Figure 4.5 show that pyrolytic lignin mainly contains aromatic structures with 2–5 fused rings (i.e., with wavelength of 290–390 nm) but little amount of mono-ring aromatics. For the char sample at 100 °C, there are only slight changes in the fluorescence intensity. A further increase in temperature leads to the gradual decrease in the UV fluorescence intensity for aromatic structures of different fused ring sizes. Small aromatic rings (< 290 nm for mono-ring), which are mostly phenolic monomers, release easily at 150 °C and almost disappear at temperatures above 250 °C. There is also a significant reduction in the UV fluorescence intensity for the aromatic structures with 2–3 fused rings at 150 °C. It is also evident that the peak shifts towards larger aromatic ring structures (with 3–5 fused rings) as temperature increases, especially at temperatures above 250 °C. At 350 °C, almost all the aromatic structures with 2–5 fused rings are released as volatiles or polymerized into char.

Table 4.3: Relative content analysis for <sup>13</sup>C CP/MAS NMR spectra

	Pyrolytic lignin	Chars prepared at various temperatures					
		100°C	150°C	200°C	250°C	300°C	350°C
Aliphatic (%)	28.05	28.02	27.68	27.22	26.92	25.69	20.69
Methoxyl (%)	20.06	20.84	20.11	19.02	17.42	16.09	14.96
Aromatic (%)	44.40	43.84	44.16	44.32	46.04	48.11	53.68
Carbonyl (%)	7.49	7.30	8.04	9.43	9.62	10.12	10.66
Aromaticity (%)	61.28	61.01	61.47	61.95	63.10	65.19	72.18

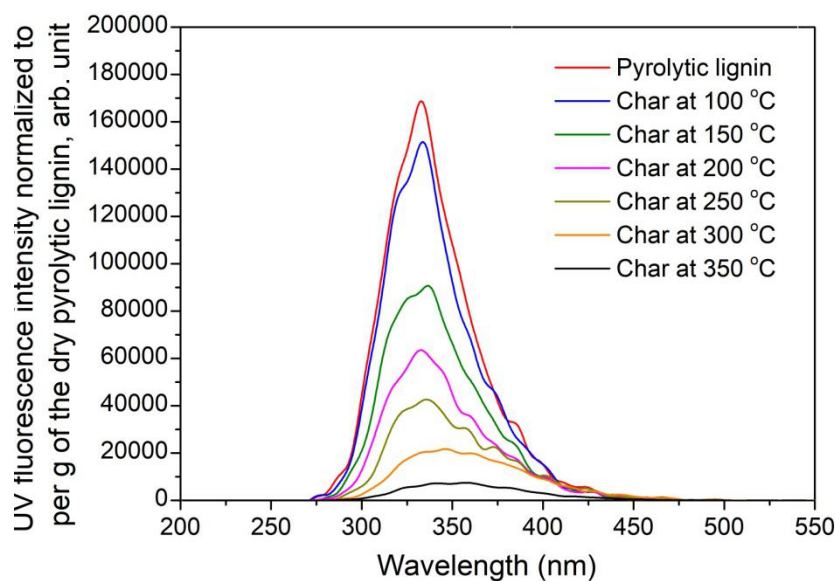


Figure 4.5: UV Fluorescence spectra of the solutions obtained from the extraction of pyrolytic lignin and its chars prepared at 100–350 °C using chloroform-methanol solvent mixture (4:1 v/v)

#### 4.5 Discussions on Thermal Decomposition Mechanism of Pyrolytic Lignin

The above results on the yields and structural changes in chars during thermal decomposition of pyrolytic lignin provide some new insights into reaction mechanisms of pyrolytic lignin at 100–350 °C. First, the thermal decomposition of the pyrolytic lignin starts with the light aromatic oligomers at a temperature as low as 100 °C, while the heavy aromatic oligomers start to decompose at a higher temperature of ~150 °C. The chars at temperatures above > 300 °C consist of mainly heavy aromatic oligomers that are insoluble in  $\text{CH}_2\text{Cl}_2$ . Second, chars prepared at elevated temperatures (e.g., 350 °C) are primarily formed from the heavy fraction of pyrolytic lignin, due to the considerably higher char yield (i.e., ~34% at 350 °C) of the  $\text{CH}_2\text{Cl}_2$ -insoluble fraction compared to that (~7% at 350 °C) of the  $\text{CH}_2\text{Cl}_2$ -soluble fraction. Interactions take place between the light and heavy fractions during thermal decomposition, leading to the formation of more char. This is evident by the fact that the char yields of the pyrolytic lignin at different temperatures are ~8% higher than those calculated based on the percentages of the  $\text{CH}_2\text{Cl}_2$ -soluble and  $\text{CH}_2\text{Cl}_2$ -insoluble fractions in the pyrolytic lignin. The results indicate that the presence of heavy aromatic oligomers suppress the release of light aromatic species, promoting the polymerization reactions to produce more char. Third, the thermal



decomposition of the pyrolytic lignin leads to the reductions in various functional groups (i.e., hydroxyl, aliphatic C–H, carbonyl, guaiacyl and syringyl groups) at 100 °C, while the aromatic C–H and the methoxyl groups start to decrease at 150 °C. Such functional groups continue to reduce with increasing temperature. In contrast, the contribution of aromatic structure increases as temperature increases as a result of enhanced polymerization reactions. The elemental composition and NMR results suggest that such polymerization reactions become important at temperatures > 250 °C, leading to an increase in char aromaticity. Therefore, the bio-oil upgrading temperature should be lower than 250 °C in order to suppress the coke formation.

#### **4.6 Conclusions**

The study reports the formation and characteristics of chars produced from the thermal decomposition of pyrolytic lignin under inert conditions at 100–350 °C. The results show that thermal decomposition of the pyrolytic lignin starts from the light aromatic oligomers (i.e., the CH<sub>2</sub>Cl<sub>2</sub>-soluble fraction) in the pyrolytic lignin at a temperature as low as 100 °C, while the heavy aromatic oligomers (i.e., the CH<sub>2</sub>Cl<sub>2</sub>-insoluble fraction) is more stable and starts to decompose at ~150 °C. The chars prepared at high temperatures (e.g., 350 °C) are mainly produced from the heavy aromatic oligomers, due to the low char yields of the light aromatic oligomers at high temperatures. Strong interactions also take place between the light and heavy aromatic oligomers, resulting in an increase in the char yield (by ~8%) during the pyrolysis of the pyrolytic lignin. The decrease in H/C ratio with increasing temperature suggests the formation of more condensed char. The reduction of various function groups during the thermal decomposition of pyrolytic lignin is mostly due to the release of aliphatic and phenolic compounds (monomers or oligomers). As pyrolysis temperature increases, the char structure becomes more aromatic due to the enhanced polymerization reactions, especially at temperatures above 250 °C.

---

## Chapter 5 Structural Changes of Chars Produced from Fast Pyrolysis of Lignin at Low Temperatures

### 5.1 Introduction

Lignin is one of the major components in lignocellulosic biomass and regarded as the largest renewable source of aromatic polymers [215-218]. It is highly branched and composed of mainly phenylpropane units that linked to each other via ether bonds and C-C bonds [219-222]. The composition and nature of lignin samples are dependent on biomass type and isolation process (e.g. organosolv [30, 223], alkali [37, 224], acid hydrolysis [225] or soda pulping [225, 226]).

Compared to those of other major components in biomass, valorization of lignin is more challenging because of lignin having heterogeneous structures with different interunit linkages. Fast pyrolysis is a promising thermochemical technology for converting lignocellulosic biomass into fuels and chemicals [163]. During fast pyrolysis, lignin can be converted to liquid (bio-oil), solid (biochar) and gas and the products derived from lignin pyrolysis have important roles in the chemical properties of bio-oil [227]. Similar as biomass fast pyrolysis [228-230], one of the major challenges for lignin fast pyrolysis technologies is its high tendency to agglomerate at temperatures pertinent to bio-oil production [27, 37, 110], because lignin easily softens and melts during pyrolysis. The formation of agglomerates can result in significant operation problems in some reactor systems (e.g., fluidized bed reactor) [225]. To develop advanced process for lignin fast pyrolysis, in-depth knowledge on lignin pyrolysis mechanism is essential.

Previous studies on lignin fast pyrolysis mainly focused on the characterization of volatile products from lignin pyrolysis using TGA or Py-GC/MS [32, 69, 172, 231]. Only scattered studies dealt with the structural changes of lignin during fast pyrolysis [37]. It is known that biomass pyrolysis proceeds with the formation of a molten intermediate liquid phase, as an important phenomenon of biomass pyrolysis [39, 163]. Those intermediates are important precursors of volatiles thus determining the

formation and properties of volatiles during pyrolysis. Extensive works have been carried out on the formation and characterisation of reaction intermediates from cellulose pyrolysis [19, 232]. For example, our previous studies [19, 233, 234] have successfully collected and characterised the reaction intermediates from cellulose pyrolysis, and identified the presence of sugar and anhydro-sugar oligomers with a wide range of degrees of polymerization (DPs) in the liquid intermediate from cellulose pyrolysis. The effect of inorganic species (i.e., Na, K, Mg, Ca) on the formation of the reaction intermediates have also been systematically investigated [235-237].

While the formation of liquid intermediates from cellulose pyrolysis have been extensively studied [19, 232, 233], the formation of such intermediates during lignin fast pyrolysis is not well understood. Some recent works [23, 36, 38] have been carried out to improve the understanding of liquid intermediates from lignin pyrolysis. For example, Garcia-Perez et al. [38] has reported the formation of liquid intermediate plays important roles in the distribution of pyrolysis product during lignin pyrolysis, i.e., via thermal ejection [23]. Dufour et al. [36] employed some in situ techniques (i.e., in situ  $^1\text{H}$  NMR, in situ high-temperature rheology) to provide new insights into lignin softening and pyrolysis. It has been found that lignin softening and solidification start at  $\sim 140$  and  $\sim 250$   $^{\circ}\text{C}$ , respectively. Most likely, the low-molecular-weight portion of lignin is responsible for the formation of liquid intermediates during lignin pyrolysis. However, there have been no studies so far to characterise the structural changes of the low- and high-molecular-weight portions of lignin during pyrolysis. Therefore, it is important to understand the structure changes of the low-molecular-weight portion of lignin during pyrolysis, especially at low temperatures ( $< 300$   $^{\circ}\text{C}$ ) where the formation of liquid intermediates becomes important.

This study employs solvent extraction [i.e., tetrahydrofuran (THF)] to separate the lignin and its char products from lignin pyrolysis into the THF-soluble (low molecular weight) and THF-insoluble (high molecular weight) portions. The structural changes of the THF-soluble portion and the whole char are then

characterised by a series of techniques to provide new insights into the lignin pyrolysis mechanism at low temperatures of 100–300 °C.

## 5.2 Char Yield of Lignin during Fast Pyrolysis and Distribution of the THF-Soluble and the THF-Insoluble Portions in the Char

Figure 5.1 presents the char yield (on a dry ash free basis) of lignin fast pyrolysis at 100–300 °C. It can be seen that lignin starts to decompose from ~150 °C, and the char yield decreases with the pyrolysis temperature, i.e., from ~92% at 150 °C to ~57% at 300 °C. To understand the change of the THF-soluble portion in the char during lignin pyrolysis at different temperatures, the raw lignin and char samples were extracted by THF to produce the THF-soluble sample, and then the solvent in the sample was removed by evaporation at 40 °C for determining the content of the THF-soluble portion. As shown in Figure 5.1, ~69% of the raw lignin is the THF-soluble. The GPC analysis results show that the Mw of the raw lignin (after acetylation) is ~4918 Da, while the weight-average molecular weight (Mw) of the THF-soluble lignin is only ~1315 Da. This is expected since the THF-soluble portion is mainly composed of the low-molecular-weight lignin, while the THF-insoluble portion consists of the high-molecular-weight lignin. The THF-soluble portion continues to decrease with increasing pyrolysis temperature, from ~69% in the raw sample to ~37% at 175 °C, then to ~11% at 225 °C. At 250 °C, the THF-soluble portion almost completely disappears. In contrast, while there is little change in the THF-insoluble portion at temperatures < 150 °C, the THF-insoluble portion increases significantly at higher temperatures, from ~31% in the raw sample to ~52% at 175 °C, then to the maximum ~67% at 250 °C. As the temperature further increases to 300 °C, the THF-insoluble portion starts to decrease.

The results indicate that lignin pyrolysis at low temperatures (i.e., < 250 °C) mainly takes place via the decomposition and polymerization of the THF-soluble portion. Since lignin softening starts at ~140 °C [36], such decomposition and polymerization reactions mainly occur in the liquid phase. The results in Figure 5.1 indicate that the decomposition reactions start at ~150 °C due to weight loss as volatiles, while the polymerization reactions start at ~175 °C as evidenced by a large increase in the THF-insoluble portion. At 250 °C, around half of the THF-soluble portion is

polymerized into the THF-insoluble portion, while the other half is decomposed as volatiles. To clearly understand the structural changes of the THF-soluble portion during lignin pyrolysis, the THF-soluble portion in the raw lignin and char samples produced from lignin pyrolysis at 100–250 °C were collected and analysed via a series of techniques, and the results are presented in the following subsections.

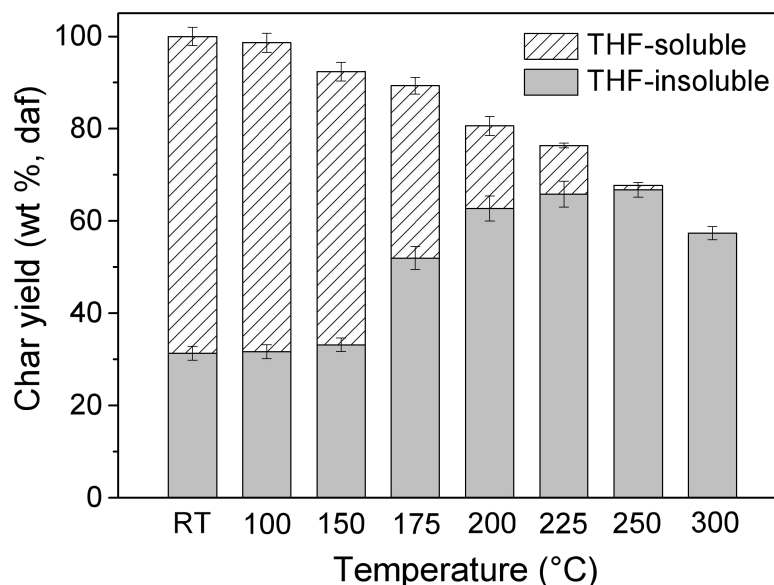


Figure 5.1: Char yield from the pyrolysis of lignin at 100–300 °C and the distribution of the THF-soluble and THF-insoluble fractions in all samples

### 5.3 Structural Changes of the THF-Soluble Portion in the Chars Produced from Lignin Fast Pyrolysis

#### 5.3.1 Elemental Composition

Table 5.1 lists the elemental compositions of the THF-soluble portions in the raw lignin and char samples produced from lignin fast pyrolysis at 100–250 °C. Compared to the raw lignin, the THF-soluble portion has slightly higher carbon and hydrogen contents but lower oxygen content. These lead to a higher H/C atomic ratio and a lower O/C atomic ratio, suggesting that the THF-soluble portion is less condensed compared to the THF-insoluble portion. As the pyrolysis temperature increases from 100 to 250 °C, the carbon content of the THF-soluble portion slightly increases from ~65.7 to ~67.0%, while the oxygen and hydrogen contents decrease from ~28.0% and ~5.7% to ~27.4% and ~5.1%, respectively. Overall, the H/C atomic ratio of the THF-soluble portion reduces from 1.00 at 100 °C to 0.91 at 250

°C, while there is only little change in the O/C atomic ratio of the THF-soluble portion. Therefore, increasing pyrolysis temperature from 100 to 250 °C only leads to small changes in the elemental composition of the THF-soluble portion.

Table 5.1: Elemental compositions of the THF-soluble portion in the raw lignin and chars prepared from lignin fast pyrolysis at various temperatures

	Raw lignin	THF-soluble portion prepared at various temperatures			
		100 °C	150 °C	200 °C	250 °C
C (wt%, daf)	64.97	65.72	66.74	66.85	67.03
H (wt%, daf)	5.72	5.47	5.36	5.14	5.09
N (wt%, daf)	0.63	0.81	0.49	0.49	0.36
O (wt%, daf)	28.67	28.00	27.41	27.52	27.42
Atomic H/C	1.06	1.00	0.96	0.92	0.91
Atomic O/C	0.33	0.32	0.31	0.31	0.31

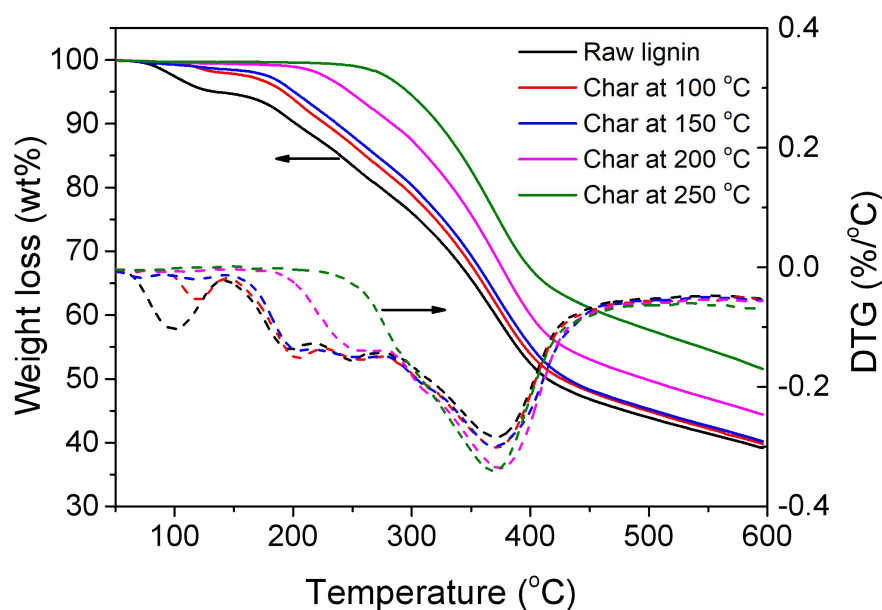


Figure 5.2: TG and DTG curves of the THF-soluble portion in the raw lignin and chars prepared at various temperatures

### 5.3.2 TG Analysis

Figure 5.2 presents the TG and DTG curves of the THF-soluble portions in the raw lignin and char samples produced from lignin fast pyrolysis at 100–250 °C. For the THF-soluble portion in the raw lignin, the weight loss starts at 150 °C after the loss of moisture or water from dehydration at 100 °C. The DTG curve has several peaks at 200, 250, 300 and 370 °C, indicating the different thermal stabilities of various

functional groups in the THF-soluble portion in the raw lignin. However, significant weight loss mainly takes place at  $\sim 370$  °C. For the THF-soluble portion in the char samples, the functional groups of lower thermal stability gradually disappear in the DTG curves as the pyrolysis temperature increases. The structural changes appears to be minimal for the THF-soluble portions in the char samples obtained at temperatures  $< 150$  °C, since only the peak at 100 °C disappears in the DTG curves. However, for the THF-soluble portion in the char sample obtained at 250 °C, several peaks (at 100, 200 and 250 °C) disappear. The losses of functional groups of low thermal stabilities also lead to a decreasing consumption of char in the TG analysis.

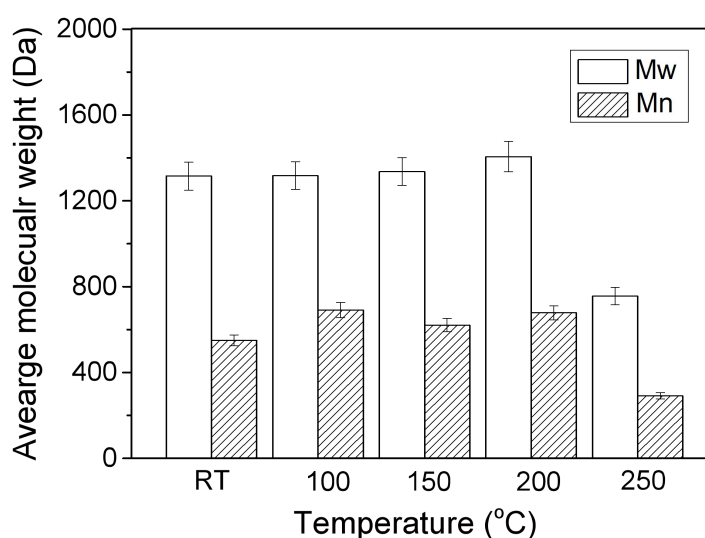


Figure 5.3: Weight-average molecular weight (Mw) and number-average molecular weight (Mn) of the THF-soluble portion in the raw lignin and chars prepared at various temperatures

### 5.3.3 GPC Analysis

Figure 5.3 presents the average molecular weight (determined by GPC) of the THF-soluble portions in the raw lignin and char samples produced from lignin fast pyrolysis at 100–250 °C. Surprisingly, there is no significant difference in the Mw of the THF-soluble portion in the chars produced at temperatures  $\leq 200$  °C. However, as the pyrolysis temperature increases to 250 °C, the Mw of the THF-soluble portion decreases substantially, by almost half from  $\sim 1407$  at 200 °C to  $\sim 756$  Da at 250 °C. This indicates that the THF-soluble portions produced at different temperatures have similar average molecular weight, in despite of the significant differences in thermal

stabilities. At 250 °C, the amount of low-molecular-weight compounds in the THF-soluble portion becomes very small.

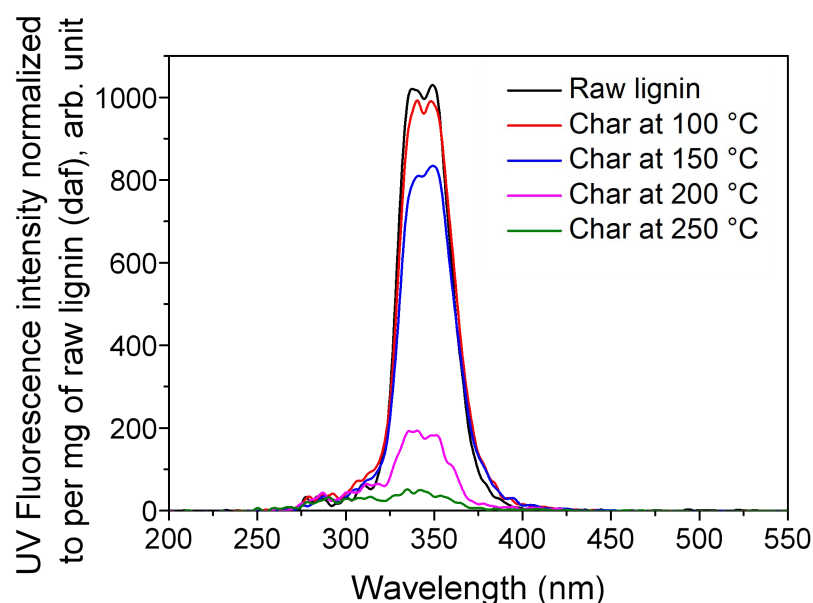


Figure 5.4: UV Fluorescence spectra of the THF-soluble portion in the raw lignin and its chars prepared at 100–300 °C

### 5.3.4 UV Fluorescence Analysis

The THF-soluble portions in the raw lignin and char samples produced from lignin fast pyrolysis at 100–250 °C were also dissolved in THF solvent for the UV fluorescence analysis. Figure 5.4 presents the UV fluorescence intensities of the THF-soluble portions normalized to the mass of the raw lignin fed into the reactor (i.e., on a basis of per mg of lignin) for comparison. It is noted that the intensities at wavelength < 290 nm, 290–340 nm and 340–390 nm represent the relative abundances of aromatic structures with mono-aromatic rings, 2–3 fused rings and 3–5 fused rings, respectively [214]. Figure 5.4 shows that the THF-soluble portion of the raw lignin mainly consists of aromatic structures with 2–5 fused rings. As the pyrolysis temperature increases, the abundance of aromatic structures of different fused rings decreases. Such a decrease is insignificant at temperatures  $\leq 150$  °C, likely due to the release of less thermally stable light aromatic oligomers into volatiles. However, such a decrease becomes significant at 200 °C. Considering the significant increase in the THF-insoluble portion at 200 °C, it is concluded that the majorities of aromatic structures in the THF-soluble portion are polymerized into more condensed aromatic structures which are insoluble in THF.



### 5.3.5 2D $^1\text{H}$ - $^{13}\text{C}$ HSQC-NMR Analysis

The THF-soluble portions in the raw lignin and char samples produced from lignin fast pyrolysis at 100–250 °C were also analyzed by 2D  $^1\text{H}$ - $^{13}\text{C}$  HSQC-NMR (see Figure 5.5). The allocation of signals in the 2D  $^1\text{H}$ - $^{13}\text{C}$  HSQC spectra are based on [238-240] and summarized in Table 5.2. It can be found that the THF-soluble portion in the raw lignin mainly includes the guaiacyl and *p*-hydroxyphenyl units linked by  $\beta$ -O-4, resinol and phenylcoumaran substructures. Similarly, there are little changes in the THF-soluble portions at temperatures  $\leq 150$  °C. However, when the temperature increases to 175 °C, the abundance of  $\beta$ -O-4, resinol and phenylcoumaran substructures start to decrease, along with part of the guaiacyl and *p*-hydroxyphenyl units. At 250 °C, there is only a small portion of guaiacyl units remaining in the THF-soluble portion, and the *p*-hydroxyphenyl units almost disappear.

Table 5.2: Assignment of the main signals in the 2D  $^1\text{H}$ - $^{13}\text{C}$  HSQC spectra [238-240]

Label	$\delta_{\text{C}}/\delta_{\text{H}}$	Assignments
A $_{\alpha}$	71.8/4.86	C $_{\alpha}$ -H $_{\alpha}$ in $\beta$ -O-4 substructures and $\gamma$ -acylated $\beta$ -O-4 substructures
A $_{\beta}$	83.6/4.38	C $_{\beta}$ -H $_{\beta}$ in $\beta$ -O-4 substructures and $\gamma$ -acylated $\beta$ -O-4 substructures
A $_{\gamma}$	60.0-60.8/3.59-3.69	C $_{\gamma}$ -H $_{\gamma}$ in $\beta$ -O-4 substructures and $\gamma$ -acylated $\beta$ -O-4 substructures
B $_{\alpha}$	84.8/4.66	C $_{\alpha}$ -H $_{\alpha}$ in resinol substructures
B $_{\beta}$	53.5/3.06	C $_{\beta}$ -H $_{\beta}$ in resinol substructures
B $_{\gamma}$	71.1/3.82	C $_{\gamma}$ -H $_{\gamma}$ in resinol substructures
C $_{\alpha}$	86.9/5.55	C $_{\alpha}$ -H $_{\alpha}$ in phenylcoumaran substructures
C $_{\beta}$	53.2/3.57	C $_{\beta}$ -H $_{\beta}$ in phenylcoumaran substructures
C $_{\gamma}$	62.8/3.74	C $_{\gamma}$ -H $_{\gamma}$ in phenylcoumaran substructures
G $_2$	110.9/6.98	C $_2$ -H $_2$ in guaiacyl units
G $_5$	114.9/6.77	C $_5$ -H $_5$ in guaiacyl units
G $_6$	119.0/6.79	C $_6$ -H $_6$ in guaiacyl units
I $_{\gamma}$	61.4/4.10	C $_{\gamma}$ -H $_{\gamma}$ in <i>p</i> -hydroxycinnamyl alcohol end groups
H $_{2,6}$	127.8/7.19	C $_{2,6}$ -H $_{2,6}$ in <i>p</i> -hydroxyphenyl units
-OCH $_3$	55.9/3.73	C-H in methoxyls

## 5.4 Structural Changes of the Chars Produced from Lignin Fast Pyrolysis

### 5.4.1 Elemental Composition

To further understand the structural changes of the whole char during lignin pyrolysis, the chars produced from produced from lignin fast pyrolysis at 100–300

°C were also analysed via elemental analysis, FT-IR and NMR. The elemental compositions of the raw lignin and char produced at 100–300 °C are summarized in Table 5.3. As the pyrolysis temperature increases from 100 to 300 °C, the carbon content of the char increases from ~63.0 to ~68.1%, while the oxygen and hydrogen contents decrease from ~31.0% and ~5.4% to ~27.1% and ~4.5%, respectively. These lead to a significant reduction in char H/C atomic ratio from 1.02 at 100 °C to 0.78 at 300 °C, but only a slight reduction in char O/C atomic ratio from 0.37 at 100 °C to 0.30 at 300 °C. This is expected because char structure becomes more condensed as the pyrolysis temperature increases. Compared to the elemental analysis results of the THF-soluble portion, the carbon and hydrogen content of the char are slightly lower, but the oxygen content is higher. For the H/C atomic ratio, there are no significant differences at temperatures  $\leq 200$  °C. However, the H/C atomic ratio of char (0.85) is lower than that of the THF-soluble portion (0.91) at 250 °C, mainly due to the polymerization of the THF-soluble portion into more condensed structures in the THF-insoluble portion.

Table 5.3: Elemental compositions of chars prepared from lignin fast pyrolysis at various temperatures

	100 °C	150 °C	175 °C	200 °C	225 °C	250 °C	300 °C
C (wt%, daf)	63.01	63.84	64.55	65.02	65.36	65.91	68.10
H (wt%, daf)	5.35	5.29	5.25	5.02	4.82	4.65	4.45
N (wt%, daf)	0.64	0.45	0.42	0.38	0.40	0.41	0.40
O (wt%, daf)	31.01	30.42	29.78	29.58	29.42	29.03	27.06
Atomic H/C	1.02	0.99	0.98	0.93	0.88	0.85	0.78
Atomic O/C	0.37	0.36	0.35	0.34	0.34	0.33	0.30

Table 5.4: Peak assignments for FT-IR spectra [35, 37, 172]

Wavenumbers (cm <sup>-1</sup> )	Assignments
3419	–OH stretches
2860-3000	Aliphatic C–H stretches
2844	O–CH <sub>3</sub> stretch of methoxyl group
1612	C=O stretching conjugated to aromatic ring
1513	Aromatic ring stretch
1221-1234	C–C plus C–O
1155	Aromatic C–H stretching of guaiacyl ring
1125	Aromatic C–H stretching of syringyl ring
1033	C–O stretch in primary alcohol

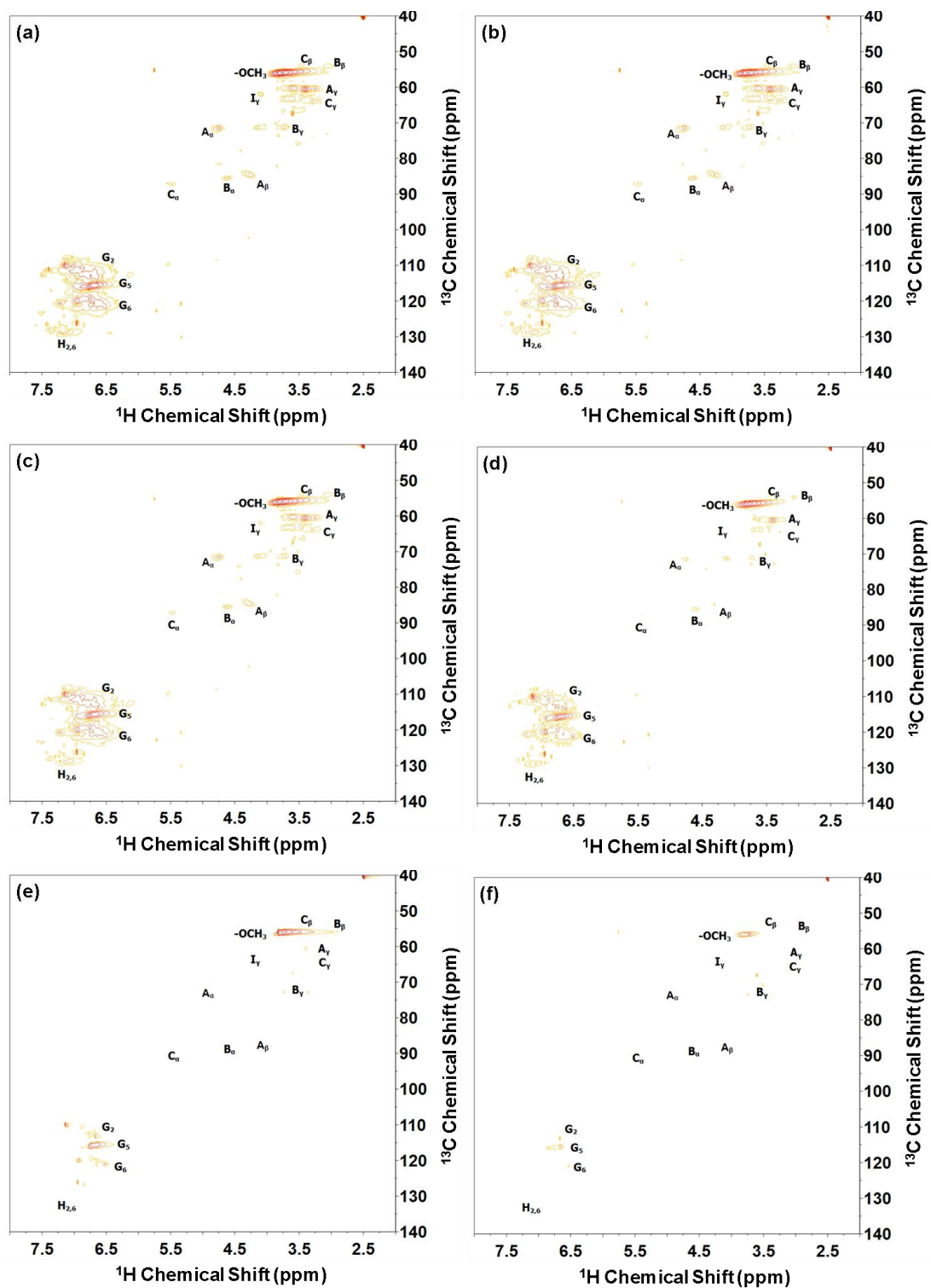


Figure 5.5: 2D  $^1\text{H}$ - $^{13}\text{C}$  HSQC spectra of the THF-soluble portion in the raw lignin and its chars prepared at 100–300 °C. (a) THF-soluble portion in the raw lignin; (b) THF-soluble portion in the char prepared at 100 °C; (c) THF-soluble portion in the char prepared at 150 °C; (d) THF-soluble portion in the char prepared at 175 °C; (e) THF-soluble portion in the char prepared at 200 °C; (f) THF-soluble portion in the char prepared at 250 °C

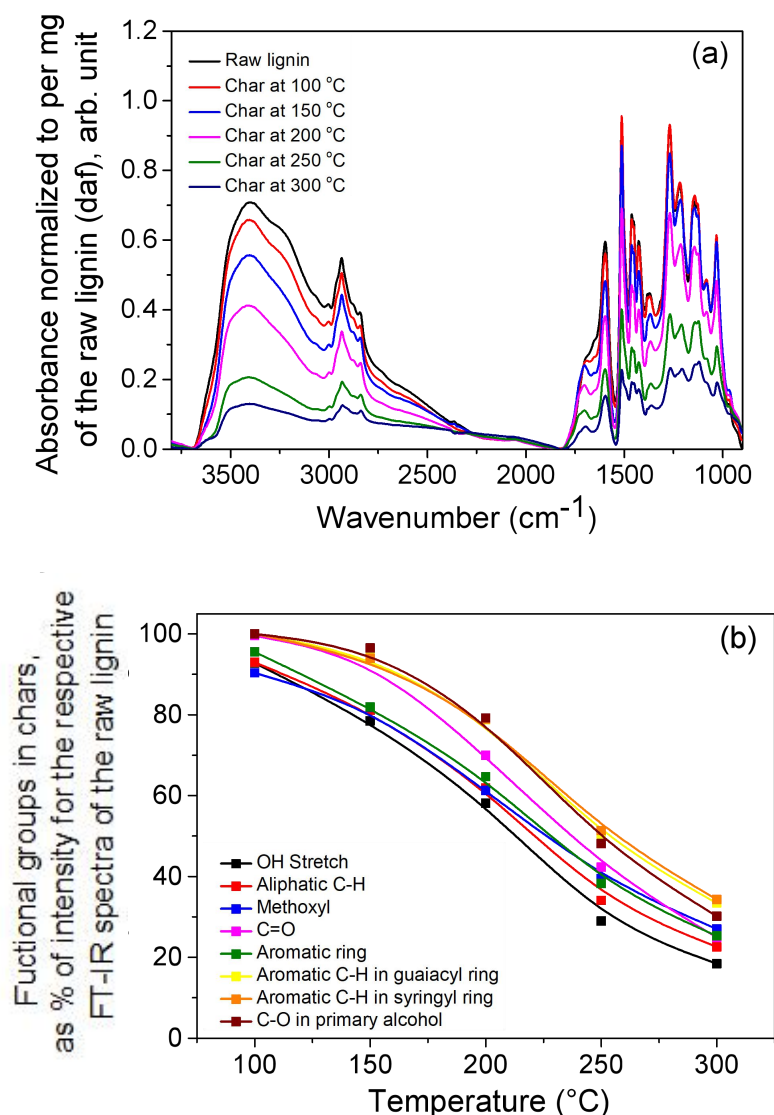


Figure 5.6: Panel (a) FT-IR spectra of the lignin and its chars prepared at 100–300 °C. Panel (b) % Functional groups in chars at 100–300 °C, expressed as % the intensity of respective FT-IR spectra for the raw lignin

#### 5.4.2 FT-IR Analysis

The FT-IR spectra of the lignin and char samples were acquired to study the changes in functional group during lignin fast pyrolysis at 100–300 °C. The peak assignment of FT-IR spectra was based on previous literature [37, 172] and summarized in Table 5.4. As shown in Figure 5.6a, the main functional groups of the FT-IR spectra are observed to be –OH stretching (3419 cm<sup>-1</sup>), aliphatic C–H (2938 cm<sup>-1</sup>), methoxyl CH<sub>3</sub> stretch (2844 cm<sup>-1</sup>), C=O stretch (1704 cm<sup>-1</sup>), aromatic ring stretch (1513 cm<sup>-1</sup>) and C–O (1033 cm<sup>-1</sup>). To compare the changes of various functional groups during lignin pyrolysis at various temperatures, the absorbance intensities of the spectra

were normalized to per mg (daf) of the raw lignin, as presented in Figure 5.6a. The intensities of all functional groups decrease as the pyrolysis temperature increases. The reductions in the functional groups were further calculated as the percentages of the initial intensities in the raw lignin and the results are presented in Figure 5.6b. The broad peak of the –OH stretching at 3300–3450  $\text{cm}^{-1}$  shows a decreased intensity as the pyrolysis temperature increases. This indicates the loss of some alcoholic/phenolic groups mainly from the THF-soluble portion of the raw lignin. This can be attributed to the cleavage of hydroxyl groups bonded to the carbon  $\text{C}_\beta$  or  $\text{C}_\gamma$  on the aliphatic side chains (resulting in releasing  $\text{H}_2\text{O}$  as volatiles) [31]. The peak at 2938  $\text{cm}^{-1}$  corresponding to the aliphatic C–H bonds exhibits a similar trend as the O–H stretching. This can be attributed to the fragmentation between  $\beta$  and  $\gamma$ -carbons in the alkyl aliphatic chains, which are thermally unstable and start to decompose at  $\sim 120$   $^\circ\text{C}$  [31]. The  $\text{CH}_3$  stretching of the methoxyl groups at 2844  $\text{cm}^{-1}$  gradually decreases with increasing temperature. The ether linkages (i.e.,  $\alpha$ -O-4,  $\beta$ -1 and  $\beta$ -O-4) bonded to the alkyl chains are known to be less stable and mostly break at  $\sim 200$   $^\circ\text{C}$  [171] so that these O– $\text{CH}_3$  groups can be easily removed from the substituted aromatic rings. The band at 1612  $\text{cm}^{-1}$  shows the presence of conjugated C=O with aromatic rings in the samples and the reduction in intensity only becomes significant at temperatures  $> 150$   $^\circ\text{C}$ . This is not surprising because the ether bonds linked to the  $\gamma$ -carbon are more resistant to the thermal decomposition [173]. The peak identified at 1513  $\text{cm}^{-1}$  is associated with the aromatic ring skeletal vibrations while the bands appeared at 1155  $\text{cm}^{-1}$  and 1125  $\text{cm}^{-1}$  show the existence of guaiacyl and syringyl rings in the samples. It can be seen that the intensities of these peaks decrease slowly as temperature increases from 150  $^\circ\text{C}$ , then rapidly at elevated temperatures up to 350  $^\circ\text{C}$ . This can be attributed to the rupture of the bonds between those monomers (e.g., guaiacol, syringol and catechol), resulting in the release of the phenolic compounds in the form of monomers or oligomers. Some of the aromatic rings are still present in the structure because the temperature is not high enough to break the more thermally stable bonds such as phenyl 5-5 and ether 4-O-5 [171, 175].

### 5.4.3 $^{13}\text{C}$ CP/MAS NMR Analysis

To provide detailed information about the carbon structure of the raw lignin and its char samples,  $^{13}\text{C}$  CP/MAS NMR spectra were acquired to semi-quantitatively

determine the changes in the carbon structure, as shown in Figure 5.7. The assignment of different carbon structures is based on the literature [72, 209, 210]. Generally, the chemical shift at 10–50 ppm and 50–90 ppm are assigned to the aliphatic C–C carbon and the oxygenated alkyl carbons (i.e., Ar-OCH<sub>3</sub> and C- $\alpha,\beta,\gamma$ ), respectively. The signals at 102–155 ppm correspond to aromatic carbons (i.e., guaiacyl, syringyl and p-hydroxyphenyl units). The region between 160–200 ppm is assigned to the carbonyl or carboxyl groups.

To compare the changes of carbon structure at different temperatures, the contributions of typical carbon structures were determined based on the integrated intensity of each carbon structure normalized to the total intensity of all carbon structures, and the results are presented in Table 6. It can be seen that the raw lignin is mainly composed of aromatic and methoxyl carbon structures, with contribution of ~60 and ~28%, respectively. Only small portions of aliphatic (~10%) and carbonyl (~2%) carbon structures are present in the raw lignin. As the pyrolysis temperature increases from 100 to 300 °C, the aliphatic carbon structures gradually decrease. This is expected due to the release of less thermal stable alkyl side chains as volatiles, such as the phenylpropane chains in lignin. The relative intensity of the methoxyl group shows a slightly reduction at 200 °C, but decreases drastically at 300 °C. This can be attributed to the loss of methoxyl substituents from the aromatic rings as a result of the decomposition of the common ether bonds linkages in lignin (i.e.  $\alpha$ -O-4,  $\beta$ -1 and  $\beta$ -O-4), known to commence at ~200 °C [171]. It is important to highlight that the aromatic carbon of the chars increases significantly from ~59% at 100 °C to ~73% at 300 °C. This clearly demonstrates that the char is mainly composed of aromatic structures at 300 °C, in consistence with the results on char aromaticity presented in Table 6. As a result, the aromaticity of the char increases progressively as the pyrolysis temperature increases, i.e., from ~86% for lignin to ~91% for the char prepared at 300 °C. It was suggested that the highly aromatic char structures are likely formed from the liquid intermediate structures via homolytic radical reactions during lignin pyrolysis [212]. The softened lignin particles formed a mass of matrix with mobile species in liquid phase, mainly due to the side chain cleavage and loss of some volatile gases when heating, as supported by other literature works [36,37]. As temperature increases, the mobile species that stabilized the intermediates decrease,

resulting in the formation of cross-linked and condensed aromatic char structures [36].

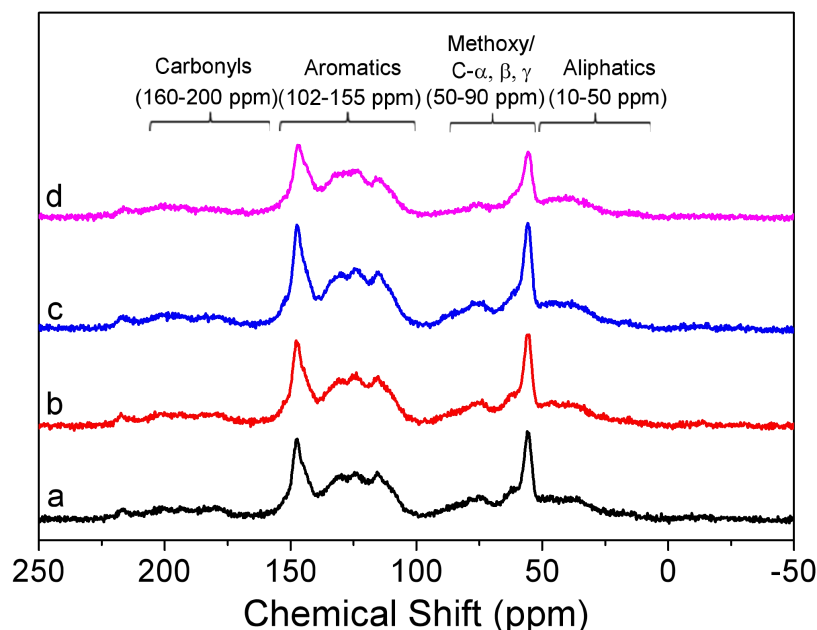


Figure 5.7: Solid  $^{13}\text{C}$  CP/MAS NMR spectra of the lignin and its chars prepared at 100–300 °C. Legends: (a) lignin; (b) char prepared at 100 °C; (c) char prepared at 200 °C; (d) char prepared at 300 °C

Table 5.5: Relative content analysis for  $^{13}\text{C}$  CP/MAS NMR spectra

	Raw lignin	Chars prepared at various temperatures		
		100 °C	200 °C	300 °C
Aliphatic (%)	9.66	9.06	8.59	7.01
Methoxyl (%)	28.49	28.24	27.60	19.51
Aromatic (%)	59.54	59.48	62.40	73.30
Carbonyl (%)	2.31	3.22	1.41	0.18
Aromaticity (%)	86.04	86.78	87.90	91.27

## 5.5 Conclusions

The work presents a systematic study to understand the structural changes of chars (particularly the low-molecular-weight portion) produced from fast pyrolysis of lignin at low temperatures of 100–300 °C. Our results show that the low temperature pyrolysis of lignin mainly proceeds with the pyrolysis of the low-molecular-weight portion (i.e., the THF-soluble portion) via decomposition reactions into volatiles and polymerization reactions into the high-molecular-weight portion (i.e., the THF-insoluble portion). The decomposition of the THF-soluble portion starts at ~150 °C,

mainly due to the loss of the hydroxyl groups as well as the alkyl aliphatic chains. Significant decomposition of the THF-soluble portion occurs at  $\sim 175$  °C, mainly because of the cleavage of weak ether bonds linked with  $\beta$ -carbon or  $\gamma$ -carbon, resulting in demethoxylation and release of some phenolic monomers or oligomers. Significant polymerization reactions start at  $\sim 175$  °C, leading to the increase of the THF-insoluble portion from  $\sim 31\%$  in the raw lignin to  $\sim 67\%$  in the char produced at 250 °C. Majority of the functional groups such as hydroxyl, methoxyl, aliphatic and carbonyl/carboxyl gradually decrease with increasing pyrolysis temperature, resulting in the formation of more condensed char as evidenced by the decreased H/C atomic ratio (i.e., 0.78 at 300 °C) and the increased aromaticity (i.e.,  $\sim 91\%$  at 300 °C) from NMR analysis.



---

## Chapter 6 Interactions between Low- and High-molecular-weight Portions of Lignin during Fast Pyrolysis at Low Temperatures

### 6.1 Introduction

Lignocellulosic biomass has received increasing attentions as a potential feedstock for renewable fuels and chemicals production due to its abundant availability worldwide [16, 26, 54, 218]. Lignin is a major component in lignocellulosic biomass, which is cross-linked by three main monomers (i.e., synapyl, coniferyl and *p*-coumaryl alcohols) [241, 242]. Lignin is considered as an important feedstock for producing renewable aromatic biochemicals and biofuels [243-250]. However, due to its heterogeneous, complex and highly branched polymeric structure, the valorization of lignin in biorefineries is very challenging [219, 221].

Lignin pyrolysis has been widely studied to understand the fundamental pyrolysis mechanism [27, 225, 251-254]. However, the softening and melting of lignin easily take place during pyrolysis at low temperatures [36, 38], leading to significant operation problems in fluidised bed reactor systems due to the formation of agglomerates [228, 230, 255, 256]. This is mainly because of the heterogeneous nature of lignin, which consists of both the low-molecular-weight (LMW) and high-molecular-weight (HMW) portions. The pyrolysis of LMW portion of lignin easily produces some species of low melting points, which form a liquid intermediate phase at low temperatures. Therefore, it is important to have a better understanding of the pyrolysis behaviours of different portions of lignin and their interactions during pyrolysis.

Solvent extraction is a good method to separate the lignin into different portions of various molecular weights. Our previous work [257] has separated the pyrolytic lignin into the light and heavy portions using  $\text{CH}_2\text{Cl}_2$ , in order to understand their behaviours and potential interactions during pyrolysis. Indeed, strongly interactions were identified between the light and heavy aromatic compounds in pyrolytic lignin, leading to the formation to additional char. However,  $\text{CH}_2\text{Cl}_2$  is not suitable for lignin extraction due to much higher molecular weight of lignin. Recently, various

solvents have been tested for lignin dissolution [190], and tetrahydrofuran (THF) was identified as a suitable solvent to dissolve majority of lignin due to its close solubility parameter to the solubility parameter of lignin [190]. In fact, THF has been widely used in gel permeation chromatography (GPC) analysis of lignin-derived products for determining the molecular weight distribution [258, 259]. Using the THF extraction, our recent study [260] has successfully characterised the structures of the THF-soluble and -insoluble portions of chars produced during lignin pyrolysis at low temperatures. It was found that lignin pyrolysis at low temperatures mainly proceeded with the THF-soluble portion via decomposition reactions into volatiles and polymerization reactions into the THF-insoluble portion [260].

To further understand the interactions between different portions of lignin during fast pyrolysis, this study employs the THF extraction to separate the lignin into the LMW (THF-soluble) and HMW (THF-insoluble) portions. Then, both the LMW and HMW lignin samples were subjected to fast pyrolysis experiments individually to understand their pyrolysis behaviours. Special attentions are paid to investigate the interactions between the LMW and HMW portions of lignin during fast pyrolysis, and the effect of interactions on char structural changes during the whole lignin pyrolysis.

## 6.2 Characterization of the Raw, LMW and HMW Lignin Samples

Via THF extraction, ~68.7 wt% of the raw lignin was recovered as the LMW portion, and ~31.3 wt% of lignin was precipitated as the HMW portion. The physical and chemical properties of the raw, LMW and HMW lignin samples were characterised using a series of techniques to understand their structural differences. Compared to the raw lignin, the LMW lignin has a higher volatile matter content but a lower fixed carbon content, while the HMW lignin has a lower volatile matter content but a higher fixed carbon content. As for elemental analysis, the carbon and hydrogen contents of the LHW lignin are slightly higher, but the oxygen content is lower. In contrast, the carbon and hydrogen contents of the HMW lignin are slightly lower, but the oxygen content is slightly higher. Determined by GPC analysis, the weight-average molecular weight (Mw) of the LMW lignin is ~1315 Da. After the acetylation pretreatment, the Mw of the raw and HMW lignin samples are

determined to be  $\sim 4918$  and  $\sim 6378$  Da, respectively, which are considerably higher than that of the LMW lignin.

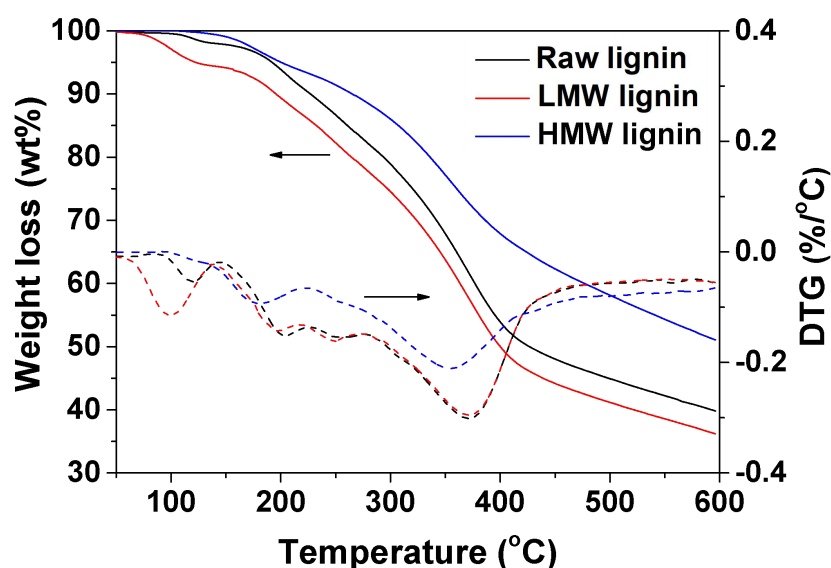


Figure 6.1: Weight losses and DTG curves of the raw, LMW and HMW lignin samples

To better understand the thermal stability of the three lignin samples, TGA experiments were performed and the results are shown in Figure 6.1. It can be seen that the HMW lignin is more thermally stable than the LMW lignin, due to its higher onset temperature and lower weight loss. The thermal decomposition of the LMW lignin starts at  $\sim 90$  °C, and the DTG curves have several peaks at 100, 200, 250, and 370 °C, respectively, demonstrating the presence of various functional groups that have different thermal stabilities in the LMW lignin. On the other hand, the HMW lignin starts to decompose at  $\sim 150$  °C, and the DTG curves have mainly three peaks at 175, 250 and 350 °C, with much lower weight loss. This leads to a higher final char yield for the HMW lignin, obviously due to its higher molecular weight. In contrast, the weight loss of the raw lignin is only slightly lower than that of the LMW lignin.

The functional groups of the three lignin samples were also investigated via the FT-IR spectroscopy and the results normalized to the unit mass of each lignin sample are compared in Figure 6.2. The peak assignments of the FT-IR spectra were based on existing literature [37, 172], as summarized in Table 6.1. It can be seen that most of

the common groups such as hydroxyl –OH, aliphatic C–H, carbonyl C=O, aromatic rings and C–O groups are present in all lignin samples but with slightly different intensities. However, the LMW lignin has higher intensities of the aromatic rings stretching at 1513–1125  $\text{cm}^{-1}$  and the C=O stretching that unconjugated to ketones/carbonyl/esters groups at 1704  $\text{cm}^{-1}$  than the other two lignin samples. This can be contributed to more aromatic structures that could be detected from the LMW lignin, since part of the highly condensed structures in the HMW lignin may be hardly detected by FT-IR analysis.

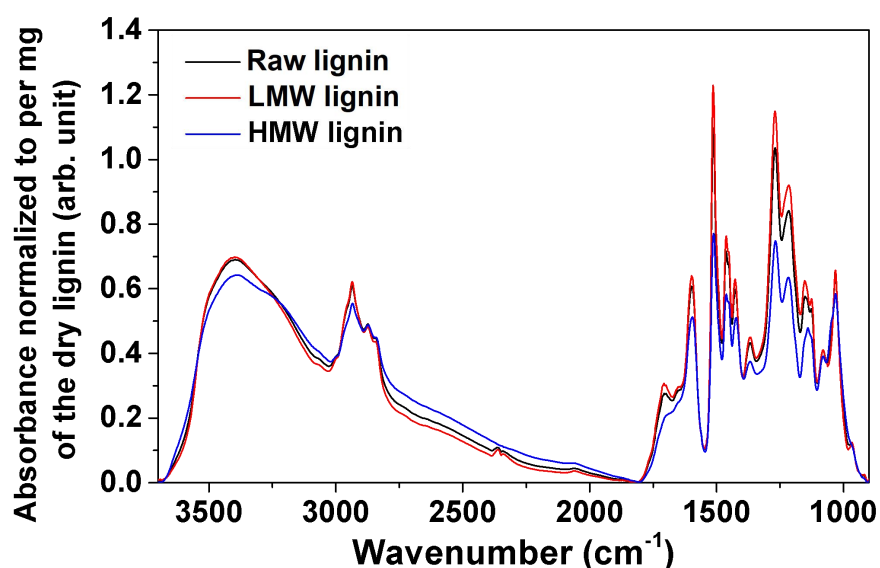


Figure 6.2: FT-IR spectra of the raw, LMW and HMW lignin samples normalized to the unit mass (per mg on a dry basis) of each sample.

Table 6.1: Peak assignments for FT-IR spectra [35, 37, 172]

Wavenumbers ( $\text{cm}^{-1}$ )	Assignments
3419	–OH stretches
2860-3000	Aliphatic C–H stretches
2844	O–CH <sub>3</sub> stretch of methoxyl group
1704	C=O stretching unconjugated to ketone, carbonyl and ester
1612	C=O stretching conjugated to aromatic ring
1513	Aromatic ring stretches
1221-1234	C–C plus C–O
1155	Aromatic C–H stretching of guaiacyl ring
1125	Aromatic C–H stretching of syringyl ring
1033	C–O stretches in primary alcohol

### 6.3 Interactions between the LMW and HMW Portions of Lignin Evidenced by Char Yields

The raw, LMW and HMW lignin samples were pyrolyzed at 100 – 300 °C under fast pyrolysis conditions and the char yields (on a daf basis) at different temperatures are compared in Figure 6.3. The char yields during the fast pyrolysis of the lignin samples at the same temperature follow an order of the HMW lignin > the raw lignin > the LMW lignin. For the raw lignin sample, the char yield decreases with increasing pyrolysis temperature, from ~96 wt% at 100 °C to ~59 wt% at 300 °C. The HMW lignin exhibits the highest thermal stability, with its char yield gradually decreasing from ~99 wt% to ~71 wt% when the temperature increases from 100 to 300 °C. Compared to the HMW lignin, the LMW lignin decomposes more rapidly as the temperature increases, with the char yield decreasing from ~94 wt% at 100 °C to ~38 wt% at 300 °C. As expected, the LMW lignin has the highest weight loss among the lignin samples under the same pyrolysis conditions, due to the presence of mostly light compounds in the LMW lignin.

The char yields of the raw lignin at various temperatures are further compared with those calculated based on the percentages of the LMW and HMW portions in the raw lignin and their corresponding char yields via addition, in order to identify the potential interactions between the LMW and HMW portions of lignin during pyrolysis. As shown in Figure 6.3, the char yield from the raw lignin is consistently higher than that calculated from its LMW and the HMW portions via addition, confirming the existence of interactions between the LMW and the HMW portions of lignin during pyrolysis under the same conditions. In addition, such a difference gradually increases with temperature, i.e., from 0.5wt% at 100 °C to 10.7wt% at 300 °C, indicating that such interactions lead to the formation of more char at higher temperatures. Compared to the pyrolysis of the LMW and HMW portions of lignin individually, the volatiles produced are more difficult to evaporate when the LMW and HMW lignin samples are pyrolyzed together (i.e., the pyrolysis of the raw lignin). This can be contributed to the formation of the liquid intermediate phase from the pyrolysis of the LMW lignin. Once a liquid intermediate phase is formed during pyrolysis, the formed volatiles must diffuse from liquid bulk to gas-liquid interface to escape the liquid intermediate phase, leading to reduced release of volatiles and

enhanced secondary reactions of volatiles in the liquid intermediate phase to form more char [163].

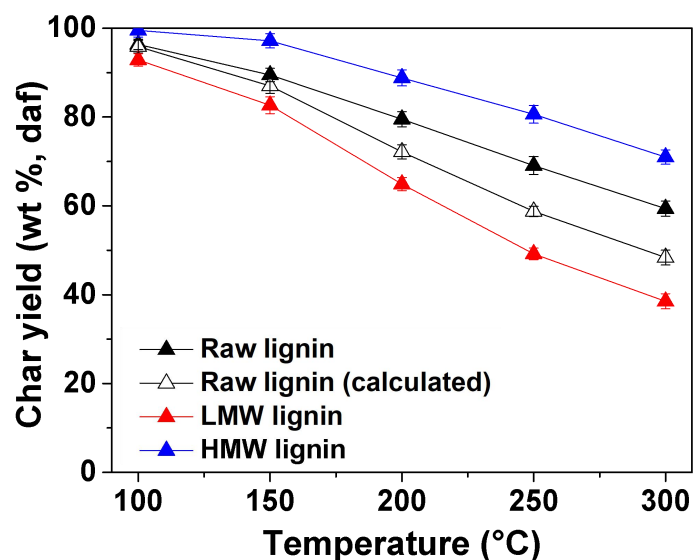


Figure 6.3: Char yields from the pyrolysis of the raw, LMW and HMW lignin samples at 100–300 °C. The calculated char yields are based on percentages of the LMW and HMW portions in the raw lignin and their corresponding char yields

#### 6.4 Interactions between the LMW and HMW Portions of Lignin Evidenced by Char Structural Changes

##### 6.4.1 Changes in Elemental Composition

Table 6.2 presents the elemental compositions of chars produced from the fast pyrolysis of the raw, LMW and HMW lignin samples at various pyrolysis temperatures. The carbon contents of char samples increases with temperature, accompanied by the decreased hydrogen and oxygen contents. The gradual loss of oxygen in the char indicates that the oxygen-containing functional groups in the pyrolysing sample is thermally unstable and start to rupture even at 100 °C. The atomic H/C and O/C ratios of the char samples decrease with increasing pyrolysis temperature. For instance, the atomic H/C and O/C ratios of the char from the raw lignin pyrolysis decrease from 1.08 and 0.34 at 100 °C to 0.85 and 0.26 at 300 °C, respectively. Similarly, for the chars from the LMW and HMW lignin, the atomic H/C ratios decrease from 1.10 and 1.15 at 100 °C to 0.92 and 0.87 at 300 °C, respectively. This indicates the formation of at least two-ring aromatic structures in the char at high temperatures, since the atomic H/C ratio of char at 300 °C is <1. The

atomic O/C ratios also slightly decrease from 0.33 and 0.36 at 100 °C to 0.27 and 0.28 at 300 °C, respectively. Such experimental results demonstrate that the char structure becomes more condensed as the pyrolysis temperature increases. It should be noted that the atomic O/C and H/C ratios of char from the raw lignin at high temperatures (i.e., 300 °C) are even lower than those from the LMW and HMW lignin. Such results show that the interactions between the LMW and HMW portions of lignin lead to enhanced polymerization reactions of oxygenated groups to form more condensed structures in the char.

Table 6.2: Elemental compositions of the chars produced from the fast pyrolysis of the raw, LMW and HMW lignin at various temperatures.

	T (°C)	Elemental Analysis (wt%, daf)				Atomic H/C	Atomic O/C
		C	H	N	O*		
Raw lignin	100	64.59	5.81	0.32	29.29	1.08	0.34
	150	65.36	5.80	0.24	28.60	1.07	0.33
	200	65.89	5.41	0.24	28.46	0.99	0.32
	250	66.83	5.17	0.23	27.77	0.93	0.31
	300	70.04	4.98	0.27	24.71	0.85	0.26
LMW lignin	100	65.47	5.98	0.18	28.38	1.10	0.33
	150	65.68	5.83	0.20	28.29	1.07	0.32
	200	66.99	5.56	0.20	27.25	1.00	0.31
	250	67.33	5.42	0.20	27.04	0.97	0.30
	300	69.45	5.34	0.20	25.01	0.92	0.27
HMW lignin	100	63.17	6.07	0.38	30.38	1.15	0.36
	150	63.78	6.06	0.33	29.83	1.14	0.35
	200	63.85	5.44	0.32	30.39	1.02	0.36
	250	65.84	5.23	0.33	28.60	0.95	0.33
	300	68.96	5.00	0.33	25.71	0.87	0.28

\*By difference.

#### 6.4.2 Changes in Functional Groups

The chars produced from the raw, LMW and HMW lignin samples were characterized by FT-IR spectroscopy to understand the differences in functional group changes. Figure 6.4 shows the FT-IR spectra of the chars produced from the pyrolysis of the raw, LMW and HMW lignin samples at 100–300 °C. The main functional groups to be examined are –OH stretches (3419 cm<sup>-1</sup>), aliphatic C–H bonds (2938 cm<sup>-1</sup>), methoxyl O–CH<sub>3</sub> stretches (2844 cm<sup>-1</sup>), C=O bonds stretches (1704 cm<sup>-1</sup>), aromatic ring vibrations (1513 cm<sup>-1</sup>) and C–O bonds (1033 cm<sup>-1</sup>). The

presented spectra of the char samples were all normalized to the unit mass (per mg on a dry basis) of the lignin sample fed into the reactor for direct comparisons.

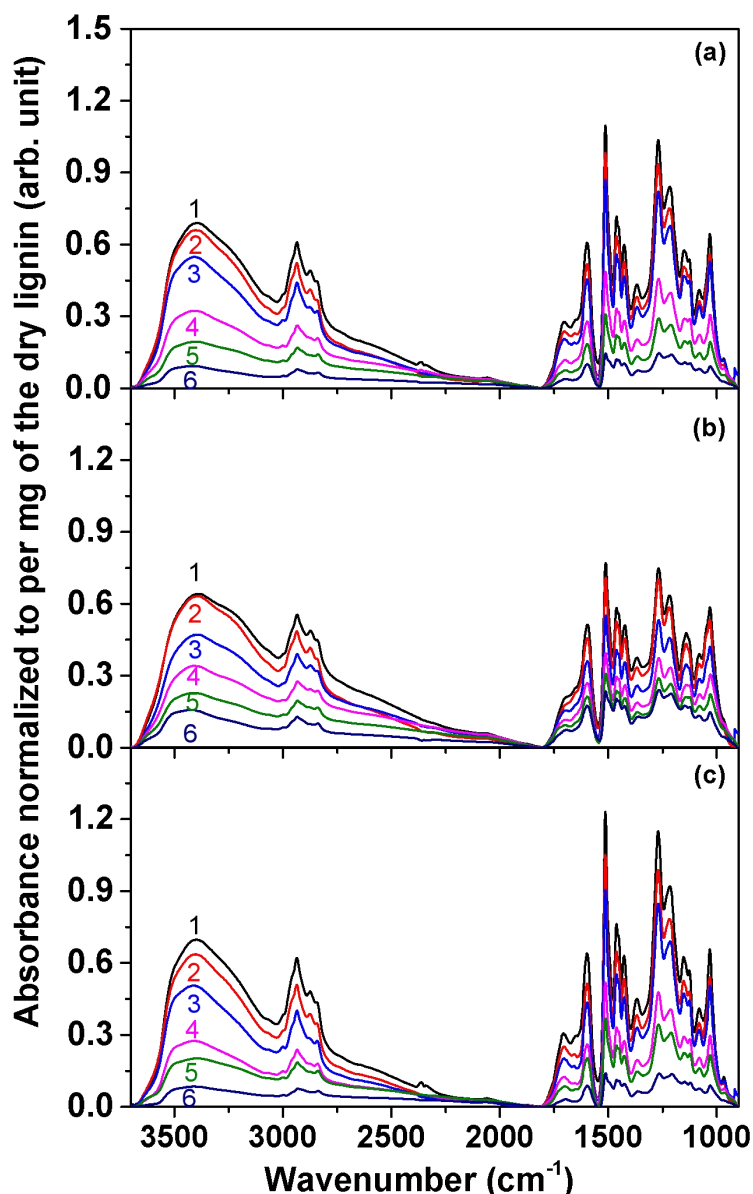


Figure 6.4: FT-IR spectra of the chars from the pyrolysis of the raw, LMW and HMW lignin samples at 100–300 °C, normalized to the unit mass (per mg on a dry basis) of each lignin sample. Panel (a) chars from the raw lignin: (1) raw lignin; (2) char at 100 °C; (3) char at 150 °C; (4) char at 200 °C; (5) char at 250 °C; (6) char at 300 °C. Panel (b) chars from the HMW lignin pyrolysis: (1) HMW lignin; (2) char at 100 °C; (3) char at 150 °C; (4) char at 200 °C; (5) char at 250 °C; (6) char at 300 °C. Panel (c) chars from the LMW lignin pyrolysis: (1) LMW lignin; (2) char at 100 °C; (3) char at 150 °C; (4) char at 200 °C; (5) char at 250 °C; (6) char at 300 °C.



Similar trends are observed for all the lignin samples. The intensities of functional groups of the chars all reduce with increasing pyrolysis temperature. The broad peak at above  $3000\text{ cm}^{-1}$  decreases with increasing temperature, due to the loss of hydroxyl groups that are mostly bonded with  $C_{\beta}$  or  $C_{\gamma}$  of carbon side chains [31, 173]. The peak in the region of  $2860 - 3000\text{ cm}^{-1}$  corresponds to the aliphatic C–H stretching. For the HMW lignin, its pyrolysis begins with the decomposition of aliphatic carbons, since negligible reductions in the –OH and other groups can be found at  $100\text{ }^{\circ}\text{C}$ , but those functional groups gradually decrease as temperature increases to  $300\text{ }^{\circ}\text{C}$ . On the other hand, most of the functional groups such as hydroxyl–OH, aliphatic C–H, carbonyl C=O and aromatic C–H bonds in the LMW lignin decrease noticeably at a low temperature of  $100\text{ }^{\circ}\text{C}$ . The methoxyl groups at  $2844\text{ cm}^{-1}$  indicate the losses of O–CH<sub>3</sub> groups from the substituted aromatics structures by the ether linkages (i.e.,  $\alpha$ -O-4,  $\beta$ -1 and  $\beta$ -O-4) [171, 261, 262]. The bands between  $1704$  and  $1612\text{ cm}^{-1}$  which represent the carbonyl groups that are unconjugated and conjugated to aromatic rings also decrease with increasing temperature. The bands at  $1513 - 1125\text{ cm}^{-1}$  comprise of aromatic ring vibrations, aromatic C–H of guaiacyl and syringyl rings. For the LMW lignin, the intensities of various functional groups reduce sharply when temperature increases from  $100$  to  $300\text{ }^{\circ}\text{C}$ . In contrast, those for the HMW lignin decrease slowly as temperature increases from  $100$  to  $300\text{ }^{\circ}\text{C}$ , because of the higher intensities of various functional groups for the chars from HMW lignin pyrolysis.

In order to understand the effect of the interactions between the LMW and HMW portions of lignin on the changes in functional groups during the raw lignin pyrolysis, the differences between the FT-IR spectra of the raw lignin chars and those calculated based on the percentages of the LMW and HMW portions in the raw lignin and their corresponding FT-IR spectra of chars produced at various pyrolysis temperatures were determined at various pyrolysis temperatures, and the results are shown in Figure 6.5. It can be found that the differences between the FT-IR spectra of the raw lignin char and the calculated spectra initially increase when temperature increases from  $100$  to  $150\text{ }^{\circ}\text{C}$ , suggesting that more functional groups are retained in the chars due to the interactions between the LMW and HMW portions of lignin. This is consistent with the increased char formation as pyrolysis temperature increases (see Figure 6.3). However, the FT-IR signals start to reduce as the temperature further increases, and almost reach zero when the temperature increases

to 200 °C. At higher temperatures > 200 °C, the differences between the FT-IR spectra of the raw lignin char and the calculated spectra even become negative, indicating that less intensities could be detected in the raw lignin chars compared to those calculated based on its LMW and HMW portions. Generally, the loss of oxygenated functional groups can be due to two reasons: (1) the evaporation of the oxygenated species after diffusion through the liquid intermediate phase and (2) the polymerization of the oxygenated species in the liquid intermediate phase [263]. High temperature enhances the formation of liquid intermediate phase, further suppressing the release of the oxygenated species in the volatiles due to increased polymerization reactions. Therefore, such increased polymerization reactions can lead to the loss of more oxygenated functional groups at increased temperatures. This can be confirmed by the lower atomic O/C ratios for the chars from the raw lignin sample at high temperature (i.e., 300 °C), showing more condensed structures in the chars.

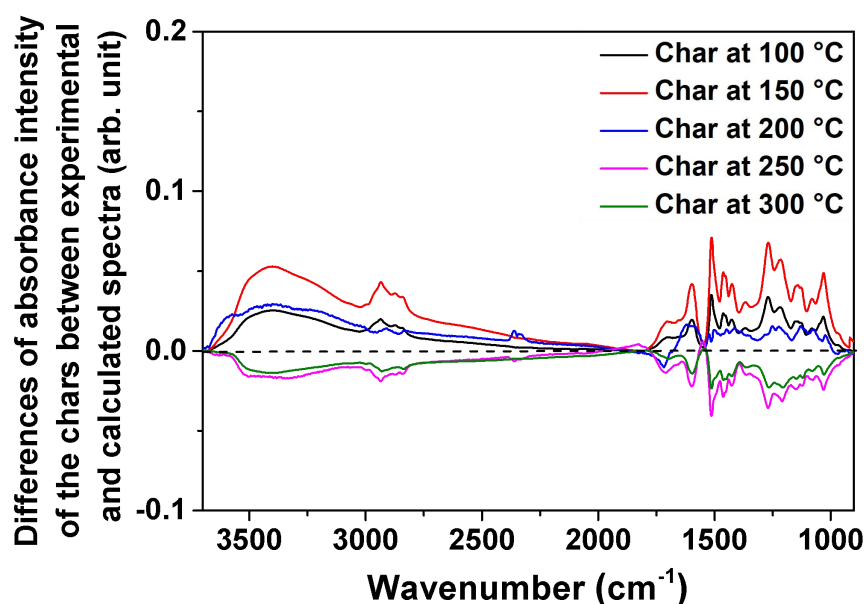


Figure 6.5: Differences between the FT-IR spectra of the raw lignin chars and the calculated spectra based on the percentages of the LMW and HMW portions in the raw lignin and their corresponding FT-IR spectra of chars produced at 100–300 °C

### 6.4.3 Changes in Aromatic Structures

Since lignin mainly consists of aromatic structures, it is important to understand the changes of the aromatic structures during lignin pyrolysis. The lignin and its char

samples were dissolved in THF, and the THF-soluble fractions of the samples were analysed by a UV fluorescence spectrometer to investigate the changes in the aromatic ring structures during lignin pyrolysis. The UV fluorescence spectra of the lignin samples and their chars produced at different temperatures are shown in Figure 6.6. It should be mentioned that the UV fluorescence intensities of the chars produced from the HMW lignin are extremely weak, hence the data are not presented in this study. It can be seen that the LMW lignin is mainly composed of aromatic ring structures with fused rings of 2–5 (e.g., mono-ring for wavelength < 290 nm, 2–3 fused rings for wavelength at 290–340 nm and 3–5 fused rings for wavelength at 340–390 nm [257, 260]). To facilitate the comparison, all the UV fluorescence intensities were normalized to the unit mass (per mg on a dry basis) of the lignin sample fed into the reactor for direct comparisons. For the pyrolysis of the LMW lignin, the UV fluorescence intensities decrease gradually when temperature increases from 100 to 300 °C, due to the decomposition of the weakly bonded light aromatic compounds. For the pyrolysis of the raw lignin, the UV fluorescence intensities decrease slowly as temperature increases to 150 °C. However, significant reductions in the UV fluorescence intensities can be found when temperature increases to 200 °C, and almost no signals can be detected at temperatures > 250 °C.

To understand the effect of the interactions between the LMW and HMW portions of lignin on the changes in aromatic structures during the raw lignin pyrolysis, the differences between the UV fluorescence intensities of the raw lignin chars and the calculated UV fluorescence intensities based on the percentage of the LMW portion in the raw lignin and their corresponding UV fluorescence intensities of chars produced at various pyrolysis temperatures were determined. As shown in Figure 6.7, the differences in the UV fluorescence intensities between the raw lignin chars and the calculated results are small at 100 °C, indicating there are only minor interactions at low temperatures. However, such differences increase as temperature increases to 150 °C, mainly in the wavelength range of 320–370 nm, suggesting the formation of more aromatic structures of 3–4 fused rings in the char from the raw lignin. At 200 °C, it is interesting to see the large negative intensities in the wavelength range of 290–390 nm, indicating that less aromatic structures of 2–5 fused rings are present in the char from the raw lignin. Since only the THF-soluble portion of char sample can be detected by the UV fluorescence analysis, it seems that the interactions between

the LMW and HMW portions of lignin lead to the formation of more condensed aromatic structures which are insoluble in THF, thus showing the negative intensities. As the temperature further increases, such negative intensities starts to decrease, due to reduced UV fluorescence intensities for the char from the LMW lignin at increased temperatures. The results are consistent with the char yields and the FT-IR results presented above.

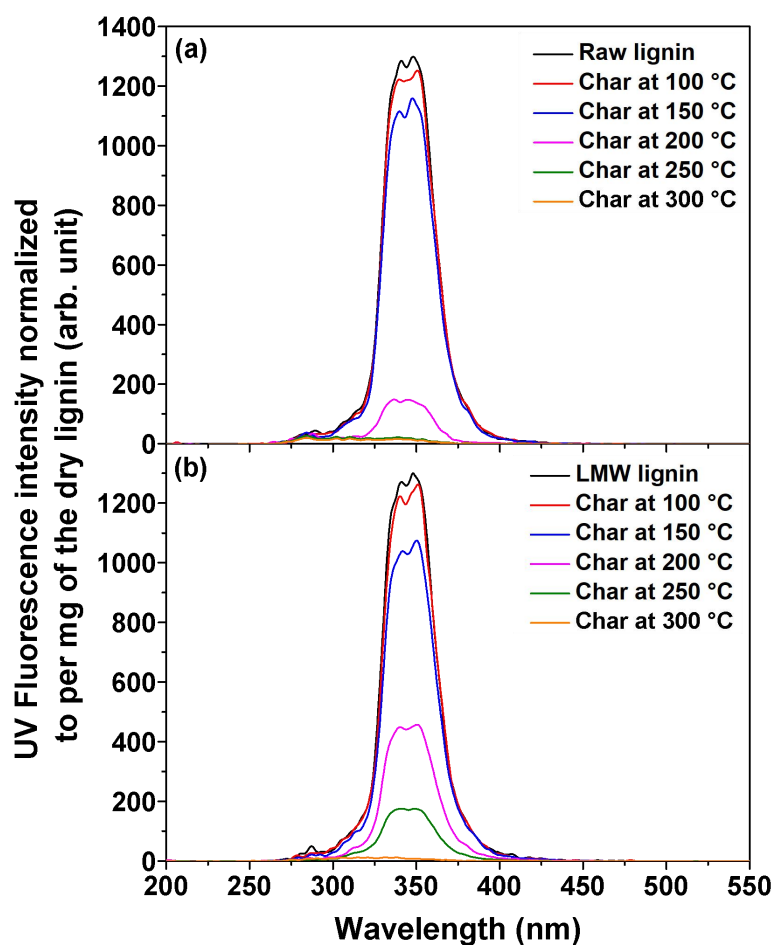


Figure 6.6: UV Fluorescence spectra of the chars from the pyrolysis of the raw and LMW lignin samples at 100–300 °C. Panel (a) chars from the raw lignin. Panel (b) chars from the LMW lignin

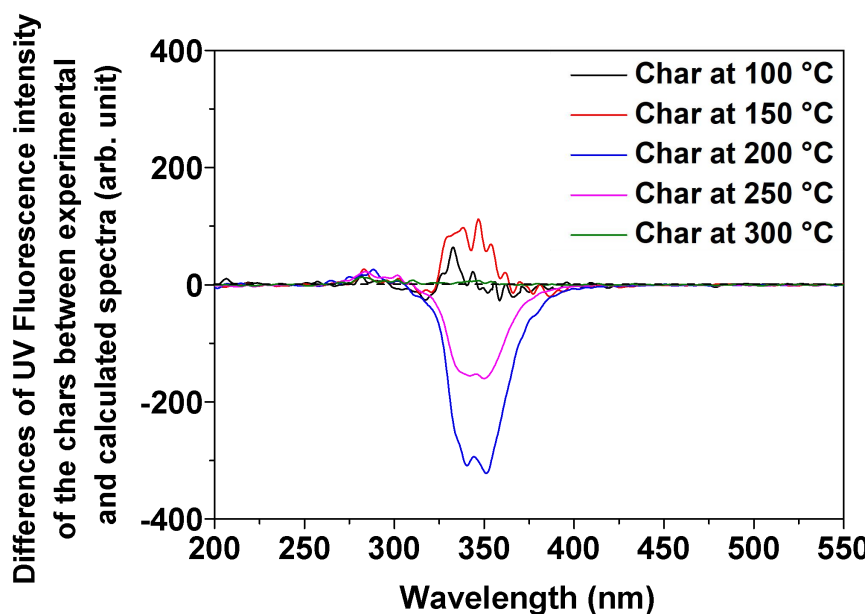


Figure 6.7: Differences between the UV fluorescence intensities of the raw lignin chars and the calculated UV fluorescence intensities based on the percentages of the LMW portion in the raw lignin and their corresponding UV fluorescence intensities of chars produced at 100–300 °C

### 6.5 Discussion on the Interactions between the LHW and HMW Portions of Lignin during Pyrolysis

The above results clearly demonstrate the interactions between the LMW and HMW portions of lignin during pyrolysis. Due to the presence of mainly light compounds in the LMW lignin, the pyrolysis of the LMW lignin can start at a temperature of ~100 °C, lower than that (i.e., ~150°C) of the HMW lignin. The interactions between the LMW and HMW portions of lignin can be clearly seen at 150 °C, because a difference between the char yield of the raw lignin and that calculated based on the LMW and HMW portions of lignin can be found at that temperature. This is probably due to the softening and melting of lignin to form a liquid intermediate phase at ~140 °C [36]. Due to the formation of a liquid phase, the evaporation of small compounds produced from the HMW portion becomes more difficult, leading to a higher char yield for the raw lignin. Such a difference in the char yield increases with pyrolysis temperature, indicating the enhanced interactions between the LMW and HMW portions of lignin at increased temperatures.

The interactions between the LMW and HMW portions of lignin can affect the char structural changes during lignin pyrolysis. At 100 °C, such interactions have small effect on the char structure during lignin pyrolysis, as shown from the differences between the FT-IR (see Figure 6.5) and UV Fluorescence spectra (see Figure 6.7) of the raw lignin char and those calculated based on the THF-soluble and the THF-insoluble lignin. However, the effect of interactions increases with temperature. At 150 °C, obvious differences in the FT-IR and UV Fluorescence spectra between the raw lignin char and those calculated results can be seen. At higher temperatures (> 200 °C), the effect of interactions become more significant, since the differences between the FT-IR and UV Fluorescence spectra of the raw lignin char and those calculated results even become negative. This clearly shows that the interactions between the LMW and HMW portions of lignin lead to the enhanced polymerization of various functional groups to form more char.

Therefore, the results in this study provide direct evidence to show the interactions between the LMW and HMW portions of lignin during pyrolysis. Due to the presence of mainly light compounds, the LMW lignin can easily melt during pyrolysis at a low temperature, leading to the formation of a liquid phase. The formation of a liquid phase suppresses the release of the volatiles produced from both the LMW and HMW portions of lignin, hence promoting the secondary reactions (i.e., polymerization reactions) within the liquid phase to form more char with more condensed structures.

## 6.6 Conclusions

This study reports the interactions between of the LMW and HMW portions of lignin during pyrolysis at low temperatures of 100–300 °C. Due to the present of mostly light compounds in the LMW lignin, its pyrolysis starts at a lower temperature (i.e., 100 °C) than that (i.e., ~150°C) of the HMW lignin, and its char yield reduces more significantly as pyrolysis temperature increases. When comparing the differences in the char yields between the raw lignin pyrolysis and those calculated based on the LMW and HMW portions of lignin, obvious interactions between the LMW and HMW portions of lignin can be observed even at a low temperature of ~150°C, leading to the formation of more char from the whole lignin pyrolysis. Such interactions are enhanced at higher pyrolysis temperatures, evidenced by an increase

in the char yield difference between the raw lignin and the calculated results as temperature increases, i.e., from 0.5wt% at 100 °C to 10.7wt% at 300 °C. The interactions not only increase the char yield but also change the char structures during the whole lignin pyrolysis. Our results show that the interactions between the LMW and HMW portions of lignin enhance the polymerization reactions of oxygenated functional groups and aromatic structures with fused rings of 2–5 to form more condensed aromatic structures with lower atomic O/C and H/C ratios.

---

## Chapter 7 Effect of Cellulose-Lignin Interactions on Char Structural Changes during Fast Pyrolysis at Low Temperatures

### 7.1 Introduction

Lignocellulosic biomass is a renewable feedstock widely utilized in thermochemical processes such as pyrolysis [264] and comprises of three major components (cellulose, hemicellulose and lignin) [265]. Each component exhibits different pyrolysis behaviour upon heating. Under non-catalytic conditions, hemicellulose decomposes rapidly at  $\sim 220$  °C, followed by cellulose decomposition at  $\sim 300$  °C, while lignin decomposes over a wide range of temperatures from 160 to 900 °C [127, 266]. The differences in properties and compositions of these biomass components strongly affect both pyrolysis mechanisms and product distributions [267, 268].

During lignocellulosic biomass pyrolysis, different biomass components may interact with each other. Hosoya et al. [268] observed significant interactions between cellulose and lignin at 800 °C, while interactions between cellulose and hemicellulose are weak. On one hand, the presence of cellulose inhibits the polymerization of lignin-derived species and enhances the formation of light compounds (such as guaiacol) from lignin. On the other hand, the presence of lignin also influences cellulose pyrolysis. It is known that cellulose pyrolysis mainly produces anhydro-sugars (i.e., levoglucosan) as primary products [233], which tend to polymerize into char within the liquid intermediate phase, or evaporate into volatiles [269]. The presence of lignin not only suppresses the polymerization of levoglucosan into char, but also promotes the formation of some light compounds such as furfural, 5-HMF and acetic acid [269, 270].

However, previous studies on the interactions of cellulose and lignin mainly focused on the characterisation of the volatiles from co-pyrolysis of cellulose and lignin [46, 268, 270, 271]. The knowledge on the characteristics and properties of chars produced from co-pyrolysis of lignin and cellulose is limited, while such knowledge is essential to understanding the pyrolysis mechanism of lignocellulosic biomass.



Therefore, the main objective of this study is to understand the effect of cellulose-lignin interactions on char structure changes during co-pyrolysis of cellulose and lignin at 100–350 °C.

## 7.2 Yields and Properties of the Chars Produced from the Fast Pyrolysis of Cellulose, Lignin and Cellulose-lignin Mixture

Figure 7.1 presents the char yields of the fast pyrolysis of cellulose, lignin and cellulose-lignin mixture at 100–350 °C. Cellulose decomposition is slow at temperatures < 250 °C, with char yields reducing from ~99% at 100 °C to ~96% at 250 °C, but becomes substantial at temperatures >250 °C with a char yield of only ~6% at 350 °C. Compared to cellulose, lignin decomposes gradually as temperature increases, with char yields reducing from ~96% at 100 °C to ~46% at 350 °C. For cellulose-lignin mixture, the char yield decreases gradually from ~98% at 100 °C to ~64% at 300 °C, but decreases rapidly to ~34% at 350 °C. The char yields were also calculated based on the mass ratio (1:1) of cellulose and lignin in the mixture and the individual char yields at various temperatures, assuming the pyrolysis of cellulose and lignin takes place independently. The experimental and calculated char yields are also compared in Figure 7.1. It can be clearly seen that the calculated char yields are higher than the experimental results at 250 °C or below, with the difference increasing from ~2% at 150 °C to ~6% at 250 °C. There is almost no difference between the char yields from experiment and calculation at 300 °C, but such a difference increases to ~8% at 350 °C. These results clearly demonstrate the existence of cellulose-lignin interactions during co-pyrolysis of cellulose and lignin.

The sugar contents (i.e., glucose) of char samples from the fast pyrolysis of cellulose, lignin and cellulose-lignin at 100–350 °C were determined via acid hydrolysis, with the results presented in Figure 7.2. After post hydrolysis, all sugar structures in the char samples are converted into glucose. Very little amount of glucose (i.e., ~0.1%) could be detected from lignin post hydrolysis. The glucose yield of the char from cellulose decreases progressively with temperature, from ~98% at 100 °C to ~58% at 300 °C, then to zero at 350 °C, indicating the complete destruction of sugar structures at 350 °C. For the cellulose-lignin mixture, the glucose yield of the char reduces from ~49% at 100 °C to ~22% at 300 °C, then to zero at 350 °C. To study the effect of cellulose-lignin interactions on the sugar structures, the sugar yields of the chars

were also calculated based on the mass ratio (1:1) of cellulose and lignin in the mixture and their corresponding glucose yields at various temperatures, and the experimental and calculated results are also presented in Figure 7.2. It can be seen that there are no obvious differences between the experimental and calculated sugar yields at 150 °C or below. However, the glucose yields from experiments are slightly lower than the calculated results at temperatures > 150°C, demonstrating that the presence of lignin indeed affects the decomposition of sugar structures during cellulose pyrolysis. The difference between the experimental and calculated sugar yields increases slightly from ~5% at 200 °C and ~7% at 300 °C. At 350°C, since all sugar structures are decomposed, there are no differences between the experimental and calculated results. Clearly, these results demonstrate that the presence of lignin enhances the decomposition of sugar structures during cellulose pyrolysis, leading to reduced sugar yields in the char.

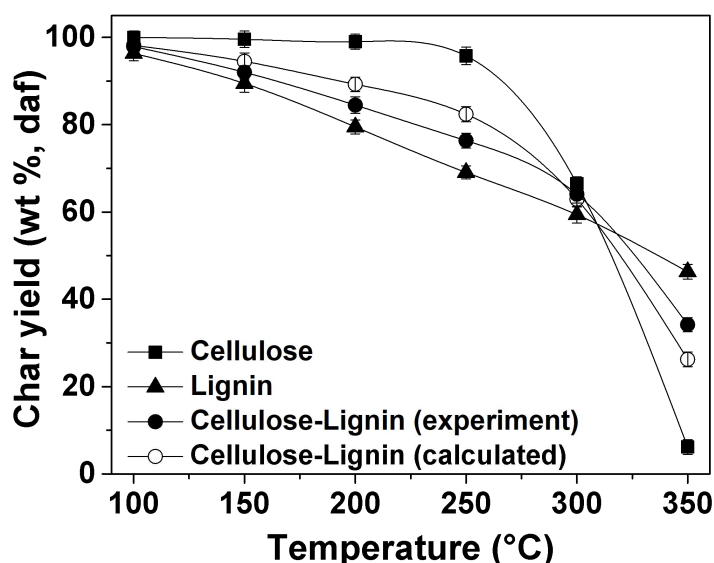


Figure 7.1: Char yield from the pyrolysis of lignin, cellulose and cellulose-lignin mixture at 100–350 °C

The elemental compositions of all raw samples and chars are listed in Table 7.1. The carbon content of cellulose char only increases slightly from ~42.7% at 100 °C to ~47.5% at 350 °C, accompanied by the decreasing hydrogen and oxygen contents from ~6.1 to ~5.1.2% at 100 °C to ~5.5 and ~46.9% at 350 °C, respectively. This leads to reductions in the atomic H/C and O/C ratios from 1.72 and 0.90 at 100 °C to 1.39 and 0.74 at 350 °C, respectively. In comparison, the carbon content of lignin

char increases from ~64.6 to ~71.4% with increasing temperature from 100 to 350 °C, accompanied by the decreasing hydrogen and oxygen contents from ~5.8 and ~23.9% at 100 °C to ~5.0 to ~23.4% at 350 °C, respectively. This leads to a reduction in the H/C atomic ratio from 1.08 at 100 °C to 0.84 at 350 °C, as expected because lignin char becomes more condensed as temperature increases. As for the chars from the cellulose-lignin mixture, the carbon content also increases from ~52.8% at 100 °C to ~58.8% at 350 °C, with the hydrogen and oxygen contents reducing from ~6.0 to ~40.2% at 100 °C and ~5.4 to ~35.7% at 350 °C. The atomic H/C and O/C ratios also decrease from 1.33 and 0.56 at 100 °C to 1.10 and 0.46 at 350 °C, respectively. To further investigate the effect of cellulose-lignin interactions on elemental composition of char during co-pyrolysis, the calculated atomic ratios of H/C and O/C based on the mass ratio (1:1) of cellulose and lignin in the mixture and their corresponding elemental compositions at various temperatures are also presented in Table 7.1 for comparisons. The experimental H/C ratio is slightly lower than the calculated H/C ratio at 250 °C or below, but higher at temperatures >250 °C. Similar trends can be observed for the O/C ratio. The results further demonstrate that the cellulose-lignin interactions enhance cellulose decomposition at temperatures  $\leq$  250 °C but suppress the condensation reactions at temperatures > 250 °C.

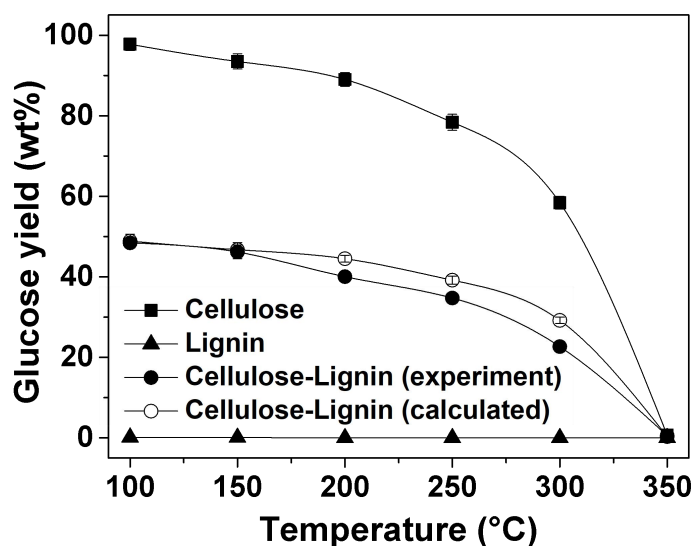


Figure 7.2: Glucose yields from pyrolysis of cellulose, lignin and cellulose-lignin mixture at 100–350 °C

Table 7.1: Elemental compositions of the chars from the pyrolysis of cellulose, lignin and cellulose-lignin mixture at 100–350 °C.

Samples	T (°C)	Elemental Analysis (wt%, daf)				Atomic H/C		Atomic O/C	
		C	H	N	O <sup>a</sup>	exp	cal <sup>b</sup>	exp	cal <sup>b</sup>
Cellulose	RT	42.7	6.2	-	51.1	1.74	-	0.90	-
	100	42.7	6.1	-	51.2	1.72	-	0.90	-
	150	42.8	6.1	-	51.1	1.72	-	0.90	-
	200	43.0	6.1	-	51.0	1.70	-	0.89	-
	250	43.6	6.0	-	50.4	1.66	-	0.87	-
	300	45.2	5.9	-	48.9	1.56	-	0.81	-
	350	47.5	5.5	-	46.9	1.39	-	0.74	-
Lignin	RT	63.3	6.1	0.4	30.2	1.15	-	0.36	-
	100	64.6	5.8	0.3	29.3	1.08	-	0.34	-
	150	65.4	5.8	0.2	28.6	1.07	-	0.33	-
	200	65.9	5.4	0.2	28.5	0.99	-	0.32	-
	250	66.8	5.2	0.2	27.8	0.93	-	0.31	-
	300	70.0	5.0	0.3	24.7	0.85	-	0.26	-
	350	71.4	5.0	0.2	23.4	0.84	-	0.25	-
Cellulose -Lignin	RT	52.8	6.1	0.1	40.9	1.39	1.39	0.58	0.58
	100	53.8	6.0	0.1	40.2	1.33	1.34	0.56	0.57
	150	54.0	5.8	0.1	40.1	1.28	1.32	0.56	0.57
	200	54.7	5.6	0.1	39.6	1.23	1.31	0.54	0.55
	250	54.9	5.6	0.1	39.4	1.21	1.22	0.54	0.53
	300	56.1	5.5	0.1	38.3	1.18	1.13	0.51	0.48
	350	58.8	5.4	0.1	35.7	1.10	1.06	0.46	0.44

### 7.3 Structural Changes of the Chars Produced from the Fast Pyrolysis of Cellulose, Lignin and Cellulose-lignin Mixture

The structures of chars from cellulose, lignin and cellulose-lignin mixture were further characterised by a series of analytic instruments including FT-IR, UV fluorescence and NMR. The FT-IR spectra of the raw samples and their chars produced from pyrolysis at 100–350 °C are shown in Figure 7.3. The presented spectra of the char samples were all normalized to the unit mass (per mg on a dry basis) of the raw sample for direct comparisons. The peak assignments of various functional groups are summarized in Table 7.2. For the cellulose chars, the main peaks identified are –OH stretches (3352 cm<sup>-1</sup>), C–H bonds (2900 cm<sup>-1</sup>), C=O bonds (1730 cm<sup>-1</sup>), OH of methyl or absorbed H<sub>2</sub>O (1638 cm<sup>-1</sup>) and C–O–C vibrations (1050 cm<sup>-1</sup>). According to the spectra shown in Figure 7.3, the absorbance intensities of the char show slight decreases at low temperatures ( $\leq 250$  °C), and significant changes are only observed when the temperature increases to 300 °C. The slow decrease of –OH stretching at 3352 cm<sup>-1</sup> can be attributed to dehydration reactions of

hydroxyl groups [272, 273]. The band associated to C–H at  $2900\text{cm}^{-1}$  shows the rupture of aliphatic groups of alkyl compounds in cellulose char. It is important to point out that the peak at  $1730\text{ cm}^{-1}$  begins to form at  $\geq 300\text{ }^\circ\text{C}$ , indicating the formation of new C=O functional groups (via mechanisms such as dehydration, ring opening and polymerization reactions [274]). The band observed at  $1638\text{ cm}^{-1}$  is reported as the –OH bending (due to the absorption of water [273]), known to be produced from dehydration reactions of polysaccharides to form anhydro-sugars [274]. The peak at  $1050\text{ cm}^{-1}$  is the C–O–C bridge stretching of pyranose saccharide rings, and its intensity decreases with temperature.

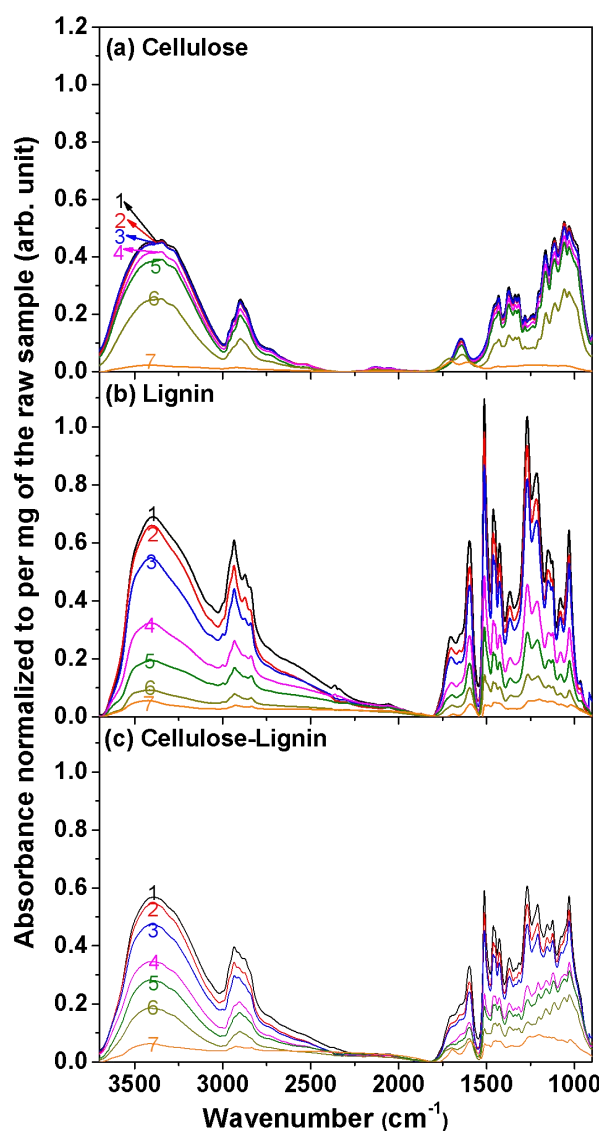


Figure 7.3: FT-IR spectra of the chars from the pyrolysis of cellulose, lignin and cellulose-lignin mixture at  $100\text{--}350\text{ }^\circ\text{C}$ . Panel (a) cellulose and its chars: (1) cellulose; (2)  $100\text{ }^\circ\text{C}$ ; (3)  $150\text{ }^\circ\text{C}$ ; (4)  $200\text{ }^\circ\text{C}$ ; (5)  $250\text{ }^\circ\text{C}$ ; (6)  $300\text{ }^\circ\text{C}$ ; (7)  $350\text{ }^\circ\text{C}$ . Panel (b) lignin and its chars: (1) raw lignin; (2)  $100\text{ }^\circ\text{C}$ ; (3)  $150\text{ }^\circ\text{C}$ ; (4)  $200\text{ }^\circ\text{C}$ ; (5)

250 °C; (6) 300 °C; (7) 350 °C. Panel (c) cellulose-lignin mixture and its chars: (1) cellulose-lignin mixture; (2) 100 °C; (3) 150 °C; (4) 200 °C; (5) 250 °C; (6) 300 °C; (7) 350 °C.

As for the lignin chars, the main functional groups also reduce as temperature increases, including –OH stretches ( $3419\text{ cm}^{-1}$ ), aliphatic C–H ( $2938\text{ cm}^{-1}$ ), –CH<sub>3</sub> stretches ( $2844\text{ cm}^{-1}$ ), C=O bonds ( $1704\text{ cm}^{-1}$ ), aromatic ring vibrations ( $1513\text{ cm}^{-1}$ ) and C–O bonds ( $1033\text{ cm}^{-1}$ ). However, the absorbance intensities of the lignin chars show obvious reductions even at 150 °C, which is expected since lignin decomposition starts at a lower temperature (i.e.,  $\sim 100\text{ °C}$ ) than that ( $\sim 200\text{ °C}$ ) for cellulose [260]. It is noted that the intensities at 350 °C are very weak. This can be attributed to the transformation of these functional groups into highly aromatic structures (invisible to FT-IR) via various reactions (e.g. fragmentation, demethylation and decarbonylation [275]), eliminating aliphatic and phenolic components [276, 277].

Table 7.2: Peak assignments for FT-IR spectra of lignin [35, 37, 172] and of cellulose samples [278-280].

Components	Wavenumbers ( $\text{cm}^{-1}$ )	Assignments
Cellulose	3352	OH stretching
	2900	CH stretching
	1730	C=O groups
	1638	Absorbed water by –OH fibers
	1430	CH <sub>2</sub> bending vibrations
	1375	CH deformation vibrations
	1240	OH in plane bending
	1050	C–O–C of pyranose ring
Lignin	3419	OH stretching
	2860-3000	Aliphatic CH stretching
	2844	CH <sub>3</sub> stretching of methoxyl group
	1704	C=O unconjugated to ketones, carbonyl and esters
	1612	C=O stretching conjugated to aromatic ring
	1513	Aromatic ring stretching
	1221-1234	C–C plus C–O
	1155	Aromatic CH stretching of guaiacyl ring
1125	Aromatic CH stretching of syringyl ring	
1033	C–O stretch in primary alcohol	

For the chars from cellulose-lignin mixture, all the absorption bands decrease with increasing temperature. The major difference lies in the wavenumber of 1000–1700  $\text{cm}^{-1}$ . The intensities of various functional groups gradually decrease as temperature increases. However, the spectra of the chars at 1000–1700  $\text{cm}^{-1}$  appear to decrease greatly at 200 °C, mainly due to lignin pyrolysis. The –OH stretching and aliphatic groups C–H decrease with increasing temperature, showing the release of alkyl chains substituent and phenolic compounds (monomers or oligomers). The aromatic bands mostly between 1513 and 1125  $\text{cm}^{-1}$  also decrease with increasing temperature. Major reductions in functional groups take place at 300 °C, mainly due to cellulose pyrolysis. The C–O–C bonds derived from saccharides decrease rapidly and majority of them diminish at 350 °C.

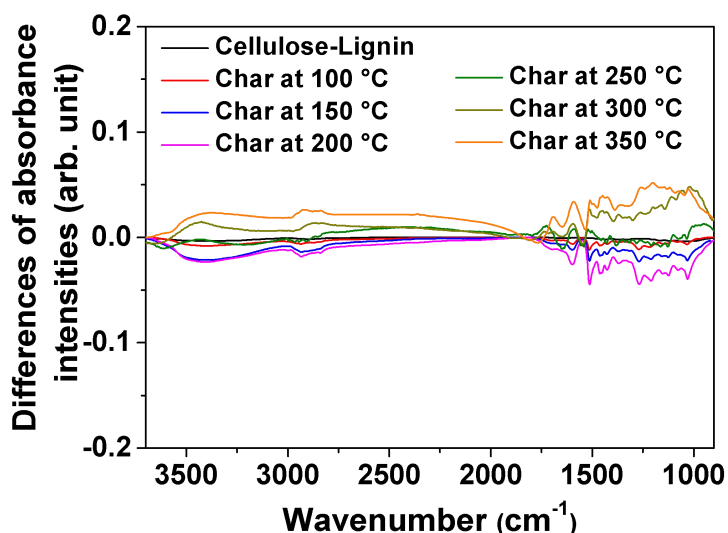


Figure 7.4: Differences between the experimental and calculated FT-IR absorbance intensities of chars for the pyrolysis of cellulose-lignin mixture at 100–350 °C

The FT-IR spectra of the chars from experiments were compared with the calculated spectra based on the mass ratio (1:1) of cellulose and lignin in the mixture and the corresponding FT-IR spectra of chars produced from pyrolysis individually. The differences between the experimental and calculated intensities of the spectra (i.e., subtracting the calculated spectra from the experimental spectra) are presented in Figure 7.4. At temperatures  $\leq 200$  °C, negative intensities between the experimental and calculated FT-IR spectra can be seen, i.e. the experimental results are lower than the calculated results. Since the reactions of cellulose pyrolysis are minimal at temperatures  $< 200$  °C, the results indicate that the releases of lignin-derived

volatiles are enhanced during co-pyrolysis of cellulose and lignin. However, positive intensities between the experimental and calculated FT-IR spectra can be found at temperatures  $\geq 300$  °C, indicating that more chemical functional groups from cellulose are retained in the chars at 300 °C and above.

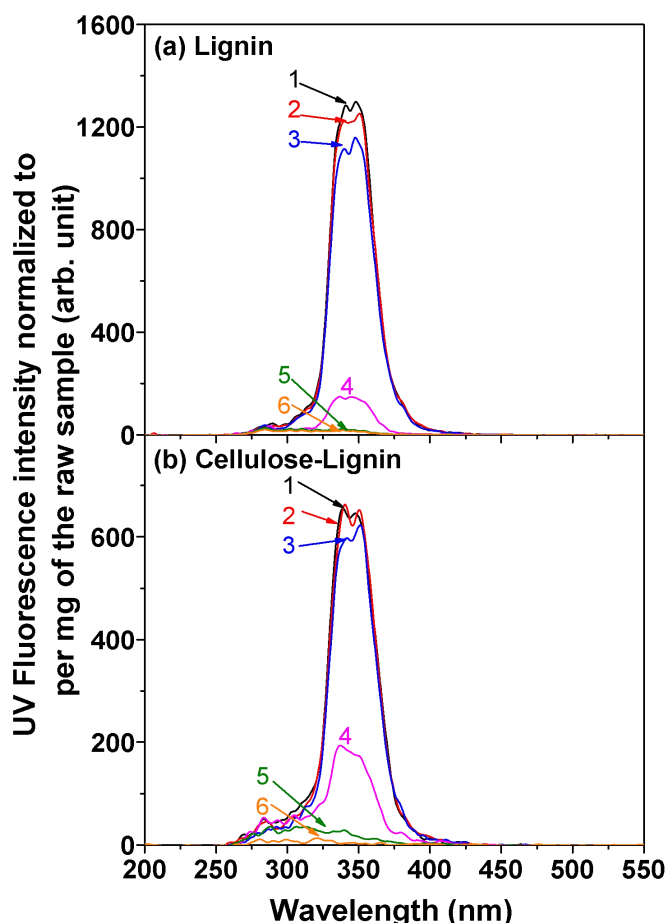


Figure 7.5: UV fluorescence spectra of the chars from the pyrolysis of lignin and cellulose-lignin mixture at 100–300 °C. Panel (a) lignin and its chars: (1) lignin; (2) 100 °C; (3) 150 °C; (4) 200 °C; (5) 250 °C; (6) 300 °C. Panel (b) cellulose-lignin mixture and its chars: (1) cellulose-lignin mixture; (2) 100 °C; (3) 150 °C; (4) 200 °C; (5) 250 °C; (6) 300 °C

The lignin, cellulose-lignin mixture and respective char samples were dissolved in THF, and the dissolved samples were analysed by UV fluorescence spectrometer to investigate the changes of the aromatic fused ring structures during pyrolysis. Figure 7.5 shows the UV fluorescence spectra of the chars produced from the pyrolysis of lignin and cellulose-lignin mixture at 100–300 °C. It should be noted that there are no UV fluorescence intensities from the cellulose chars. For the chars from lignin



and cellulose-lignin mixture, a broad peak can be seen from the spectra in the wavelength range of 250–400 nm, with mono ring at < 290 nm, 2–3 fused rings at 290–340 nm, 3–5 fused rings at 340–390 nm [257]. To enable direct comparisons, all the UV fluorescence spectra were normalized to the unit mass (per mg on a dry basis) of the raw sample, and the results are shown in Figure 7.5. For lignin pyrolysis, the UV fluorescence intensities decrease slowly as temperature increases to 150 °C, indicating the slow release of light lignin compounds (i.e., the so-called low-molecular-weight portion of lignin [281]). However, significant reductions in the UV fluorescence intensities can be found at 200 °C, and almost no signals can be detected at 250 °C. This can be attributed to the softening and melting of lignin at ~140 °C, generating a liquid intermediate phase that suppresses the release of volatile compounds from lignin hence forming a char with more aromatic characteristics. The UV fluorescence intensities of the chars from the pyrolysis of cellulose-lignin mixture follow a similar trend, but the reductions in aromatic fused ring structures are much slower at 200 °C, indicating polymerization of lignin-derived aromatic structures being suppressed during co-pyrolysis.

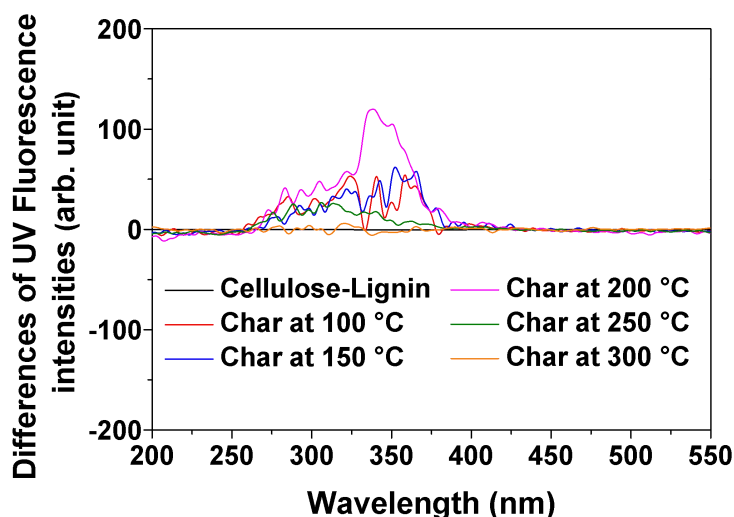


Figure 7.6: Differences between the experimental and calculated UV fluorescence intensity of the chars for the pyrolysis of cellulose-lignin mixture at 100–300 °C

The UV fluorescence intensities of the chars from experiments were also compared with the calculated spectra based on the mass ratio (1:1) of cellulose and lignin in the mixture and their corresponding UV fluorescence intensities of chars produced at various temperatures. The differences between the experimental and calculated UV

fluorescence intensities (i.e., subtracting the calculated intensities from the experimental intensities) are plotted in Figure 7.6. The experimental results are higher than the calculated results, due to the positive UV fluorescence intensities between the experimental and calculated results. As the temperature increases, the differences of UV fluorescence intensities increase slowly and reach maximum at 200 °C, followed by decreases as temperature further increases. More aromatic structures of 2–5 fused rings are retained in the char during co-pyrolysis of lignin and cellulose, especially at 200 °C, demonstrating that the presence of cellulose suppresses the polymerization of aromatic structures in lignin during co-pyrolysis of cellulose and lignin.

The solid state  $^{13}\text{C}$  CP/MAS NMR analysis was also used to study the changes of carbon structure in the chars from the pyrolysis of cellulose, lignin and cellulose-lignin mixture, and the results are presented in Figure 7.7. The assignment of carbons in cellulose are listed as: C1 at 100–108 ppm, combination of C2/C3/C5 at 70–78 ppm, C4 at 81–91 ppm and C6 at 60–66 ppm [282]. For cellulose pyrolysis, there are negligible changes in the spectra of chars at temperatures  $\leq 200$  °C, as expected. At 300 °C, the spectrum shows the decomposition of sugar structures, since cellulose decomposition starts at 250 °C. The sharp resonance peaks of the NMR spectra of cellulose char also disappear at 300 °C. For lignin pyrolysis, the carbon groups are assigned as follows: aliphatic C at 10–50 ppm, methoxyl C at 50–90 ppm, aromatic C at 102–155 ppm and carbonyl C at 160–220 ppm [283]. The spectra of lignin chars show decreasing peaks of aliphatic and methoxyl carbons, but increasing peaks of aromatic carbons as temperature increases from 100 to 300 °C. The NMR spectra indicate that the aliphatic and methoxyl carbon structures are gradually transformed into more condensed aromatic structures as temperature increases during lignin pyrolysis.

The spectra of chars from the pyrolysis of cellulose-lignin mixture show overlapping characters from both lignin and cellulose structures. As the temperature increases from 100 to 300 °C, the NMR spectra show decreasing aliphatic and methoxyl carbon structures from lignin, while the sugar structures from cellulose only experience slight reductions at 300 °C. It is interesting to see that the sugar structures are still present in the char from cellulose-lignin co-pyrolysis even at 300 °C, in

contrast to the significant destruction of sugar structures during cellulose pyrolysis alone. The results demonstrate that part of sugar structures are preserved during co-pyrolysis of cellulose and lignin.

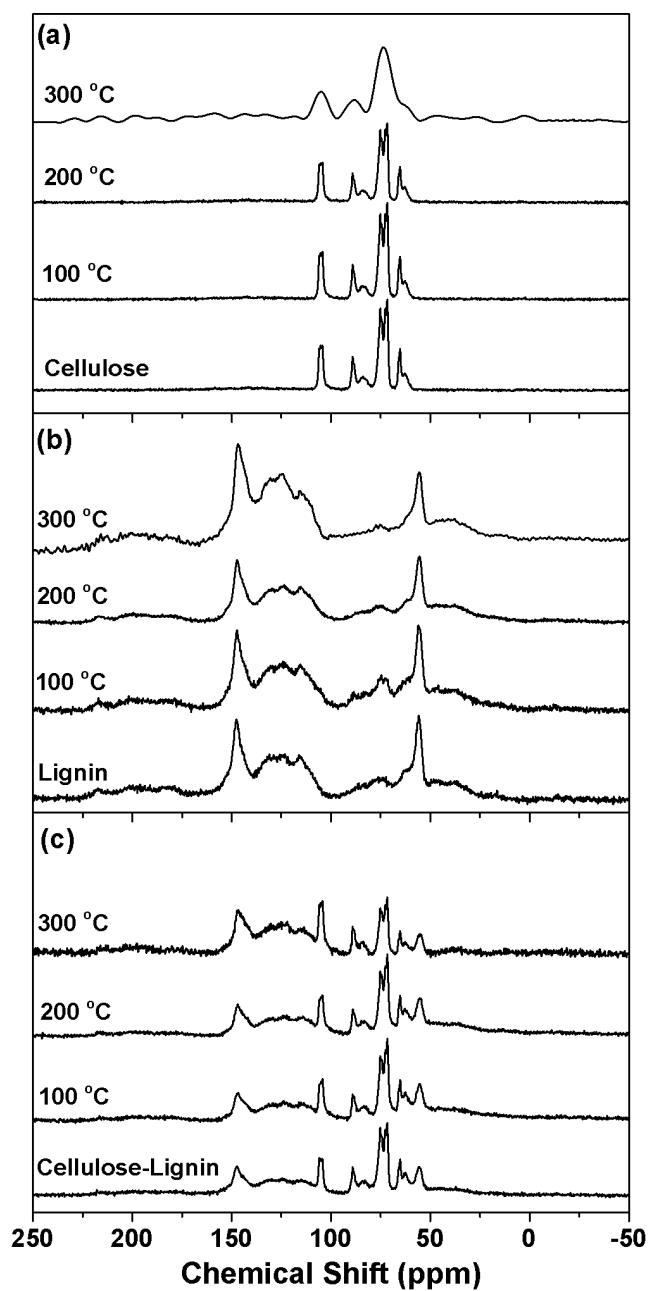


Figure 7.7:  $^{13}\text{C}$  CP/MAS NMR spectra of the chars from the pyrolysis of cellulose, lignin and cellulose-lignin mixture at 100–300 °C. (a) Cellulose and its chars; (b) lignin and its chars; (c) cellulose-lignin mixture and its chars.

#### 7.4 Discussion on the Cellulose-lignin Interactions during Co-pyrolysis of Cellulose and Lignin

The experimental results presented in this study clearly demonstrate the existence of interactions between cellulose and lignin during co-pyrolysis. The cellulose-lignin interactions affect both char yields and char structures during co-pyrolysis. At temperatures  $\leq 250$  °C, pyrolysis of cellulose-lignin mixture leads lower char yields than the theoretically-calculated values (assuming no synergies), with the differences between the experimental and calculated char yields increasing from  $\sim 2\%$  at 150 °C to  $\sim 6\%$  at 250 °C. This demonstrates the presence of cellulose enhances the release of lignin-derived compounds, due to the hydrogen donation from the cellulose-derived compounds to stabilize the reactive species from lignin pyrolysis. The hydrogen could be the mobile protons possibly generated from the cellulose-derived products in the liquid intermediates during cellulose-lignin pyrolysis, as evidenced by Shrestha et al. [36] in their in situ  $^1\text{H}$  NMR experiments. It is known that reaction intermediates (mainly sugar and anhydro-sugar oligomers) can be produced from cellulose pyrolysis even at 150 °C [284]. Those intermediates can easily participate in lignin pyrolysis reactions as hydrogen donors. Eventually, this leads to suppressed polymerization of lignin-derived species and increased release of light compounds from lignin pyrolysis, resulting in reduced char yields. Meanwhile, the UV fluorescence spectra (see Figure 7.6) also indicate more retention of aromatic structures with 2-5 fused rings during co-pyrolysis of cellulose and lignin. Since the reaction intermediates from cellulose pyrolysis are involved in lignin pyrolysis reactions as hydrogen donors, the sugar content in the char from co-pyrolysis of cellulose and lignin is also slightly reduced, compared to the calculated sugar content.

At temperatures  $> 250$  °C, cellulose pyrolysis becomes more important. Due to the enhanced destruction of sugar structures at temperatures  $\leq 250$  °C, the volatiles released from cellulose pyrolysis are reduced hence increasing the char formation from cellulose. This is supported by the FT-IR and NMR results (see Figure 7.4), which show increased retention of cellulose structures at temperatures  $> 250$  °C. As a result, pyrolysis of cellulose-lignin mixture leads higher char yields than the theoretically-calculated values, with the difference between the experimental and calculated char yields increasing from  $\sim 1\%$  at 300 °C to  $\sim 8\%$  at 350 °C.

## 7.5 Conclusions

This study reports the effect of cellulose-lignin interactions on the structural changes of chars during fast pyrolysis at 100–350 °C. Co-pyrolysis of cellulose and lignin leads to a reduced char yield at low temperatures ( $\leq 250$  °C) but an increased char yield at high temperatures ( $> 250$  °C), compared to the calculated char yield from the pyrolysis of cellulose and lignin individually. At temperatures  $\leq 250$  °C, the retention of lignin functional groups is found to reduce in the char from co-pyrolysis of cellulose and lignin, likely due to the formation of reaction intermediates (i.e., anhydro-sugars) from cellulose pyrolysis, which can stabilize the reactive species from lignin pyrolysis as hydrogen donors. This leads to enhanced evaporation and suppressed polymerization of lignin-derived species, thus reducing the char yield. The differences between the experimental and calculated char yields increase with temperature, from ~2% at 150 °C to ~6% at 250 °C. As a result, the destruction of sugar structures in cellulose is enhanced at temperatures  $\leq 250$  °C, as evidenced by reduced sugar content of the char. This leads to increased char formation from cellulose pyrolysis at temperatures  $> 250$  °C, as evidenced by increased retention of cellulose functional groups in the char from co-pyrolysis of cellulose and lignin. The difference between the experimental and calculated char yields increases from ~1% at 300 °C to ~8% at 350 °C.

---

## Chapter 8 Conclusions and Recommendations

### 8.1 Conclusions

This research work leads to a better understanding on the current knowledge of lignin and its derived compounds pyrolysis mechanisms, particularly at low temperatures. This chapter summarizes the key findings from this present study and outlines the recommendations for future study in this research area.

#### 8.1.1 Thermal Decomposition of Pyrolytic Lignin under Inert Conditions at Low Temperatures

- The major reduction in char yield is contributed by the light lignin-derived aromatic oligomers, which can easily decomposed during fast pyrolysis.
- The presences of both light and heavy lignin-derived aromatic oligomers interact with each other and enhanced the char formation during the thermal decomposition reaction.
- The main reactions take place during the pyrolysis of pyrolytic lignin include the cleavage of aliphatic, demethylation and decarbonylation, mainly due to the rupture of ether linkages in the pyrolytic lignin structure, resulting in the release of phenolic compounds.
- The chars produced from pyrolysis of pyrolytic lignin at higher temperature (i.e.,  $T > 300\text{ }^{\circ}\text{C}$ ) consist of mainly heavy lignin-derived aromatic oligomers.
- The presence of mostly heavy aromatic oligomers in the char from pyrolytic lignin pyrolysis at temperature  $> 250\text{ }^{\circ}\text{C}$  tends to polymerize, leads to the formation of more char.

#### 8.1.2 Structural Changes of Chars Produced from Fast Pyrolysis of Lignin at Low Temperatures

- The low-molecular-weight portion of lignin is appeared to be an important precursor of not only volatiles formation due to decomposition but also char formation via polymerization reactions.
- The low-molecular-weight portion of lignin can be easily undergo melting and softening to form a liquid intermediate phase at low temperatures, and affects the char structures during pyrolysis.

- The polymerization reactions become increasingly significant at temperature  $\geq 175$  °C, resulting in the transformation of THF-soluble portion into the THF-insoluble portion.
- Further elevating the pyrolysis temperature  $> 250$  °C leading to the formation of more condensed char structure due to the major depletion of hydroxyl, aliphatic, methoxyl and carbonyl/carboxyl groups.

### **8.1.3 Interactions between Low- and High-molecular-weight Portions of Lignin during Fast Pyrolysis at Low Temperatures**

- The interactions between the low- and high-molecular-weight portions of lignin also lead to the formation of more char with condensed structures.
- The formation of liquid intermediate mainly due to the decomposition of the low-molecular-weight species in lignin at low temperature of 100 °C, suppressed the release of volatiles from both THF-soluble and THF-insoluble portions.
- The reaction temperature seems to affect the interactions between the low-molecular-weight species in lignin, thus change the char structures during pyrolysis.
- Above temperature of 200 °C, the polymerization reactions of the oxygenated compounds are greatly enhanced to form char with larger aromatic ring and condensed structure.

### **8.1.4 Effect of Cellulose-lignin Interactions on Char Structural Changes during Fast Pyrolysis at Low Temperatures**

- The interactions between cellulose and lignin not only affect the char yield but also the char structure during the co-pyrolysis of cellulose and lignin even at low temperatures.
- The reduction in char yield is mainly due to the enhanced evaporation of lignin-derived species and the cellulose-derived products suppress the polymerization of aromatic structure in lignin at low temperatures ( $\leq 250$  °C).
- The presence of reaction intermediates in molten phase, mainly produced from cellulose pyrolysis at lower temperature of 150 °C, actively participate as hydrogen donors to stabilize the reactive species from lignin pyrolysis.

- At higher temperatures ( $> 250$  °C), additional char formation apparently due to enhanced polymerization of cellulose-derived species.

## **8.2 Recommendations**

Based on the findings from the present study, the following new research gaps are recommended for future work:

- It is desired to further characterize the char products, especially those produced from higher pyrolysis reaction temperatures to understand the form of the structure that retained in char, as some analysis techniques could only analyse the soluble portion via solvent extraction.
- Further investigations on the reaction intermediates formation in liquid phase, considering the in situ analysis.
- It is also desired to study the effect of loading various AAEM species (e.g., NaCl, KCl, MgCl<sub>2</sub> and CaCl<sub>2</sub>) on the intermediates formation mechanisms during the pyrolysis reaction of lignin and its derived compounds.
- Current study focusing on the homogeneous mixture of cellulose and lignin, in a mass ratio of 1:1 for the interactions investigation. Extended research can be studied on the heterogeneous structure of cellulose-lignin mixture or in variety of mixing ratio, to examine their influence on pyrolysis mechanisms.



## REFERENCES

- [1] D. Iribarren, J.F. Peters, J. Dufour, Life cycle assessment of transportation fuels from biomass pyrolysis, *Fuel* 97 (2012) 812-821.
- [2] M. Lenzen, R. Schaeffer, Historical and potential future contributions of power technologies to global warming, *Climatic Change* 112 (3) (2012) 601-632.
- [3] Enerdata. Global Energy Statistical Yearbook 2018. Available from: <https://yearbook.enerdata.net/total-energy/world-consumption-statistics.html>.
- [4] A.V. Bridgwater, Renewable fuels and chemicals by thermal processing of biomass, *Chemical Engineering Journal* 91 (2) (2003) 87-102.
- [5] M. Ni, D.Y.C. Leung, M.K.H. Leung, K. Sumathy, An overview of hydrogen production from biomass, *Fuel Processing Technology* 87 (5) (2006) 461-472.
- [6] H. Abdullah, H. Wu, Biochar as a Fuel: 1. Properties and Grindability of Biochars Produced from the Pyrolysis of Mallee Wood under Slow-Heating Conditions, *Energy & Fuels* 23 (8) (2009) 4174-4181.
- [7] Y. Yu, J. Bartle, C.-Z. Li, H. Wu, Mallee Biomass as a Key Bioenergy Source in Western Australia: Importance of Biomass Supply Chain, *Energy & Fuels* 23 (6) (2009) 3290-3299.
- [8] G.W. Huber, S. Iborra, A. Corma, Synthesis of Transportation Fuels from Biomass: Chemistry, Catalysts, and Engineering, *Chemical Reviews* 106 (9) (2006) 4044-4098.
- [9] S. Pang, Advances in thermochemical conversion of woody biomass to energy, fuels and chemicals, *Biotechnology Advances* (2018)
- [10] S.V. Pisupati, A.H. Tchapda, Thermochemical Processing of Biomass, in *Advances in Bioprocess Technology*, P. Ravindra, Editor. 2015, Springer International Publishing: Cham. p. 277-314.
- [11] A. Demirbas, Combustion characteristics of different biomass fuels, *Progress in Energy and Combustion Science* 30 (2) (2004) 219-230.
- [12] Chan Seung Park, Partho Sarothi Roy, S.H. Kim, Current Developments in Thermochemical Conversion of Biomass to Fuels and Chemicals, Intech Open, 2018,
- [13] S.K. Sansaniwal, M.A. Rosen, S.K. Tyagi, Global challenges in the sustainable development of biomass gasification: An overview, *Renewable and Sustainable Energy Reviews* 80 (2017) 23-43.
- [14] A.V. Bridgwater, D. Meier, D. Radlein, An overview of fast pyrolysis of biomass, *Organic Geochemistry* 30 (12) (1999) 1479-1493.
- [15] Q. Lu, W.-Z. Li, X.-F. Zhu, Overview of fuel properties of biomass fast pyrolysis oils, *Energy Conversion and Management* 50 (5) (2009) 1376-1383.
- [16] S. Czernik, A.V. Bridgwater, Overview of Applications of Biomass Fast Pyrolysis Oil, *Energy & Fuels* 18 (2) (2004) 590-598.
- [17] T. Kan, V. Strezov, T.J. Evans, Lignocellulosic biomass pyrolysis: A review of product properties and effects of pyrolysis parameters, *Renewable and Sustainable Energy Reviews* 57 (2016) 1126-1140.
- [18] A.S. Pollard, M.R. Rover, R.C. Brown, Characterization of bio-oil recovered as stage fractions with unique chemical and physical properties, *Journal of Analytical and Applied Pyrolysis* 93 (2012) 129-138.

- 
- [19] Y. Yu, D. Liu, H. Wu, Characterization of Water-Soluble Intermediates from Slow Pyrolysis of Cellulose at Low Temperatures, *Energy & Fuels* 26 (12) (2012) 7331-7339.
- [20] J.B. Wooten, J.I. Seeman, M.R. Hajaligol, Observation and Characterization of Cellulose Pyrolysis Intermediates by  $^{13}\text{C}$  CPMAS NMR. A New Mechanistic Model, *Energy & Fuels* 18 (1) (2004) 1-15.
- [21] S. Wang, X. Guo, T. Liang, Y. Zhou, Z. Luo, Mechanism research on cellulose pyrolysis by Py-GC/MS and subsequent density functional theory studies, *Bioresource Technology* 104 (2012) 722-728.
- [22] Q. Lu, X.-c. Yang, C.-q. Dong, Z.-f. Zhang, X.-m. Zhang, X.-f. Zhu, Influence of pyrolysis temperature and time on the cellulose fast pyrolysis products: Analytical Py-GC/MS study, *Journal of Analytical and Applied Pyrolysis* 92 (2) (2011) 430-438.
- [23] J. Montoya, B. Pecha, F.C. Janna, M. Garcia-Perez, Micro-explosion of liquid intermediates during the fast pyrolysis of sucrose and organosolv lignin, *Journal of Analytical and Applied Pyrolysis* 122 (2016) 106-121.
- [24] A.R. Teixeira, K.G. Mooney, J.S. Kruger, C.L. Williams, W.J. Suszynski, L.D. Schmidt, D.P. Schmidt, P.J. Dauenhauer, Aerosol generation by reactive boiling ejection of molten cellulose, *Energy & Environmental Science* 4 (10) (2011) 4306-4321.
- [25] H. Kawamoto, M. Murayama, S. Saka, Pyrolysis behavior of levoglucosan as an intermediate in cellulose pyrolysis: polymerization into polysaccharide as a key reaction to carbonized product formation, *Journal of Wood Science* 49 (5) (2003) 469-473.
- [26] J. Zakzeski, P.C.A. Bruijninx, A.L. Jongerius, B.M. Weckhuysen, The catalytic valorization of lignin for the production of renewable chemicals, *Chemical Reviews* 110 (6) (2010) 3552-3599.
- [27] W. Mu, H. Ben, A. Ragauskas, Y. Deng, Lignin Pyrolysis Components and Upgrading—Technology Review, *BioEnergy Research* 6 (4) (2013) 1183-1204.
- [28] J.C. Hicks, Advances in C–O Bond Transformations in Lignin-Derived Compounds for Biofuels Production, *The Journal of Physical Chemistry Letters* 2 (18) (2011) 2280-2287.
- [29] M. Brebu, T. Tamminen, I. Spiridon, Thermal degradation of various lignins by TG-MS/FTIR and Py-GC-MS, *Journal of Analytical and Applied Pyrolysis* 104 (2013) 531-539.
- [30] P.J. de Wild, W.J.J. Huijgen, H.J. Heeres, Pyrolysis of wheat straw-derived organosolv lignin, *Journal of Analytical and Applied Pyrolysis* 93 (2012) 95-103.
- [31] D. Ferdous, A.K. Dalai, S.K. Bej, R.W. Thring, Pyrolysis of Lignins: Experimental and Kinetics Studies, *Energy & Fuels* 16 (6) (2002) 1405-1412.
- [32] E. Jakab, O. Faix, F. Till, Thermal decomposition of milled wood lignins studied by thermogravimetry/mass spectrometry, *Journal of Analytical and Applied Pyrolysis* 40-41 (1997) 171-186.
- [33] Q. Liu, S. Wang, Y. Zheng, Z. Luo, K. Cen, Mechanism study of wood lignin pyrolysis by using TG-FTIR analysis, *Journal of Analytical and Applied Pyrolysis* 82 (1) (2008) 170-177.
- [34] D.K. Shen, S. Gu, K.H. Luo, S.R. Wang, M.X. Fang, The pyrolytic degradation of wood-derived lignin from pulping process, *Bioresource Technology* 101 (15) (2010) 6136-6146.
-

- [35] S. Wang, H. Lin, B. Ru, W. Sun, Y. Wang, Z. Luo, Comparison of the pyrolysis behavior of pyrolytic lignin and milled wood lignin by using TG-FTIR analysis, *Journal of Analytical and Applied Pyrolysis* 108 (2014) 78-85.
- [36] B. Shrestha, Y. le Brech, T. Ghislain, S. Leclerc, V. Carré, F. Aubriet, S. Hoppe, P. Marchal, S. Pontvianne, N. Brosse, A. Dufour, A Multitechnique Characterization of Lignin Softening and Pyrolysis, *ACS Sustainable Chemistry & Engineering* 5 (8) (2017) 6940-6949.
- [37] R.K. Sharma, J.B. Wooten, V.L. Baliga, X. Lin, W. Geoffrey Chan, M.R. Hajaligol, Characterization of chars from pyrolysis of lignin, *Fuel* 83 (11) (2004) 1469-1482.
- [38] S. Zhou, B. Pecha, M. van Kuppevelt, A.G. McDonald, M. Garcia-Perez, Slow and fast pyrolysis of Douglas-fir lignin: Importance of liquid-intermediate formation on the distribution of products, *Biomass and Bioenergy* 66 (2014) 398-409.
- [39] A. Dufour, M. Castro-Díaz, P. Marchal, N. Brosse, R. Olcese, M. Bouroukba, C. Snape, In Situ Analysis of Biomass Pyrolysis by High Temperature Rheology in Relations with <sup>1</sup>H NMR, *Energy & Fuels* 26 (10) (2012) 6432-6441.
- [40] V. Baliga, R. Sharma, D. Miser, T. McGrath, M. Hajaligol, Physical characterization of pyrolyzed tobacco and tobacco components, *Journal of Analytical and Applied Pyrolysis* 66 (1) (2003) 191-215.
- [41] C. Chen, D. Jin, X. Ouyang, L. Zhao, X. Qiu, F. Wang, Effect of structural characteristics on the depolymerization of lignin into phenolic monomers, *Fuel* 223 (2018) 366-372.
- [42] T. Hosoya, H. Kawamoto, S. Saka, Cellulose-hemicellulose and cellulose-lignin interactions in wood pyrolysis at gasification temperature, *Journal of Analytical and Applied Pyrolysis* 80 (1) (2007) 118-125.
- [43] Q. Liu, Z. Zhong, S. Wang, Z. Luo, Interactions of biomass components during pyrolysis: A TG-FTIR study, *Journal of Analytical and Applied Pyrolysis* 90 (2) (2011) 213-218.
- [44] S. Wang, X. Guo, K. Wang, Z. Luo, Influence of the interaction of components on the pyrolysis behavior of biomass, *Journal of Analytical and Applied Pyrolysis* 91 (1) (2011) 183-189.
- [45] N. Worasuwannarak, T. Sonobe, W. Tanthapanichakoon, Pyrolysis behaviors of rice straw, rice husk, and corncob by TG-MS technique, *Journal of Analytical and Applied Pyrolysis* 78 (2) (2007) 265-271.
- [46] J. Yu, N. Paterson, J. Blamey, M. Millan, Cellulose, xylan and lignin interactions during pyrolysis of lignocellulosic biomass, *Fuel* 191 (2017) 140-149.
- [47] J. Zhang, Y.S. Choi, C.G. Yoo, T.H. Kim, R.C. Brown, B.H. Shanks, Cellulose-Hemicellulose and Cellulose-Lignin Interactions during Fast Pyrolysis, *ACS Sustainable Chemistry & Engineering* 3 (2) (2015) 293-301.
- [48] J. Pérez, J. Muñoz-Dorado, T. de la Rubia, J. Martínez, Biodegradation and biological treatments of cellulose, hemicellulose and lignin: an overview, *International Microbiology* 5 (2) (2002) 53-63.
- [49] Y. Horikawa, T. Itoh, J. Sugiyama, Preferential Uniplanar Orientation of Cellulose Microfibrils Reinvestigated by the FTIR Technique, *Cellulose* 13 (3) (2006) 309-316.
- [50] E.M. Rubin, Genomics of cellulosic biofuels, *Nature* 454 (2008) 841.

- [51] S. Wang, G. Dai, H. Yang, Z. Luo, Lignocellulosic biomass pyrolysis mechanism: A state-of-the-art review, *Progress in Energy and Combustion Science* 62 (2017) 33-86.
- [52] J.D. Murphy, K. McCarthy, Ethanol production from energy crops and wastes for use as a transport fuel in Ireland, *Applied Energy* 82 (2) (2005) 148-166.
- [53] N. Sonil, A.K. Janusz, K.D. Ajay, Lignocellulosic Biomass: A Review of Conversion Technologies and Fuel Products, *Current Biochemical Engineering* 3 (1) (2016) 24-36.
- [54] D. Mohan, C.U. Pittman, P.H. Steele, Pyrolysis of Wood/Biomass for Bio-oil: A Critical Review, *Energy & Fuels* 20 (3) (2006) 848-889.
- [55] Y. Yu, X. Lou, H. Wu, Some Recent Advances in Hydrolysis of Biomass in Hot-Compressed Water and Its Comparisons with Other Hydrolysis Methods, *Energy & Fuels* 22 (1) (2008) 46-60.
- [56] G.W. Huber, J.A. Dumesic, An overview of aqueous-phase catalytic processes for production of hydrogen and alkanes in a biorefinery, *Catalysis Today* 111 (1) (2006) 119-132.
- [57] T. Kondo, C. Sawatari, A Fourier transform infra-red spectroscopic analysis of the character of hydrogen bonds in amorphous cellulose, *Polymer* 37 (3) (1996) 393-399.
- [58] I. Kögel-Knabner, The macromolecular organic composition of plant and microbial residues as inputs to soil organic matter, *Soil Biology and Biochemistry* 34 (2) (2002) 139-162.
- [59] F.S. Chakar, A.J. Ragauskas, Review of current and future softwood kraft lignin process chemistry, *Industrial Crops and Products* 20 (2) (2004) 131-141.
- [60] J.L. McCarthy, Lignin chemistry, technology, and utilization : a brief history, *Lignin : historical, biological, and material perspectives* (2000) 2-99.
- [61] S. Nanda, J. Maley, J.A. Kozinski, A.K. Dalai, Physico-Chemical Evolution in Lignocellulosic Feedstocks During Hydrothermal Pretreatment and Delignification, *Journal of Biobased Materials and Bioenergy* 9 (3) (2015) 295-308.
- [62] S. Beis, S. Mukkamala, N. Hill, J. Joseph, C. Baker, B. Jensen, E. Stemmler, C. Wheeler, B. Frederick, A. van Heiningen, A. Berg, W.J. DeSisto, FAST PYROLYSIS OF LIGNINS, *BioResources; Vol 5, No 3* (2010) (2010)
- [63] C.A. Mullen, A.A. Boateng, Catalytic pyrolysis-GC/MS of lignin from several sources, *Fuel Processing Technology* 91 (11) (2010) 1446-1458.
- [64] M. Wang, M. Leitch, C. Xu, Synthesis of phenol-formaldehyde resol resins using organosolv pine lignins, *European Polymer Journal* 45 (12) (2009) 3380-3388.
- [65] S.S. Mankar, A.R. Chaudhari, I. Soni, Lignin in phenol-formaldehyde adhesives, *International Journal of Knowledge Engineering* 3 (1) (2012) 116-118.
- [66] E. Gnansounou, A. Pandey, Chapter 1 - Classification of Biorefineries Taking into Account Sustainability Potentials and Flexibility, in *Life-Cycle Assessment of Biorefineries*, E. Gnansounou and A. Pandey, Editors. 2017, Elsevier: Amsterdam. p. 1-39.
- [67] I.A. Pearl, *The chemistry of lignin*, Edward Arnold (Publishers) Ltd., London, 1967, xiii + 339 pp.
- [68] J. Gierer, Chemistry of delignification, *Wood Science and Technology* 19 (4) (1985) 289-312.

- [69] G. Jiang, D.J. Nowakowski, A.V. Bridgwater, A systematic study of the kinetics of lignin pyrolysis, *Thermochimica Acta* 498 (1) (2010) 61-66.
- [70] D. Watkins, M. Nuruddin, M. Hosur, A. Tcherbi-Narteh, S. Jeelani, Extraction and characterization of lignin from different biomass resources, *Journal of Materials Research and Technology* 4 (1) (2015) 26-32.
- [71] X. Pan, C. Arato, N. Gilkes, D. Gregg, W. Mabee, K. Pye, Z. Xiao, X. Zhang, J. Saddler, Biorefining of softwoods using ethanol organosolv pulping: Preliminary evaluation of process streams for manufacture of fuel-grade ethanol and co-products, *Biotechnology and Bioengineering* 90 (4) (2005) 473-481.
- [72] B. Scholze, C. Hanser, D. Meier, Characterization of the water-insoluble fraction from fast pyrolysis liquids (pyrolytic lignin): Part II. GPC, carbonyl groups, and <sup>13</sup>C-NMR, *Journal of Analytical and Applied Pyrolysis* 58-59 (2001) 387-400.
- [73] B. Scholze, D. Meier, Characterization of the water-insoluble fraction from pyrolysis oil (pyrolytic lignin). Part I. PY-GC/MS, FTIR, and functional groups, *Journal of Analytical and Applied Pyrolysis* 60 (1) (2001) 41-54.
- [74] R.Y. Nsimba, C.A. Mullen, N.M. West, A.A. Boateng, Structure-Property Characteristics of Pyrolytic Lignins Derived from Fast Pyrolysis of a Lignin Rich Biomass Extract, *ACS Sustainable Chemistry & Engineering* 1 (2) (2013) 260-267.
- [75] R. Bayerbach, D. Meier, Characterization of the water-insoluble fraction from fast pyrolysis liquids (pyrolytic lignin). Part IV: Structure elucidation of oligomeric molecules, *Journal of Analytical and Applied Pyrolysis* 85 (1) (2009) 98-107.
- [76] D.V. Evtuguin, C. Pascoal Neto, J. Rocha, J.D. Pedrosa de Jesus, Oxidative delignification in the presence of molybdovanadophosphate heteropolyanions: mechanism and kinetic studies, *Applied Catalysis A: General* 167 (1) (1998) 123-139.
- [77] A. Kallioinen, A. Vaari, M. Rättö, J. Konn, M. Siika-aho, L. Viikari, Effects of bacterial treatments on wood extractives, *Journal of Biotechnology* 103 (1) (2003) 67-76.
- [78] A.A. Khan, W. de Jong, P.J. Jansens, H. Spliethoff, Biomass combustion in fluidized bed boilers: Potential problems and remedies, *Fuel Processing Technology* 90 (1) (2009) 21-50.
- [79] A. Demirbas, G. Arin, An Overview of Biomass Pyrolysis, *Energy Sources* 24 (5) (2002) 471-482.
- [80] M. Balat, M. Balat, E. Kırtay, H. Balat, Main routes for the thermo-conversion of biomass into fuels and chemicals. Part 1: Pyrolysis systems, *Energy Conversion and Management* 50 (12) (2009) 3147-3157.
- [81] M.F. Demirbas, M. Balat, Biomass pyrolysis for liquid fuels and chemicals: A review, *Journal of Scientific and Industrial Research* 66 (10) (2007) 797-804.
- [82] D.A. Laird, R.C. Brown, J.E. Amonette, J. Lehmann, Review of the pyrolysis platform for coproducing bio-oil and biochar, *Biofuels, Bioproducts and Biorefining* 3 (5) (2009) 547-562.
- [83] C.E. Brewer, K. Schmidt-Rohr, J.A. Satrio, R.C. Brown, Characterization of biochar from fast pyrolysis and gasification systems, *Environmental Progress & Sustainable Energy* 28 (3) (2009) 386-396.

- [84] N. Rogovska, D.A. Laird, S.J. Rathke, D.L. Karlen, Biochar impact on Midwestern Mollisols and maize nutrient availability, *Geoderma* 230-231 (2014) 340-347.
- [85] A. Demirbas, Determination of calorific values of bio-chars and pyro-oils from pyrolysis of beech trunkbarks, *Journal of Analytical and Applied Pyrolysis* 72 (2) (2004) 215-219.
- [86] A. Demirbaş, Properties of charcoal derived from hazelnut shell and the production of briquettes using pyrolytic oil, *Energy* 24 (2) (1999) 141-150.
- [87] A. Sharma, V. Pareek, D. Zhang, Biomass pyrolysis—A review of modelling, process parameters and catalytic studies, *Renewable and Sustainable Energy Reviews* 50 (2015) 1081-1096.
- [88] K. Weber, P. Quicker, Properties of biochar, *Fuel* 217 (2018) 240-261.
- [89] A.V. McBeath, R.J. Smernik, M.P.W. Schneider, M.W.I. Schmidt, E.L. Plant, Determination of the aromaticity and the degree of aromatic condensation of a thermosequence of wood charcoal using NMR, *Organic Geochemistry* 42 (10) (2011) 1194-1202.
- [90] D.B. Wiedemeier, S. Abiven, W.C. Hockaday, M. Keiluweit, M. Kleber, C.A. Masiello, A.V. McBeath, P.S. Nico, L.A. Pyle, M.P.W. Schneider, R.J. Smernik, G.L.B. Wiesenberg, M.W.I. Schmidt, Aromaticity and degree of aromatic condensation of char, *Organic Geochemistry* 78 (2015) 135-143.
- [91] K.B. Cantrell, P.G. Hunt, M. Uchimiya, J.M. Novak, K.S. Ro, Impact of pyrolysis temperature and manure source on physicochemical characteristics of biochar, *Bioresource Technology* 107 (2012) 419-428.
- [92] Y. Chun, G. Sheng, C.T. Chiou, B. Xing, Compositions and Sorptive Properties of Crop Residue-Derived Chars, *Environmental Science & Technology* 38 (17) (2004) 4649-4655.
- [93] Q. Fang, B. Chen, Y. Lin, Y. Guan, Aromatic and Hydrophobic Surfaces of Wood-derived Biochar Enhance Perchlorate Adsorption via Hydrogen Bonding to Oxygen-containing Organic Groups, *Environmental Science & Technology* 48 (1) (2014) 279-288.
- [94] J. Lehmann, J. Gaunt, M. Rondon, Bio-char sequestration in terrestrial ecosystems, *Mitigation and Adaptation Strategies for Global Change* 11 (2) (2006) 395-419.
- [95] Y. Lee, J. Park, C. Ryu, K.S. Gang, W. Yang, Y.-K. Park, J. Jung, S. Hyun, Comparison of biochar properties from biomass residues produced by slow pyrolysis at 500°C, *Bioresource Technology* 148 (2013) 196-201.
- [96] P. Quicker, K. Weber, *Biokohle*, Springer Vieweg, 2016,
- [97] L. Zhang, R. Liu, R. Yin, Y. Mei, Upgrading of bio-oil from biomass fast pyrolysis in China: A review, *Renewable and Sustainable Energy Reviews* 24 (2013) 66-72.
- [98] T. Ba, A. Chaala, M. Garcia-Perez, D. Rodrigue, C. Roy, Colloidal Properties of Bio-oils Obtained by Vacuum Pyrolysis of Softwood Bark. Characterization of Water-Soluble and Water-Insoluble Fractions, *Energy & Fuels* 18 (3) (2004) 704-712.
- [99] C. Lindfors, E. Kuoppala, A. Oasmaa, Y. Solantausta, V. Arpiainen, Fractionation of Bio-Oil, *Energy & Fuels* 28 (9) (2014) 5785-5791.
- [100] A. Demirbas, The influence of temperature on the yields of compounds existing in bio-oils obtained from biomass samples via pyrolysis, *Fuel Processing Technology* 88 (6) (2007) 591-597.

- 
- [101] A. Oasmaa, E. Kuoppala, Y. Solantausta, Fast Pyrolysis of Forestry Residue. 2. Physicochemical Composition of Product Liquid, *Energy & Fuels* 17 (2) (2003) 433-443.
- [102] K. Sipilä, E. Kuoppala, L. Fagernäs, A. Oasmaa, Characterization of biomass-based flash pyrolysis oils, *Biomass and Bioenergy* 14 (2) (1998) 103-113.
- [103] C.R. Vitasari, G.W. Meindersma, A.B. de Haan, Water extraction of pyrolysis oil: The first step for the recovery of renewable chemicals, *Bioresource Technology* 102 (14) (2011) 7204-7210.
- [104] M. Garcia-Perez, S. Wang, J. Shen, M. Rhodes, W.J. Lee, C.-Z. Li, Effects of Temperature on the Formation of Lignin-Derived Oligomers during the Fast Pyrolysis of Mallee Woody Biomass, *Energy & Fuels* 22 (3) (2008) 2022-2032.
- [105] M.P. Pandey, C.S. Kim, Lignin Depolymerization and Conversion: A Review of Thermochemical Methods, *Chemical Engineering & Technology* 34 (1) (2010) 29-41.
- [106] X. Shi, J. Wang, A comparative investigation into the formation behaviors of char, liquids and gases during pyrolysis of pinewood and lignocellulosic components, *Bioresource Technology* 170 (2014) 262-269.
- [107] Y. Zhao, L. Deng, B. Liao, Y. Fu, Q.-X. Guo, Aromatics Production via Catalytic Pyrolysis of Pyrolytic Lignins from Bio-Oil, *Energy & Fuels* 24 (10) (2010) 5735-5740.
- [108] S. Baumlin, F. Broust, F. Bazer-Bachi, T. Bourdeaux, O. Herbinet, F. Toutie Ndiaye, M. Ferrer, J. Lédé, Production of hydrogen by lignins fast pyrolysis, *International Journal of Hydrogen Energy* 31 (15) (2006) 2179-2192.
- [109] A. Effendi, H. Gerhauser, A.V. Bridgwater, Production of renewable phenolic resins by thermochemical conversion of biomass: A review, *Renewable and Sustainable Energy Reviews* 12 (8) (2008) 2092-2116.
- [110] P. Azadi, O.R. Inderwildi, R. Farnood, D.A. King, Liquid fuels, hydrogen and chemicals from lignin: A critical review, *Renewable and Sustainable Energy Reviews* 21 (2013) 506-523.
- [111] Y. Solantausta, N.-O. Nylund, M. Westerholm, T. Koljonen, A. Oasmaa, Wood-pyrolysis oil as fuel in a diesel-power plant, *Bioresource Technology* 46 (1) (1993) 177-188.
- [112] S. Panigrahi, S.T. Chaudhari, N.N. Bakhshi, A.K. Dalai, Production of Synthesis Gas/High-Btu Gaseous Fuel from Pyrolysis of Biomass-Derived Oil, *Energy & Fuels* 16 (6) (2002) 1392-1397.
- [113] M. Balat, An Overview of the Properties and Applications of Biomass Pyrolysis Oils, *Energy Sources, Part A: Recovery, Utilization, and Environmental Effects* 33 (7) (2011) 674-689.
- [114] P.T. Williams, P.A. Horne, Characterisation of oils from the fluidised bed pyrolysis of biomass with zeolite catalyst upgrading, *Biomass and Bioenergy* 7 (1) (1994) 223-236.
- [115] P.M. Mortensen, J.D. Grunwaldt, P.A. Jensen, K.G. Knudsen, A.D. Jensen, A review of catalytic upgrading of bio-oil to engine fuels, *Applied Catalysis A: General* 407 (1) (2011) 1-19.
- [116] D.C. Elliott, T.R. Hart, Catalytic Hydroprocessing of Chemical Models for Bio-oil, *Energy & Fuels* 23 (2) (2009) 631-637.
-

## REFERENCES

- [117] M. Sakaguchi, A.P. Watkinson, N. Ellis, Steam Gasification of Bio-Oil and Bio-Oil/Char Slurry in a Fluidized Bed Reactor, *Energy & Fuels* 24 (9) (2010) 5181-5189.
- [118] D. Rennard, R. French, S. Czernik, T. Josephson, L. Schmidt, Production of synthesis gas by partial oxidation and steam reforming of biomass pyrolysis oils, *International Journal of Hydrogen Energy* 35 (9) (2010) 4048-4059.
- [119] J.T. Oladeji, E.A. Itabiyi, P.O. Okekunle, A comprehensive review of biomass pyrolysis as a process of renewable energy generation, *Journal of Natural Sciences Research* 5 (5) (2015) 99-105.
- [120] D. Monarca, A. Colantoni, M. Cecchini, L. Longo, L. Vecchione, M. Carlini, A. Manzo, Energy Characterization and Gasification of Biomass Derived by Hazelnut Cultivation: Analysis of Produced Syngas by Gas Chromatography, *Mathematical Problems in Engineering* 2012 (2012) 9.
- [121] V. Strezov, T.J. Evans, C. Hayman, Thermal conversion of elephant grass (*Pennisetum Purpureum* Schum) to bio-gas, bio-oil and charcoal, *Bioresource Technology* 99 (17) (2008) 8394-8399.
- [122] T. Qu, W. Guo, L. Shen, J. Xiao, K. Zhao, Experimental Study of Biomass Pyrolysis Based on Three Major Components: Hemicellulose, Cellulose, and Lignin, *Industrial & Engineering Chemistry Research* 50 (18) (2011) 10424-10433.
- [123] M.N. Uddin, W.M.A.W. Daud, H.F. Abbas, Effects of pyrolysis parameters on hydrogen formations from biomass: a review, *RSC Advances* 4 (21) (2014) 10467-10490.
- [124] A.K. Hossain, P.A. Davies, Pyrolysis liquids and gases as alternative fuels in internal combustion engines – A review, *Renewable and Sustainable Energy Reviews* 21 (2013) 165-189.
- [125] A. Domínguez, Y. Fernández, B. Fidalgo, J.J. Pis, J.A. Menéndez, Bio-syngas production with low concentrations of CO<sub>2</sub> and CH<sub>4</sub> from microwave-induced pyrolysis of wet and dried sewage sludge, *Chemosphere* 70 (3) (2008) 397-403.
- [126] J. Akhtar, N. Saidina Amin, A review on operating parameters for optimum liquid oil yield in biomass pyrolysis, *Renewable and Sustainable Energy Reviews* 16 (7) (2012) 5101-5109.
- [127] H. Yang, R. Yan, H. Chen, D.H. Lee, C. Zheng, Characteristics of hemicellulose, cellulose and lignin pyrolysis, *Fuel* 86 (12) (2007) 1781-1788.
- [128] R. Zanzi, K. Sjöström, E. Björnbom, Rapid pyrolysis of agricultural residues at high temperature, *Biomass and Bioenergy* 23 (5) (2002) 357-366.
- [129] R. Fahmi, A.V. Bridgwater, I. Donnison, N. Yates, J.M. Jones, The effect of lignin and inorganic species in biomass on pyrolysis oil yields, quality and stability, *Fuel* 87 (7) (2008) 1230-1240.
- [130] E. Biagini, F. Barontini, L. Tognotti, Devolatilization of Biomass Fuels and Biomass Components Studied by TG/FTIR Technique, *Industrial & Engineering Chemistry Research* 45 (13) (2006) 4486-4493.
- [131] Y. Wang, L. Wu, C. Wang, J. Yu, Z. Yang, Investigating the influence of extractives on the oil yield and alkane production obtained from three kinds of biomass via deoxy-liquefaction, *Bioresource Technology* 102 (14) (2011) 7190-7195.
- [132] P.A. Horne, P.T. Williams, Influence of temperature on the products from the flash pyrolysis of biomass, *Fuel* 75 (9) (1996) 1051-1059.



- [133] M. Garcia-Perez, X.S. Wang, J. Shen, M.J. Rhodes, F. Tian, W.-J. Lee, H. Wu, C.-Z. Li, Fast Pyrolysis of Oil Mallee Woody Biomass: Effect of Temperature on the Yield and Quality of Pyrolysis Products, *Industrial & Engineering Chemistry Research* 47 (6) (2008) 1846-1854.
- [134] M.I. Jahirul, M. Rasul, A. Chowdhury, N. Ashwath, Biofuels Production through Biomass Pyrolysis—A Technological Review, 2012, 4952-5001.
- [135] J. Li, R. Yan, B. Xiao, X. Wang, H. Yang, Influence of Temperature on the Formation of Oil from Pyrolyzing Palm Oil Wastes in a Fixed Bed Reactor, *Energy & Fuels* 21 (4) (2007) 2398-2407.
- [136] D.S. Scott, J. Piskorz, M.A. Bergougnou, R. Graham, R.P. Overend, The role of temperature in the fast pyrolysis of cellulose and wood, *Industrial & Engineering Chemistry Research* 27 (1) (1988) 8-15.
- [137] R. Azargohar, S. Nanda, J.A. Kozinski, A.K. Dalai, R. Sutarto, Effects of temperature on the physicochemical characteristics of fast pyrolysis bio-chars derived from Canadian waste biomass, *Fuel* 125 (2014) 90-100.
- [138] S.-W. Park, C.-H. Jang, Effects of pyrolysis temperature on changes in fuel characteristics of biomass char, *Energy* 39 (1) (2012) 187-195.
- [139] W.C. Park, A. Atreya, H.R. Baum, Experimental and theoretical investigation of heat and mass transfer processes during wood pyrolysis, *Combustion and Flame* 157 (3) (2010) 481-494.
- [140] Z. Luo, S. Wang, Y. Liao, J. Zhou, Y. Gu, K. Cen, Research on biomass fast pyrolysis for liquid fuel, *Biomass and Bioenergy* 26 (5) (2004) 455-462.
- [141] V. Strezov, B. Moghtaderi, J.A. Lucas, Thermal study of decomposition of selected biomass samples, *Journal of Thermal Analysis and Calorimetry* 72 (3) (2003) 1041-1048.
- [142] N. Ozbay, A.E. Pütün, E. Pütün, Bio-oil production from rapid pyrolysis of cottonseed cake: product yields and compositions, *International Journal of Energy Research* 30 (7) (2006) 501-510.
- [143] E. Salehi, J. Abedi, T. Harding, Bio-oil from Sawdust: Pyrolysis of Sawdust in a Fixed-Bed System, *Energy & Fuels* 23 (7) (2009) 3767-3772.
- [144] M.L. Boroson, J.B. Howard, J.P. Longwell, W.A. Peters, Product yields and kinetics from the vapor phase cracking of wood pyrolysis tars, *AIChE Journal* 35 (1) (1989) 120-128.
- [145] D.S. Scott, P. Majerski, J. Piskorz, D. Radlein, A second look at fast pyrolysis of biomass—the RTI process, *Journal of Analytical and Applied Pyrolysis* 51 (1) (1999) 23-37.
- [146] I.-Y. Eom, J.-Y. Kim, T.-S. Kim, S.-M. Lee, D. Choi, I.-G. Choi, J.-W. Choi, Effect of essential inorganic metals on primary thermal degradation of lignocellulosic biomass, *Bioresource Technology* 104 (2012) 687-694.
- [147] G.N. Richards, G. Zheng, Influence of metal ions and of salts on products from pyrolysis of wood: Applications to thermochemical processing of newsprint and biomass, *Journal of Analytical and Applied Pyrolysis* 21 (1) (1991) 133-146.
- [148] F.-X. Collard, J. Blin, A. Bensakhria, J. Valette, Influence of impregnated metal on the pyrolysis conversion of biomass constituents, *Journal of Analytical and Applied Pyrolysis* 95 (2012) 213-226.
- [149] P.T. Williams, P.A. Horne, The role of metal salts in the pyrolysis of biomass, *Renewable Energy* 4 (1) (1994) 1-13.

- [150] M. Nik-Azar, M.R. Hajaligol, M. Sohrabi, B. Dabir, Mineral matter effects in rapid pyrolysis of beech wood, *Fuel Processing Technology* 51 (1) (1997) 7-17.
- [151] N.A. Öztaş, Y. Yürüm, Pyrolysis of Turkish Zonguldak bituminous coal. Part 1. Effect of mineral matter, *Fuel* 79 (10) (2000) 1221-1227.
- [152] K. Raveendran, A. Ganesh, K.C. Khilar, Influence of mineral matter on biomass pyrolysis characteristics, *Fuel* 74 (12) (1995) 1812-1822.
- [153] F.-X. Collard, J. Blin, A review on pyrolysis of biomass constituents: Mechanisms and composition of the products obtained from the conversion of cellulose, hemicelluloses and lignin, *Renewable and Sustainable Energy Reviews* 38 (2014) 594-608.
- [154] M. Van de Velden, J. Baeyens, A. Brems, B. Janssens, R. Dewil, Fundamentals, kinetics and endothermicity of the biomass pyrolysis reaction, *Renewable Energy* 35 (1) (2010) 232-242.
- [155] J.-P. Lange, Lignocellulose conversion: an introduction to chemistry, process and economics, *Biofuels, Bioproducts and Biorefining* 1 (1) (2007) 39-48.
- [156] A.M. Azeez, D. Meier, J. Odermatt, Temperature dependence of fast pyrolysis volatile products from European and African biomasses, *Journal of Analytical and Applied Pyrolysis* 90 (2) (2011) 81-92.
- [157] P. Morf, P. Hasler, T. Nussbaumer, Mechanisms and kinetics of homogeneous secondary reactions of tar from continuous pyrolysis of wood chips, *Fuel* 81 (7) (2002) 843-853.
- [158] L. Wei, S. Xu, L. Zhang, H. Zhang, C. Liu, H. Zhu, S. Liu, Characteristics of fast pyrolysis of biomass in a free fall reactor, *Fuel Processing Technology* 87 (10) (2006) 863-871.
- [159] F. Shafizadeh, Pyrolytic Reactions and Products of Biomass, in *Fundamentals of Thermochemical Biomass Conversion*, R.P. Overend, T.A. Milne, and L.K. Mudge, Editors. 1985, Springer Netherlands: Dordrecht. p. 183-217.
- [160] F. Shafizadeh, *Wood Technology*, Am. Chem. Soc. (1977) 57-81.
- [161] G. Lv, S. Wu, Analytical pyrolysis studies of corn stalk and its three main components by TG-MS and Py-GC/MS, *Journal of Analytical and Applied Pyrolysis* 97 (2012) 11-18.
- [162] Y.-C. Lin, J. Cho, G.A. Tompsett, P.R. Westmoreland, G.W. Huber, Kinetics and mechanism of cellulose pyrolysis, *The Journal of Physical Chemistry C* 113 (46) (2009) 20097-20107.
- [163] M.S. Mettler, D.G. Vlachos, P.J. Dauenhauer, Top ten fundamental challenges of biomass pyrolysis for biofuels, *Energy & Environmental Science* 5 (7) (2012) 7797-7809.
- [164] J.J.M. Orfão, F.J.A. Antunes, J.L. Figueiredo, Pyrolysis kinetics of lignocellulosic materials—three independent reactions model, *Fuel* 78 (3) (1999) 349-358.
- [165] Y. Peng, S. Wu, The structural and thermal characteristics of wheat straw hemicellulose, *Journal of Analytical and Applied Pyrolysis* 88 (2) (2010) 134-139.
- [166] D.K. Shen, S. Gu, A.V. Bridgwater, Study on the pyrolytic behaviour of xylan-based hemicellulose using TG-FTIR and Py-GC-FTIR, *Journal of Analytical and Applied Pyrolysis* 87 (2) (2010) 199-206.

- [167] S. Wang, B. Ru, H. Lin, W. Sun, Pyrolysis behaviors of four O-acetyl-preserved hemicelluloses isolated from hardwoods and softwoods, *Fuel* 150 (2015) 243-251.
- [168] X. Wang, R. Rinaldi, Solvent Effects on the Hydrogenolysis of Diphenyl Ether with Raney Nickel and their Implications for the Conversion of Lignin, *ChemSusChem* 5 (8) (2012) 1455-1466.
- [169] R. Parthasarathi, R.A. Romero, A. Redondo, S. Gnanakaran, Theoretical Study of the Remarkably Diverse Linkages in Lignin, *The Journal of Physical Chemistry Letters* 2 (20) (2011) 2660-2666.
- [170] H. Kawamoto, S. Horigoshi, S. Saka, Pyrolysis reactions of various lignin model dimers, *Journal of Wood Science* 53 (2) (2007) 168-174.
- [171] T. Nakamura, H. Kawamoto, S. Saka, Pyrolysis behavior of Japanese cedar wood lignin studied with various model dimers, *Journal of Analytical and Applied Pyrolysis* 81 (2) (2008) 173-182.
- [172] S. Wang, K. Wang, Q. Liu, Y. Gu, Z. Luo, K. Cen, T. Fransson, Comparison of the pyrolysis behavior of lignins from different tree species, *Biotechnology Advances* 27 (5) (2009) 562-567.
- [173] E. Jakab, O. Faix, F. Till, T. Székely, Thermogravimetry/mass spectrometry study of six lignins within the scope of an international round robin test, *Journal of Analytical and Applied Pyrolysis* 35 (2) (1995) 167-179.
- [174] Y. Huang, Z. Wei, Z. Qiu, X. Yin, C. Wu, Study on structure and pyrolysis behavior of lignin derived from corn cob acid hydrolysis residue, *Journal of Analytical and Applied Pyrolysis* 93 (2012) 153-159.
- [175] T. Faravelli, A. Frassoldati, G. Migliavacca, E. Ranzi, Detailed kinetic modeling of the thermal degradation of lignins, *Biomass and Bioenergy* 34 (3) (2010) 290-301.
- [176] H. Kawamoto, S. Saka, Role of Side-Chain Hydroxyl Groups in Pyrolytic Reaction of Phenolic  $\beta$ -Ether Type of Lignin Dimer, *Journal of Wood Chemistry and Technology* 27 (2) (2007) 113-120.
- [177] R. Brežný, V. Mihalov, V. Kováčik, Low Temperature Thermolysis of Lignins - I. Reactions of  $\beta$ -O-4 Model Compounds, *International Journal of the Biology, Chemistry, Physics and Technology of Wood*. 37 (4) (1983) 199-204.
- [178] M. Foston, G.A. Nunnery, X. Meng, Q. Sun, F.S. Baker, A. Ragauskas, NMR a critical tool to study the production of carbon fiber from lignin, *Carbon* 52 (2013) 65-73.
- [179] H. Kawamoto, S. Saka, Condensation Reactions of Some Lignin Related Compounds at Relatively Low Pyrolysis Temperature AU - Nakamura, Takeshi, *Journal of Wood Chemistry and Technology* 27 (2) (2007) 121-133.
- [180] T. Hosoya, H. Kawamoto, S. Saka, Secondary reactions of lignin-derived primary tar components, *Journal of Analytical and Applied Pyrolysis* 83 (1) (2008) 78-87.
- [181] S. Zhou, M. Garcia-Perez, B. Pecha, A.G. McDonald, S.R.A. Kersten, R.J.M. Westerhof, Secondary Vapor Phase Reactions of Lignin-Derived Oligomers Obtained by Fast Pyrolysis of Pine Wood, *Energy & Fuels* 27 (3) (2013) 1428-1438.
- [182] P.R. Patwardhan, D.L. Dalluge, B.H. Shanks, R.C. Brown, Distinguishing primary and secondary reactions of cellulose pyrolysis, *Bioresource Technology* 102 (8) (2011) 5265-5269.

## REFERENCES

- [183] S. Wu, D. Shen, J. Hu, H. Zhang, R. Xiao, Cellulose-hemicellulose interactions during fast pyrolysis with different temperatures and mixing methods, *Biomass and Bioenergy* 95 (2016) 55-63.
- [184] T. Hosoya, H. Kawamoto, S. Saka, Solid/liquid- and vapor-phase interactions between cellulose- and lignin-derived pyrolysis products, *Journal of Analytical and Applied Pyrolysis* 85 (1) (2009) 237-246.
- [185] C.E. Greenhalf, D.J. Nowakowski, A.B. Harms, J.O. Titiloye, A.V. Bridgwater, A comparative study of straw, perennial grasses and hardwoods in terms of fast pyrolysis products, *Fuel* 108 (2013) 216-230.
- [186] H. Kawamoto, W. Hatanaka, S. Saka, Thermochemical conversion of cellulose in polar solvent (sulfolane) into levoglucosan and other low molecular-weight substances, *Journal of Analytical and Applied Pyrolysis* 70 (2) (2003) 303-313.
- [187] T. Hosoya, H. Kawamoto, S. Saka, Different pyrolytic pathways of levoglucosan in vapor- and liquid/solid-phases, *Journal of Analytical and Applied Pyrolysis* 83 (1) (2008) 64-70.
- [188] M. Garcia-Perez, A. Chaala, H. Pakdel, D. Kretschmer, C. Roy, Characterization of bio-oils in chemical families, *Biomass and Bioenergy* 31 (4) (2007) 222-242.
- [189] M. Garcia-Pèrez, A. Chaala, H. Pakdel, D. Kretschmer, D. Rodrigue, C. Roy, Evaluation of the influence of stainless steel and copper on the aging process of bio-oil, *Energy and Fuels* 20 (2) (2006) 786-795.
- [190] J. Sameni, S. Krigstin, M. Sain, Solubility of Lignin and Acetylated Lignin in Organic Solvents, 2017,
- [191] Standard test methods for analysis of wood fuels, E870-82 (reapproved 2006), 2006, ASTM-American Society for Testing and Materials.
- [192] X. Jiang, N. Ellis, Z. Zhong, Characterization of pyrolytic lignin extracted from bio-oil, *Chinese Journal of Chemical Engineering* 18 (6) (2010) 1018-1022.
- [193] M. Li, M. Zhang, Y. Yu, H. Wu, Ternary System of Pyrolytic Lignin, Mixed Solvent, and Water: Phase Diagram and Implications, *Energy & Fuels* 32 (1) (2018) 465-474.
- [194] A. Sluiter, B. Hames, R. Ruiz, C. Scarlata, J. Sluiter, D. Templeton, D. Crocker, Determination of structural carbohydrates and lignin in biomass, Technical Report NREL/TP-510-42618; National Renewable Energy Laboratory (2008)
- [195] S.B. Liaw, Y. Yu, H. Wu, Association of inorganic species release with sugar recovery during wood hydrothermal processing, *Fuel* 166 (2016) 581-584.
- [196] K. Yip, F. Tian, J.-i. Hayashi, H. Wu, Effect of Alkali and Alkaline Earth Metallic Species on Biochar Reactivity and Syngas Compositions during Steam Gasification, *Energy & Fuels* 24 (1) (2010) 173-181.
- [197] M. Shemfe, S. Gu, B. Fidalgo, Techno-economic analysis of biofuel production via bio-oil zeolite upgrading: An evaluation of two catalyst regeneration systems, *Biomass and Bioenergy* 98 (2017) 182-193.
- [198] X. Zhang, Q. Zhang, T. Wang, B. Li, Y. Xu, L. Ma, Efficient upgrading process for production of low quality fuel from bio-oil, *Fuel* 179 (2016) 312-321.
- [199] A. Renny, V. Santhosh, N. Somkuwar, D.T. Gokak, P. Sharma, S. Bhargava, Pyrolysis of de-oiled seed cake of *Jatropha Curcas* and catalytic steam

- reforming of pyrolytic bio-oil to hydrogen, *Bioresource Technology* 220 (2016) 151-160.
- [200] Y. Xu, L. Zhang, J. Chang, X. Zhang, L. Ma, T. Wang, Q. Zhang, One step hydrogenation–esterification of model compounds and bio-oil to alcohols and esters over Raney Ni catalysts, *Energy Conversion and Management* 108 (2016) 78-84.
- [201] A. Sanna, K. Ogbunike, J.M. Andrésen, Bio-coke from upgrading of pyrolysis bio-oil for co-firing, *Fuel* 88 (12) (2009) 2340-2347.
- [202] T. Hosoya, H. Kawamoto, S. Saka, Role of methoxyl group in char formation from lignin-related compounds, *Journal of Analytical and Applied Pyrolysis* 84 (1) (2009) 79-83.
- [203] C.A. Fisk, T. Morgan, Y. Ji, M. Crocker, C. Crofcheck, S.A. Lewis, Bio-oil upgrading over platinum catalysts using in situ generated hydrogen, *Applied Catalysis A: General* 358 (2) (2009) 150-156.
- [204] Y. Li, C. Zhang, Y. Liu, S. Tang, G. Chen, R. Zhang, X. Tang, Coke formation on the surface of Ni/HZSM-5 and Ni-Cu/HZSM-5 catalysts during bio-oil hydrodeoxygenation, *Fuel* 189 (2017) 23-31.
- [205] Y. Wang, S. Wang, F. Leng, J. Chen, L. Zhu, Z. Luo, Separation and characterization of pyrolytic lignins from the heavy fraction of bio-oil by molecular distillation, *Separation and Purification Technology* 152 (2015) 123-132.
- [206] X. Jiang, N. Ellis, D.K. Shen, J. Jiang, W. Dai, Z. Zhong, Thermogravimetry-FTIR Analysis of Pyrolysis of Pyrolytic Lignin Extracted from Bio-Oil, *Chemical Engineering & Technology* 35 (5) (2012) 827-833.
- [207] C. Amen-Chen, H. Pakdel, C. Roy, Production of monomeric phenols by thermochemical conversion of biomass: a review, *Bioresource Technology* 79 (3) (2001) 277-299.
- [208] Y. Yu, Y.W. Chua, H. Wu, Characterization of Pyrolytic Sugars in Bio-Oil Produced from Biomass Fast Pyrolysis, *Energy & Fuels* 30 (5) (2016) 4145-4149.
- [209] G.R. Hatfield, G.E. Maciel, O. Erbatur, G. Erbatur, Qualitative and Quantitative Analysis of Solid Lignin Samples by Carbon-13 Nuclear Magnetic Resonance Spectrometry, *Analytical Chemistry* 59 (1) (1987) 172-179.
- [210] G. Almendros, H. Knicker, F.J. González-Vila, Rearrangement of carbon and nitrogen forms in peat after progressive thermal oxidation as determined by solid-state <sup>13</sup>C- and <sup>15</sup>N-NMR spectroscopy, *Organic Geochemistry* 34 (11) (2003) 1559-1568.
- [211] T.F. Yen, J.G. Erdman, S.S. Pollack, Investigation of the Structure of Petroleum Asphaltene by X-Ray Diffraction, *Analytical Chemistry* 33 (11) (1961) 1587-1594.
- [212] H. Kawamoto, M. Ryoritani, S. Saka, Different pyrolytic cleavage mechanisms of β-ether bond depending on the side-chain structure of lignin dimers, *Journal of Analytical and Applied Pyrolysis* 81 (1) (2008) 88-94.
- [213] N. Kashimura, J.-i. Hayashi, C.-Z. Li, C. Sathe, T. Chiba, Evidence of poly-condensed aromatic rings in a Victorian brown coal, *Fuel* 83 (1) (2004) 97-107.
- [214] Y. Wang, X. Li, D. Mourant, R. Gunawan, S. Zhang, C.Z. Li, Formation of aromatic structures during the pyrolysis of bio-oil, *Energy and Fuels* 26 (1) (2012) 241-247.

- [215] A.J. Ragauskas, C.K. Williams, B.H. Davison, G. Britovsek, J. Cairney, C.A. Eckert, W.J. Frederick, J.P. Hallett, D.J. Leak, C.L. Liotta, J.R. Mielenz, R. Murphy, R. Templer, T. Tschaplinski, The Path Forward for Biofuels and Biomaterials, *Science* 311 (5760) (2006) 484.
- [216] R. Chaudhary, P.L. Dhepe, Depolymerization of Lignin Using a Solid Base Catalyst, *Energy & Fuels* 33 (5) (2019) 4369-4377.
- [217] D.K. Ratnasari, W. Yang, P.G. Jönsson, Kinetic Study of an H-ZSM-5/Al-MCM-41 Catalyst Mixture and Its Application in Lignocellulose Biomass Pyrolysis, *Energy & Fuels* 33 (6) (2019) 5360-5367.
- [218] A.P. Pinheiro Pires, J. Arauzo, I. Fonts, M.E. Domine, A. Fernández Arroyo, M.E. Garcia-Perez, J. Montoya, F. Chejne, P. Pfromm, M. Garcia-Perez, Challenges and Opportunities for Bio-oil Refining: A Review, *Energy & Fuels* 33 (6) (2019) 4683-4720.
- [219] C. Lapierre, B. Pollet, C. Rolando, New insights into the molecular architecture of hardwood lignins by chemical degradative methods, *Research on Chemical Intermediates* 21 (3) (1995) 397.
- [220] G. Neutelings, Lignin variability in plant cell walls: Contribution of new models, *Plant Science* 181 (4) (2011) 379-386.
- [221] K. M., B. T., Phenols from Lignin, *Chemical Engineering & Technology* 31 (5) (2008) 736-745.
- [222] R. Parthasarathi, R.A. Romero, A. Redondo, S. Gnanakaran, Theoretical study of the remarkably diverse linkages in lignin, *Journal of Physical Chemistry Letters* 2 (20) (2011) 2660-2666.
- [223] J. Cho, S. Chu, P.J. Dauenhauer, G.W. Huber, Kinetics and reaction chemistry for slow pyrolysis of enzymatic hydrolysis lignin and organosolv extracted lignin derived from maplewood, *Green Chemistry* 14 (2) (2012) 428-439.
- [224] H. Ben, A.J. Ragauskas, Pyrolysis of kraft lignin with additives, *Energy and Fuels* 25 (10) (2011) 4662-4668.
- [225] D.J. Nowakowski, A.V. Bridgwater, D.C. Elliott, D. Meier, P. de Wild, Lignin fast pyrolysis: Results from an international collaboration, *Journal of Analytical and Applied Pyrolysis* 88 (1) (2010) 53-72.
- [226] G. Jiang, D.J. Nowakowski, A.V. Bridgwater, Effect of the temperature on the composition of lignin pyrolysis products, *Energy and Fuels* 24 (8) (2010) 4470-4475.
- [227] A.E. Harman-Ware, J.R. Ferrell, Methods and Challenges in the Determination of Molecular Weight Metrics of Bio-oils, *Energy & Fuels* 32 (9) (2018) 8905-8920.
- [228] A. Burton, H. Wu, Mechanistic Investigation into Bed Agglomeration during Biomass Fast Pyrolysis in a Fluidized-Bed Reactor, *Energy & Fuels* 26 (11) (2012) 6979-6987.
- [229] A. Burton, H. Wu, Differences in Bed Agglomeration Behavior during the Fast Pyrolysis of Mallee Bark, Leaf, and Wood in a Fluidized-Bed Reactor at 500 °C, *Energy & Fuels* 29 (6) (2015) 3753-3759.
- [230] X. Xin, K.M. Torr, F. de Miguel Mercader, S. Pang, Insights into Preventing Fluidized Bed Material Agglomeration in Fast Pyrolysis of Acid-Leached Pine Wood, *Energy & Fuels* 33 (5) (2019) 4254-4263.
- [231] X. Jiang, Q. Lu, B. Hu, J. Liu, C. Dong, Y. Yang, Intermolecular interaction mechanism of lignin pyrolysis: A joint theoretical and experimental study, *Fuel* 215 (2018) 386-394.

- [232] J. Lédé, Cellulose pyrolysis kinetics: An historical review on the existence and role of intermediate active cellulose, *J. Anal. Appl. Pyrolysis* 94 (2012) 17-32.
- [233] X. Gong, Y. Yu, X. Gao, Y. Qiao, M. Xu, H. Wu, Formation of Anhydro-sugars in the Primary Volatiles and Solid Residues from Cellulose Fast Pyrolysis in a Wire-Mesh Reactor, *Energy & Fuels* 28 (8) (2014) 5204-5211.
- [234] D. Liu, Y. Yu, H. Wu, Differences in Water-Soluble Intermediates from Slow Pyrolysis of Amorphous and Crystalline Cellulose, *Energy & Fuels* 27 (3) (2013) 1371-1380.
- [235] D. Liu, Y. Yu, J.-i. Hayashi, B. Moghtaderi, H. Wu, Contribution of dehydration and depolymerization reactions during the fast pyrolysis of various salt-loaded celluloses at low temperatures, *Fuel* 136 (2014) 62-68.
- [236] D. Liu, Y. Yu, Y. Long, H. Wu, Effect of MgCl<sub>2</sub> loading on the evolution of reaction intermediates during cellulose fast pyrolysis at 325°C, *Proceedings of the Combustion Institute* 35 (2) (2015) 2381-2388.
- [237] Y. Yu, D. Liu, H. Wu, Formation and Characteristics of Reaction Intermediates from the Fast Pyrolysis of NaCl- and MgCl<sub>2</sub>-Loaded Celluloses, *Energy & Fuels* 28 (1) (2014) 245-253.
- [238] S.D. Mansfield, H. Kim, F. Lu, J. Ralph, Whole plant cell wall characterization using solution-state 2D NMR, *Nature Protocols* 7 (2012) 1579.
- [239] J. Dou, H. Kim, Y. Li, D. Padmakshan, F. Yue, J. Ralph, T. Vuorinen, Structural Characterization of Lignins from Willow Bark and Wood, *Journal of Agricultural and Food Chemistry* 66 (28) (2018) 7294-7300.
- [240] T.-Q. Yuan, S.-N. Sun, F. Xu, R.-C. Sun, Structural Characterization of Lignin from Triploid of *Populus tomentosa* Carr, *Journal of Agricultural and Food Chemistry* 59 (12) (2011) 6605-6615.
- [241] E. Adler, Lignin chemistry—past, present and future, *Wood Science and Technology* 11 (3) (1977) 169-218.
- [242] D.S. Argyropoulos, S.B. Menachem, Lignin, in *Biotechnology in the Pulp and Paper Industry*, K.E.L. Eriksson, et al., Editors. 1997, Springer Berlin Heidelberg: Berlin, Heidelberg. p. 127-158.
- [243] J.E. Holladay, J.F. White, J.J. Bozell, D. Johnson, Top Value-Added Chemicals from Biomass - Volume II—Results of Screening for Potential Candidates from Biorefinery Lignin, 2007.
- [244] J.-M. Lavoie, W. Baré, M. Bilodeau, Depolymerization of steam-treated lignin for the production of green chemicals, *Bioresource Technology* 102 (7) (2011) 4917-4920.
- [245] A. Toledano, L. Serrano, J. Labidi, Organosolv lignin depolymerization with different base catalysts, *Journal of Chemical Technology & Biotechnology* 87 (11) (2012) 1593-1599.
- [246] S.-C. Qi, J.-i. Hayashi, S. Kudo, L. Zhang, Catalytic hydrogenolysis of kraft lignin to monomers at high yield in alkaline water, *Green Chemistry* 19 (11) (2017) 2636-2645.
- [247] J. Hu, S. Wu, X. Jiang, R. Xiao, Structure–Reactivity Relationship in Fast Pyrolysis of Lignin into Monomeric Phenolic Compounds, *Energy & Fuels* 32 (2) (2018) 1843-1850.
- [248] D. Gschwend, S. Müller, A. Wokaun, F. Vogel, Optimum Fuel for Spark Ignition Engines from Lignin Pyrolysis Oil, *Energy & Fuels* 32 (9) (2018) 9388-9398.

- [249] J. Ye, M. Zhou, J. Zhao, H. Xia, J. Xu, W. Tan, J. Jiang, Continuous Steam-Assisted Low-Temperature Pyrolysis of Alkali Lignin and Selective Production of Guaiacol Components in a Fixed-Bed Reactor, *Energy & Fuels* (2019), DOI: 10.1021/acs.energyfuels.1029b01501.
- [250] L.A. Dodge, R.M. Kalinoski, L. Das, J. Bursavich, P. Muley, D. Boldor, J. Shi, Sequential Extraction and Characterization of Lignin-Derived Compounds from Thermochemically Processed Biorefinery Lignins, *Energy & Fuels* 33 (5) (2019) 4322-4330.
- [251] S. Zhou, M. Garcia-Perez, B. Pecha, S.R.A. Kersten, A.G. McDonald, R.J.M. Westerhof, Effect of the Fast Pyrolysis Temperature on the Primary and Secondary Products of Lignin, *Energy & Fuels* 27 (10) (2013) 5867-5877.
- [252] A.J. Yanez, P. Natarajan, W. Li, R. Mabon, L.J. Broadbelt, Coupled Structural and Kinetic Model of Lignin Fast Pyrolysis, *Energy & Fuels* 32 (2) (2018) 1822-1830.
- [253] G. Dai, Q. Zou, S. Wang, Y. Zhao, L. Zhu, Q. Huang, Effect of Torrefaction on the Structure and Pyrolysis Behavior of Lignin, *Energy & Fuels* 32 (4) (2018) 4160-4166.
- [254] L. Khachatryan, M. Barekati-Goudarzi, D. Kekejian, G. Aguilar, R. Asatryan, G.G. Stanley, D. Boldor, Pyrolysis of Lignin in Gas-Phase Isothermal and cw-CO<sub>2</sub> Laser Powered Non-Isothermal Reactors, *Energy & Fuels* 32 (12) (2018) 12597-12606.
- [255] V. Lago, C. Greenhalf, C. Briens, F. Berruti, Mixing and operability characteristics of mechanically fluidized reactors for the pyrolysis of biomass, *Powder Technology* 274 (2015) 205-212.
- [256] W. Gao, M. Zhang, H. Wu, Bed Agglomeration during Bio-oil Fast Pyrolysis in a Fluidized-Bed Reactor, *Energy & Fuels* 32 (3) (2018) 3608-3613.
- [257] Y.W. Chua, Y. Yu, H. Wu, Thermal decomposition of pyrolytic lignin under inert conditions at low temperatures, *Fuel* 200 (2017) 70-75.
- [258] J.R. Runyon, D.E. Barnes, J.F. Rudd, L.H. Tung, Multiple detectors for molecular weight and composition analysis of copolymers by gel permeation chromatography, *Journal of Applied Polymer Science* 13 (11) (1969) 2359-2369.
- [259] K. Okuda, M. Umetsu, S. Takami, T. Adschiri, Disassembly of lignin and chemical recovery—rapid depolymerization of lignin without char formation in water–phenol mixtures, *Fuel Processing Technology* 85 (8) (2004) 803-813.
- [260] Y.W. Chua, Y. Yu, H. Wu, Structural changes of chars produced from fast pyrolysis of lignin at 100–300 °C, *Fuel* 255 (2019) 115754.
- [261] F. Haw James, P. Schultz Tor, Carbon-13 CP/MAS NMR and FT-IR Study of Low-Temperature Lignin Pyrolysis, in *Holzforschung - International Journal of the Biology, Chemistry, Physics and Technology of Wood*, 1985. p. 289.
- [262] T. Melkior, S. Jacob, G. Gerbaud, S. Hediger, L. Le Pape, L. Bonnefois, M. Bardet, NMR analysis of the transformation of wood constituents by torrefaction, *Fuel* 92 (1) (2012) 271-280.
- [263] S. Chu, A.V. Subrahmanyam, G.W. Huber, The pyrolysis chemistry of a  $\beta$ -O-4 type oligomeric lignin model compound, *Green Chemistry* 15 (1) (2013) 125-136.
- [264] G.W. Huber, S. Iborra, A. Corma, Synthesis of Transportation Fuels from Biomass: Chemistry, Catalysts, and Engineering, *Chem. Rev.* 106 (9) (2006) 4044-4098.



- [265] S.D. Stefanidis, K.G. Kalogiannis, E.F. Iliopoulou, C.M. Michailof, P.A. Pilavachi, A.A. Lappas, A study of lignocellulosic biomass pyrolysis via the pyrolysis of cellulose, hemicellulose and lignin, *J. Anal. Appl. Pyrol.* 105 (2014) 143-150.
- [266] S. Wang, X. Guo, K. Wang, Z. Luo, Influence of the interaction of components on the pyrolysis behavior of biomass, *J. Anal. Appl. Pyrol.* 91 (1) (2011) 183-189.
- [267] S. Wu, D. Shen, J. Hu, H. Zhang, R. Xiao, Cellulose-hemicellulose interactions during fast pyrolysis with different temperatures and mixing methods, *Biomass Bioenerg.* 95 (2016) 55-63.
- [268] T. Hosoya, H. Kawamoto, S. Saka, Cellulose-hemicellulose and cellulose-lignin interactions in wood pyrolysis at gasification temperature, *J. Anal. Appl. Pyrol.* 80 (1) (2007) 118-125.
- [269] T. Hosoya, H. Kawamoto, S. Saka, Different pyrolytic pathways of levoglucosan in vapor- and liquid/solid-phases, *J. Anal. Appl. Pyrol.* 83 (1) (2008) 64-70.
- [270] J. Zhang, Y.S. Choi, C.G. Yoo, T.H. Kim, R.C. Brown, B.H. Shanks, Cellulose-Hemicellulose and Cellulose-Lignin Interactions during Fast Pyrolysis, *ACS Sustain. Chem. Eng.* 3 (2) (2015) 293-301.
- [271] T. Hosoya, H. Kawamoto, S. Saka, Solid/liquid- and vapor-phase interactions between cellulose- and lignin-derived pyrolysis products, *J. Anal. Appl. Pyrol.* 85 (1) (2009) 237-246.
- [272] M.M. Tang, R. Bacon, Carbonization of cellulose fibers—I. Low temperature pyrolysis, *Carbon* 2 (3) (1964) 211-220.
- [273] J. Scheirs, G. Camino, W. Tumiatti, Overview of water evolution during the thermal degradation of cellulose, *Eur. Polym. J.* 37 (5) (2001) 933-942.
- [274] Y.-C. Lin, J. Cho, G.A. Tompsett, P.R. Westmoreland, G.W. Huber, Kinetics and mechanism of cellulose pyrolysis, *J. Phys. Chem. C* 113 (46) (2009) 20097-20107.
- [275] T. Nakamura, H. Kawamoto, S. Saka, Pyrolysis behavior of Japanese cedar wood lignin studied with various model dimers, *J. Anal. Appl. Pyrol.* 81 (2) (2008) 173-182.
- [276] Y. Huang, Z. Wei, Z. Qiu, X. Yin, C. Wu, Study on structure and pyrolysis behavior of lignin derived from corncob acid hydrolysis residue, *J. Anal. Appl. Pyrol.* 93 (2012) 153-159.
- [277] D.K. Shen, S. Gu, K.H. Luo, S.R. Wang, M.X. Fang, The pyrolytic degradation of wood-derived lignin from pulping process, *Bioresour. Technol.* 101 (15) (2010) 6136-6146.
- [278] G. Bolio, E. Rubí, Ross-Alcudia, L. Veleva, J. Antonio, A. Barrios, G. Cadenas Madrigal, M.M. Hernandez Villegas, P. De La, C. Burelo, S. Sánchez Córdova, *Chemical Science Review and Letters* Extraction and Characterization of Cellulose from Agroindustrial Waste of Pineapple (*Ananas comosus* L. Merrill) Crowns \*Correspondence, 2016,
- [279] F. Carrillo, X. Colom, J.J. Suñol, J. Saurina, Structural FTIR analysis and thermal characterisation of lyocell and viscose-type fibres, *European Polymer Journal* 40 (9) (2004) 2229-2234.
- [280] J.I. Morán, V.A. Alvarez, V.P. Cyras, A. Vázquez, Extraction of cellulose and preparation of nanocellulose from sisal fibers, *Cellulose* 15 (1) (2008) 149-159.

## REFERENCES

---

- [281] Y.W. Chua, H. Wu, Y. Yu, Interactions between Low- and High-Molecular-Weight Portions of Lignin during Fast Pyrolysis at Low Temperatures, *Energy Fuels* (2019), DOI: 10.1021/acs.energyfuels.1029b02813.
- [282] H. Kono, S. Yunoki, T. Shikano, M. Fujiwara, T. Erata, M. Takai, CP/MAS <sup>13</sup>C NMR Study of Cellulose and Cellulose Derivatives. 1. Complete Assignment of the CP/MAS <sup>13</sup>C NMR Spectrum of the Native Cellulose, *J. Am. Chem. Soc.* 124 (25) (2002) 7506-7511.
- [283] G.R. Hatfield, G.E. Maciel, O. Erbatur, G. Erbatur, Qualitative and Quantitative Analysis of Solid Lignin Samples by Carbon-13 Nuclear Magnetic Resonance Spectrometry, *Anal. Chem.* 59 (1) (1987) 172-179.
- [284] Y. Yu, D. Liu, H. Wu, Characterization of Water-Soluble Intermediates from Slow Pyrolysis of Cellulose at Low Temperatures, *Energy Fuels* 26 (12) (2012) 7331-7339.




*Every reasonable effort has been made to acknowledge the owners of copyright material. I would be pleased to hear from any copyright owner who has been omitted or incorrectly acknowledged.*

**APPENDICES**

**APPENDIX A      ATTRIBUTION OF AUTHORSHIP**




I. Publication paper “Thermal Decomposition of Pyrolytic Lignin under Inert Conditions at Low Temperatures. *Fuel* **2017**, Vol (200), pages 70-75.”

Authors and full affiliations:

	Conception and design	Acquisition of data & method	Data conditioning & manipulation	Analysis & statistical method	Interpretation & discussion	Final Approval
Yee Wen Chua	X	X	X	X	X	
I acknowledge that these represent my contribution to the above research output.						
Signed: 						
Dr Yun Yu	X	X	X	X	X	X
I acknowledge that these represent my contribution to the above research output.						
Signed: 						
Prof Hongwei Wu	X	X	X	X	X	X
I acknowledge that these represent my contribution to the above research output.						
Signed: 						

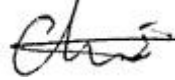


II. Publication paper “Structural changes of chars produced from fast pyrolysis of lignin at 100–300 °C, *Fuel* **2019**, Vol (255), pages 115754.”

Authors and full affiliations:

	Conception and design	Acquisition of data & method	Data conditioning & manipulation	Analysis & statistical method	Interpretation & discussion	Final Approval
Yee Wen Chua	X	X	X	X	X	
I acknowledge that these represent my contribution to the above research output.						
Signed: 						
Dr Yun Yu	X	X	X	X	X	X
I acknowledge that these represent my contribution to the above research output.						
Signed: 						
Prof Hongwei Wu	X	X	X	X	X	X
I acknowledge that these represent my contribution to the above research output.						
Signed: 						


III. Publication paper “Interactions between Low- and High-molecular-weight Portions of Lignin during Fast Pyrolysis at Low Temperatures, Energy & Fuels **2019**, DOI: 10.1021/acs.energyfuels.9b02813.”

Authors and full affiliations:

	Conception and design	Acquisition of data & method	Data conditioning & manipulation	Analysis & statistical method	Interpretation & discussion	Final Approval
Yee Wen Chua	X	X	X	X	X	
I acknowledge that these represent my contribution to the above research output. Signed: 						
Dr Yun Yu	X	X	X	X	X	X
I acknowledge that these represent my contribution to the above research output. Signed: 						
Prof Hongwei Wu	X	X	X	X	X	X
I acknowledge that these represent my contribution to the above research output. Signed: 						


**APPENDIX B      COPYRIGHT PERMISSION STATEMENTS**

- I. *Chapter 4, reprinted with permission from (Yee Wen Chua, Yun Yu and Hongwei Wu. Thermal Decomposition of Pyrolytic Lignin under Inert Conditions at Low Temperatures, Fuel 2017, 200: 70-75.) Copyright (2017) from Elsevier.*



**RightsLink<sup>®</sup>**

Home
Help
Live Chat
Yee Wen Chua ▾



**Thermal decomposition of pyrolytic lignin under inert conditions at low temperatures**

Author: Yee Wen Chua, Yun Yu, Hongwei Wu

Publication: Fuel

Publisher: Elsevier

Date: 15 July 2017

© 2017 Elsevier Ltd. All rights reserved.

Please note that, as the author of this Elsevier article, you retain the right to include it in a thesis or dissertation, provided it is not published commercially. Permission is not required, but please ensure that you reference the journal as the original source. For more information on this and on your other retained rights, please visit: <https://www.elsevier.com/about/our-business/policies/copyright#Author-rights>

BACK
CLOSE WINDOW

II. Chapter 5, reprinted with permission from (Yee Wen Chua, Yun Yu and Hongwei Wu. *Structural Changes of Chars Produced from Fast Pyrolysis of Lignin at 100–300 °C*, *Fuel* **2019**, 255: 115754.) Copyright (2019) from Elsevier.



RightsLink®



Home



Help



Live Chat



Yee Wen Chua ▾



Structural changes of chars produced from fast pyrolysis of lignin at 100–300 °C

Author: Yee Wen Chua, Yun Yu, Hongwei Wu

Publication: Fuel

Publisher: Elsevier

Date: 1 November 2019

© 2019 Elsevier Ltd. All rights reserved.

Please note that, as the author of this Elsevier article, you retain the right to include it in a thesis or dissertation, provided it is not published commercially. Permission is not required, but please ensure that you reference the journal as the original source. For more information on this and on your other retained rights, please visit: <https://www.elsevier.com/about/our-business/policies/copyright#Author-rights>

BACK

CLOSE WINDOW

*III. Chapter 6, reprinted with permission from (Yee Wen Chua, Hongwei Wu and Yun Yu. Interactions between Low- and High-molecular-weight Portions of Lignin during Fast Pyrolysis at Low Temperatures, Energy & Fuels 2019, DOI: 10.1021/acs.energyfuels.9b02813.) Copyright (2019) from American Chemical Society.*



RightsLink®



Home



Help



Live Chat



Yee Wen Chua ▾

**Interactions between Low- and High-Molecular-Weight Portions of Lignin during Fast Pyrolysis at Low Temperatures**



Author: Yee Wen Chua, Hongwei Wu, Yun Yu

Publication: Energy & Fuels

Publisher: American Chemical Society

Date: Nov 1, 2019

Copyright © 2019, American Chemical Society

**PERMISSION/LICENSE IS GRANTED FOR YOUR ORDER AT NO CHARGE**

This type of permission/license, instead of the standard Terms & Conditions, is sent to you because no fee is being charged for your order. Please note the following:

- Permission is granted for your request in both print and electronic formats, and translations.
- If figures and/or tables were requested, they may be adapted or used in part.
- Please print this page for your records and send a copy of it to your publisher/graduate school.
- Appropriate credit for the requested material should be given as follows: "Reprinted (adapted) with permission from (COMPLETE REFERENCE CITATION). Copyright (YEAR) American Chemical Society." Insert appropriate information in place of the capitalized words.
- One-time permission is granted only for the use specified in your request. No additional uses are granted (such as derivative works or other editions). For any other uses, please submit a new request.

[BACK](#)

[CLOSE WINDOW](#)